

# Lightweight Composite Trailer Design



**Joel Luke Galos**

Department of Engineering  
University of Cambridge

This dissertation is submitted for the degree of  
*Doctor of Philosophy*

Darwin College

March 2017

## **Declaration**

I hereby declare that except where specific reference is made to the work of others, the contents of this dissertation are original and have not been submitted in whole or in part for consideration for any other degree or qualification in this, or any other university. This dissertation presents the results of research carried out in the Engineering Department of the University of Cambridge between October 2013 and October 2016. This dissertation is my own work and contains nothing which is the outcome of work done in collaboration with others, except as specified in the text and Acknowledgements. This dissertation contains fewer than 65,000 words including appendices, bibliography, footnotes, tables and equations and has fewer than 150 figures.

Joel Luke Galos  
March 2017



## **Acknowledgements**

I wish to express my most sincere thanks to my supervisor Dr. Michael Sutcliffe who afforded me the opportunity to perform doctoral research at Cambridge. He gave me patient guidance and support throughout the duration of my PhD and was always willing to make time for me when I encountered issues. It was both an honour and a pleasure to learn from such knowledgeable yet approachable man.

I would also like to extend my gratitude to my advisor Prof. David Cebon. His insightful contributions to the direction of the research were greatly appreciated. I am also indebted to him for helping me progress to the next stage of my career.

I was also fortunate to be able to learn from Prof. Golam Newaz (Wayne State University) who visited the department from January 2015 to June 2015. He offered many pieces of helpful advice, particularly throughout Chapters 3 and 4. I am also extremely grateful to him for inviting me to give a talk at Wayne State University and for hosting me in his home.

I am also grateful to Dr. Maja Piecyk (Westminster University) and Dr. Phil Greening (Heriot Watt University) who provided helpful suggestions with logistics related work.

I am highly appreciative of Prof. Nick Warrior who allowed me to make use of the composites workshop facilities at the University of Nottingham, which made the work in Chapter 4 possible. I am also thankful of the help and guidance in sandwich panel fabrication provided by Paul Johns at the University of Nottingham, as well as Alan Heaver and Dr. Carlos Pascal at Cambridge, who both assisted in mechanical testing.

I gratefully acknowledge the financial support of the members of the Centre for Sustainable Road Freight. In particular: the EPSRC, Tesco, John Lewis Partnership, Hargreaves Logistics, Wincanton and SDC Trailers. Also thanks to Fiberline Composites who generously provided glass fibre pultrusion samples for mechanical testing. Thanks are also due to Jimmy Dorian and Pete Gribbin of SDC Trailers who assisted with steel chassis modelling.

Lastly but most importantly, I would like to thank my family and friends for supporting me through good times and bad during my time at Cambridge. In particular, my parents who lovingly believed in me and very generously gave me the financial support to study at Imperial College London, which led me on the path to doctoral research at Cambridge.

## **Abstract**

This thesis explores the use of lightweight composite materials in road freight trailer design as a means of reducing the emissions of the road freight industry.

A comprehensive review of previous lightweight composite trailers and related projects was conducted; it concluded that the application of composites in trailers to-date has largely been limited by relatively high material and production costs. The review highlighted that the trailer industry could learn from the success of composites in the bridge construction industry. A statistical weight analysis of two road freight fleets and an energy consumption estimation, via a drive cycle analysis, were used to identify trailers that are particularly suited to lightweighting.

Hardwood trailer decking was identified as a prime subcomponent for composite replacement. However, there is little literature on how conventional hardwood trailer decks react to in-service loadings. This problem was addressed through a comprehensive deck damage study, which was used to benchmark novel lightweight deck systems. Several lightweight replacement composite sandwich panels were designed, built and tested. Two different pultruded GFRP decks were also examined. While pultrusions do not offer the same level of weight savings as sandwich panels, the highly cost-driven nature of the trailer industry could dictate that their integration is the most reasonable first step to introducing composites into structural subcomponents.

The final part of the thesis explores options for lightweighting the trailer chassis holistically. Trailer load cases were investigated through finite element modelling in Abaqus. A parametric model of a typical longitudinal trailer I-beam was developed using Python scripting and Abaqus. The model was expanded to analyse composite trailer structures. It showed that approximately 1,300 kg of weight could be saved by shape and material optimisation in a composite trailer.

In summary, this research has shown that short-term trailer weight reductions can be effectively achieved through subcomponent replacement, while more significant reductions can be achieved in the long-term by a ‘clean slate’ composite redesign of the trailer chassis. The lightweighting strategies presented here are poised to have an increasingly important role in reducing the emissions of the road freight industry.

# Table of contents

<b>List of figures</b>	<b>viii</b>
<b>List of tables</b>	<b>xvii</b>
<b>Nomenclature</b>	<b>xx</b>
<b>1 Introduction and review of the state-of-the-art</b>	<b>1</b>
1.1 Introduction . . . . .	1
1.2 Review of the state-of-the-art . . . . .	3
1.2.1 Holistic composite trailers . . . . .	3
1.2.2 Composite subcomponents . . . . .	8
1.2.3 Related lightweighting projects . . . . .	12
1.3 Conclusions and scope of thesis . . . . .	17
<b>2 Energy consumption, fleet logistics and strategies for lightweighting</b>	<b>18</b>
2.1 Introduction . . . . .	18
2.2 Statistical weight analysis of two different road freight fleets . . . . .	20
2.2.1 Heavy goods vehicle fleet used in grocery distribution . . . . .	20
2.2.2 Heavy goods vehicle fleet used in bulk haulage . . . . .	24
2.3 Energy consumption estimation through an idealised drive cycle analysis . .	25
2.4 Discussion . . . . .	30
2.4.1 Weight and energy consumption analysis . . . . .	30
2.4.2 Fuel tankers . . . . .	32
2.4.3 The economics of trailer lightweighting . . . . .	33
2.5 Potential strategies for the application of composites to trailers . . . . .	35
2.5.1 Staged integration of composite subcomponents . . . . .	35
2.5.2 ‘Clean-slate’ composite re-design of trailer . . . . .	38
2.6 Conclusions . . . . .	39

<b>3</b>	<b>Mechanical characterisation of hardwood trailer decking</b>	<b>40</b>
3.1	Introduction . . . . .	40
3.2	Materials and damage study methods . . . . .	42
3.2.1	Materials . . . . .	42
3.2.2	Flexural testing . . . . .	44
3.2.3	Moisture damage . . . . .	46
3.2.4	Indentation damage . . . . .	48
3.2.5	Wear testing . . . . .	50
3.3	Results and discussion . . . . .	51
3.3.1	Flexural testing . . . . .	51
3.3.2	Moisture damage . . . . .	53
3.3.3	Indentation damage . . . . .	56
3.3.4	Wear testing . . . . .	57
3.4	Conclusions . . . . .	59
<b>4</b>	<b>Lightweight sandwich panel trailer decking</b>	<b>60</b>
4.1	Introduction . . . . .	60
4.2	Material selection and detailed design . . . . .	62
4.2.1	Material selection indices . . . . .	62
4.2.2	Detailed design . . . . .	64
4.2.3	Choice of raw materials . . . . .	65
4.2.4	Failure mode maps . . . . .	66
4.3	Panel fabrication . . . . .	69
4.4	Mechanical testing . . . . .	71
4.5	Results and discussion . . . . .	73
4.6	Conclusions . . . . .	79
<b>5</b>	<b>Pultruded GFRP subcomponents</b>	<b>80</b>
5.1	Introduction . . . . .	80
5.2	Trailer decking . . . . .	82
5.2.1	Choice of off-the-shelf pultrusions . . . . .	82
5.2.2	Damage study and mechanical testing . . . . .	86
5.3	Transverse members in ‘walking-floor’ trailers . . . . .	90
5.3.1	Choice of off-the-shelf pultrusions . . . . .	90
5.3.2	Joining . . . . .	92
5.4	Conclusions . . . . .	93

<b>6</b>	<b>Lightweight chassis design</b>	<b>94</b>
6.1	Introduction . . . . .	94
6.2	Review of chassis load cases and optimisation . . . . .	95
6.2.1	Literature . . . . .	95
6.2.2	SDC Trailers . . . . .	96
6.3	Development of a lightweight chassis . . . . .	98
6.3.1	Methodology . . . . .	98
6.3.2	Shape optimisation of steel beams . . . . .	102
6.3.3	Influence of trailer decking on structural properties . . . . .	105
6.3.4	Optimisation of lightweight composite chassis . . . . .	109
6.4	Conclusions . . . . .	112
<b>7</b>	<b>Conclusions and Future Work</b>	<b>115</b>
7.1	Conclusions . . . . .	115
7.1.1	Review of the state-of-the-art . . . . .	115
7.1.2	Energy consumption and fleet logistics . . . . .	115
7.1.3	Lightweight composite subcomponents . . . . .	116
7.1.4	Lightweight composite chassis . . . . .	117
7.2	Future work . . . . .	117
	<b>References</b>	<b>119</b>
	<b>Appendix A Sandwich panel calculations</b>	<b>127</b>
A.1	Flexural rigidity . . . . .	127
A.2	Failure collapse loads . . . . .	127
A.3	Failure mode map methodology . . . . .	128
	<b>Appendix B Sandwich panel flexural testing</b>	<b>130</b>
	<b>Appendix C Balsa micrographs</b>	<b>131</b>
C.1	Intermediate density end-grain balsa . . . . .	131
C.2	High density end-grain balsa . . . . .	132
	<b>Appendix D Balsa compression testing</b>	<b>133</b>

# List of figures

1.1	Structural design of a typical 13.6 m long curtain side trailer and the approximate weight of major subcomponents (courtesy of SDC Trailers). Note that the trailer connects to the truck tractor unit at the fifth wheel attachment point toward the front of the trailer. . . . .	2
1.2	The 13.6 m Belgian made Compositrailer [1]. . . . .	4
1.3	(a) The 10 m ROADLITE trailer developed by Nottingham University and EPL composites [2]. (b) The 13.6 m CleanMould trailer developed by EPL composites and other collaborators continued on the work from the ROADLITE trailer project [3]. . . . .	5
1.4	(a) The 13.6 m carbon fibre based Phoenixx trailer developed by TTT Composite AG for German trailer manufacturer Kögel [4]. (b) The carbon fibre based Walmart concept trailer developed by American trailer manufacturer Great Dane Trailers project [5]. . . . .	5
1.5	(a) The 13.6m carbon fibre based refrigerated trailer developed by TTT Composite AG for German retailer Aldi [6]. (b) The 13.6m refrigerated GIGA trailer which uses a carbon fibre monocoque structure developed by Dutch company Talson Transport Engineering [7]. . . . .	6
1.6	(a) The carbon fibre based Omni Tanker developed by Australian company Evolution Tankers Pty Ltd. [8]. (b) Tippable composite cylindrical tanker made by French company Spitzer-Eurovac [9]. . . . .	7
1.7	(a) Carbon fibre monocoque tipper trailer developed by TTT Composite AG in collaboration with fellow German company Meierling [4]. (b) Thermoplastic based Fiby tipper developed by a collection of Dutch companies for CompositTransport [10]. . . . .	8
1.8	Oak wood trailer decking reinforced with glass fibre reinforced epoxy, developed by Havco Wood Products LLC [11]. . . . .	10

1.9	Prototype sandwich panel trailer decking with extruded aluminium tube cores and (a) GFRP face sheets and (b) CFRP face sheets [12]. . . . .	10
1.10	The Dynawheel developed by Prins Dokkum BV is the first wholly carbon fibre composite HGV wheel [13]. . . . .	11
1.11	(a) The new London Wrightbus incorporates a large structural GFRP section at the rear developed by Gurit [14]. (b) The CompoBus used in Los Angeles boasts a wholly composite design [15]. . . . .	12
1.12	The glass fibre reinforced polypropylene floor structure used in the CompoBus [16]. . . . .	13
1.13	The Friedberg Bridge uses GFRP pultrusions over two steel I-beams [17]. .	14
1.14	The Pontresina Bridge undergoing laboratory testing [17]. . . . .	14
1.15	(a) Typical cross section of the West Mill Bridge [17]. (b) Standen Hey road bridge uses GFRP deck pultrusions laid span-wise [18]. . . . .	15
1.16	(a) Pont y Ddraig footbridge, Wales. (b) Typical cross section of the Pont y Ddraig footbridge. [18] . . . . .	16
1.17	(a) Air freight container that incorporates an iso-grid floor. (b) CFRP iso-grid floor. [19] . . . . .	17
2.1	Percentage of weight and volume constrained HGVs operating in the UK, adapted from [20]. . . . .	19
2.2	Approximate densities for a range of common road freight payloads, adapted from [21]. . . . .	19
2.3	(a) A three axle 13.6 m double-deck trailer with box side-walls. (b) A three axle 13.6 m single deck curtain side trailer. . . . .	21
2.4	Probability distributions (with kernel smoothing function applied) for: (a) tractor axle weight, (b) trailer axle weight, (c) GVW and (d) a histogram of number of cages for 13.6 m double-deck box trailers combined with three axle tractors used in non-refrigerated grocery distribution. Dashed lines indicate maximum allowable values. Sample size = 188. . . . .	22
2.5	Probability distributions (with kernel smoothing function applied) for: (a) tractor axle weight, (b) trailer axle weight, (c) GVW and (d) a histogram of number of cages for 13.6 m single deck curtain side trailers combined with two axle tractors used in non-refrigerated grocery distribution. Dashed lines indicate maximum allowable values. Sample size = 59. . . . .	23

2.6	Probability distributions (with kernel smoothing function applied) for: (a) tractor axle weight, (b) trailer axle weight, (c) GVW and (d) a histogram of number of cages for 13.6 m single deck curtain side trailers combined with three axle tractors used in non-refrigerated grocery distribution. Dashed lines indicate maximum allowable values. Sample size = 31. . . . .	23
2.7	(a) Rigid '8 wheeler tipper' used in bulk haulage. (b) Steel tipping bin articulated combination with a total of six axles used in bulk haulage. . . .	24
2.8	(a) Probability distribution (with kernel smoothing function applied) for GVW for 44 tonne vehicles (sample size = 5,773) and 32 tonne vehicles (sample size = 3,572) used in bulk haulage. (b) Average GVW by payload type for 44 tonne articulated combinations (sample size = 4,719). (c) Average GVW by payload type for rigid tippers with a maximum legal GVW of 32 tonnes (sample size = 2,855). . . . .	26
2.9	Free body diagram of a lorry travelling along a straight level road. . . . .	27
2.10	Idealised long haul drive cycle over a distance of 10km, adapted from [22].	28
2.11	Estimates of energy consumption reductions that can be achieved through three scenarios involving lightweighting. The average values of GVW found in the case studies (Section 2.2) were used to establish the reference case. Note that the third scenario, which involves reducing trailer weight by 30% and increasing the payload until the vehicle reaches its maximum legal GVW (weights-out), will be difficult to achieve for single deck trailers used in grocery distribution because of their volume restrictions. However, this scenario should be achievable in bulk haulage trailers and double-deck trailers used in grocery distribution. . . . .	29
2.12	Estimates of potential weight saving opportunities from various subcomponent replacement strategies. . . . .	36
2.13	Hardwood flooring laid over steel chassis beams (view from underside of a 13.6 m flat-bed trailer at the goose-neck). . . . .	36
3.1	Micrograph of the cell structure of Finnish birch plywood, with phenolic resin adhesive used to join veneers. . . . .	43
3.2	(a) Phenolic resin coated 30 mm thick Finnish birch plywood, trade name WISA-Trans. (b) Cell structure transverse to the grain direction. (c) Hot pressed non-slip phenolic coating. (d) Cell structure parallel to the grain direction. . . . .	43



3.3	The underside of WISA-Trans birch plywood with a black phenolic resin coating and the two principal material directions defined relative to the printed arrow. . . . .	44
3.4	Specimen dimensions and test parameters used in three point bend testing. .	45
3.5	Diffusion of red dye outward from a central hole indicates that moisture has a tendency to travel parallel to the grain through vessels (visible in Figs. 3.1 and 3.2) in individual veneers. . . . .	47
3.6	Top views and surface profiles of flexural test specimens with indentation damage. (a) Three indentations and (b) six indentations across the centre of the specimen. Indentations were created with a 25.5 mm diameter hardened steel spherical indenter at an applied load of 10 kN. . . . .	49
3.7	Load cycle plot of an elastic/plastic indentation, where the area inside the hysteresis loop is defined as the plastic work of indentation. . . . .	50
3.8	Rotary abrasion test set up for accelerated wear testing. Test speed = 72 RPM, applied load = 1 kg per wheel. Not to scale. . . . .	51
3.9	Flexural strength and stiffness (determined by three point bend tests) of Finnish birch plywood plotted against moisture content by weight. Error bars plotted correspond to standard deviation. . . . .	52
3.10	Residual flexural strength (determined through three point bend tests) of Finnish birch plywood decking with varying levels of damage, plotted against the reduction in flexural stiffness. Error bars plotted correspond to standard deviation. Note that * indicates dried from 20% to 10% moisture. . . . .	53
3.11	Typical load-displacement curve and corresponding failure mechanisms for pristine Finnish birch plywood (30 mm nominal thickness) in three point bending. Inset photos correspond to the positions indicated on the load-displacement curve. . . . .	54
3.12	Typical load-displacement curve and corresponding failure mechanism for Finnish birch plywood (30 mm nominal thickness) with moisture damage in three point bending. Inset photo and micrograph correspond to the position indicated on the load-displacement curve. . . . .	55
3.13	Moisture content by weight plotted against specimen soaking time. Experimental data points are a reasonable fit with Fickian diffusion theory calculated from the through thickness diffusivity $D_x$ determined from the slope given by the first two experimental data points. . . . .	56
3.14	(a) Maximum indentation force and (b) residual dent depth plotted against plastic work of indentation. . . . .	57

3.15	Maximum wear depth of coated and uncoated Finnish birch plywood plotted against the number of revolutions of the rotary abrasion machine for four repeated tests. Three distinct stages of wear observed in the phenolic coated specimens indicated. . . . .	58
3.16	Wear of phenolic coated Finnish birch plywood after testing on rotary abrasion machine for (a) 1,000 revolutions as the tops of the non-slip phenolic coating are worn off and (b) 7,000 revolutions as the birch plywood becomes exposed. . . . .	58
4.1	Various lightweight panels can be split into three broad categories, adapted from [23]. . . . .	61
4.2	Two installation techniques commonly used with hardwood decking [24]. .	61
4.3	(a) Spacing between the transverse and longitudinal beam members in a 13.6 m flatbed chassis determines the required sandwich panel thickness. (b) Plan view of the typical (TYP) spacing between the transverse members in a 13.6 m flatbed chassis, which determines the required span length $L$ subjected to three point bending. Images courtesy of SDC Trailers. . . . .	61
4.4	The sandwich effect: comparison between homogeneous and sandwich cross-sections, adapted from [25]. . . . .	62
4.5	Material selection plot for a beam in three point bending developed in CES [26]. Orange and yellow markers indicate sandwich panels which match or exceed the performance of birch hardwood (shown in green) in three point bending. . . . .	64
4.6	Plot of relative mass against relative cost for the eight cheapest acceptable sandwich material combinations identified from the three point bending material selection plot. Unfilled markers: sandwich panels with woven GFRP face sheets. Solid markers: sandwich panels with aluminium face sheets. Key see Table 4.2. . . . .	66
4.7	Baltek SB.100 rigid end-grain balsa core sheet comprised of many constituent blocks bonded together with PVA adhesive. . . . .	67
4.8	Failure mode map for sandwich panels with a woven GFRP face sheets of thickness $t_f$ , an end-grain balsa core of thickness $t_c$ and an unsupported span length $l$ . Current design: 2.1 mm thick face sheets and 25.4 mm thick core. . . . .	68
4.9	Failure mode map for sandwich panels with aluminium face sheets of thickness $t_f$ , an end-grain balsa core of thickness $t_c$ and an unsupported span length $l$ . Current design: 1.5 mm thick top face sheet (tread plate), 1.2 mm bottom face sheet and 25.4 mm thick core. . . . .	68

4.10 (a) Woven GFRP-balsa (SB.150) sandwich panel manufactured with a single shot process (2.1 mm thick face sheets and 25.4 mm thick core) and with a non-slip polyamine epoxy coating applied. (b) Micrograph of GFRP face sheet used in sandwich panel construction, showing the presence of numerous voids introduced during the wet hand lay-up of the face sheets (typical cross section inset). . . . .	70
4.11 (a) Woven GFRP-balsa (SB.150) sandwich panel (2.1 mm thick face sheets and 25.4 mm thick core). (b) Aluminium-balsa (SB.150) sandwich panel (1.5 mm thick 5052 H32 tread plate top face sheet, 1.2 mm thick 6082 T6 bottom face sheet and 25.4 mm thick SB.150 core). Panels were constructed by bonding the face sheets to the core with methacrylate adhesive. . . . .	70
4.12 Nominal specimen dimensions and test parameters used in flexural testing, with an applied load $P$ . Test speed = 5 mm/min. . . . .	72
4.13 Panel testing setup with simulated forklift wheel contact. Test speed = 5 mm/min. . . . .	72
4.14 Schematic of ‘hole-punch’ test used to determine the apparent properties of constituent end-grain balsa blocks. . . . .	73
4.15 Typical load-displacement curves of the sandwich panels with SB.150 end-grain balsa cores in three point bending, compared to birch plywood. A full set of load-displacement curves is provided in Appendix B. . . . .	74
4.16 (a) Mean ultimate load and (b) mean flexural modulus of the sandwich panels in three point bending, compared to birch plywood. Error bars indicate standard deviation. . . . .	75
4.17 (a) Core shear failure observed in GFRP-balsa (SB.150) sandwich panels. (b) Face sheet yielding, followed by core shear failure observed in methacrylate bonded aluminium-balsa (SB.150) sandwich panels. . . . .	75
4.18 Load-displacement curves obtained from the large panel (550 × 400 × 30 mm) testing with loading through a simulated forklift wheel (180 × 80 mm). . . . .	76
4.19 Top face sheet failure observed during large panel testing of 30 mm thick woven GFRP-balsa (SB.150) single shot sandwich panel with non-slip coating. Failure propagates along one edge of the rubber pad that simulates a forklift wheel. . . . .	77
4.20 Histograms of the density of constituent blocks within single sheets of rigid Baltek SB.100 and SB.150 end-grain balsa core. Medians and standard deviations (S.D.) are also shown. . . . .	77

4.21	Variations in (a) shear strength and (b) nominal shear modulus, with density of end-grain balsa core used in sandwich panel construction. Properties determined through ‘hole-punch’ test. Dashed lines correspond to polynomial fits to experimental data. . . . .	78
5.1	Composite manufacturing processes in terms of performance and units per annum, adapted from [27]. . . . .	81
5.2	Schematic of the pultrusion process [28]. . . . .	81
5.3	(a) Dimensions of ‘Pedestrian Plank’ produced by Fiberline, Denmark. Adapted from [29]. (b) Dimensions of ‘Hollow Decking’ produced by Unicomposite Technology, China. Adapted from [30]. . . . .	83
5.4	Micrographs of 40 mm high ‘Pedestrian Plank’ decking, manufactured by Fiberline Composites, Denmark. . . . .	84
5.5	Micrographs of 28 mm high ‘Hollow Decking’, manufactured by Unicomposites, China. . . . .	85
5.6	Fibre architectures recovered during matrix burn-off testing of (a) ‘Pedestrian Plank’ and (b) ‘Hollow Decking’. . . . .	86
5.7	Moisture content by weight plotted against specimen soaking time for the two GFRP pultrusions. . . . .	87
5.8	Flexural strength and stiffness (determined by three point bend tests) of GFRP deck pultrusions plotted against soaking time in days. Error bars indicate standard deviation. . . . .	88
5.9	Load-displacement curves of pultrusion controls compared to birch plywood controls. Note that the nominal width of the birch plywood and ‘Hollow Decking’ specimens is 95 mm, however the nominal width of the ‘Pedestrian Plank’ specimens is 50 mm. . . . .	89
5.10	Maximum wear depth of various uncoated deck materials plotted against number of revolutions of the rotary abrasion machine. Minimum of two repeated tests for each material. . . . .	89
5.11	Transverse aluminium U-beams in ‘walking-floor’ trailers used in bulk haulage are a good candidate for replacement with GFRP pultrusions. . . .	90
5.12	Bolted joint connections that should be avoided with pultruded GFRP sections, as specified in the Fiberline Design Manual [29]. . . . .	92
6.1	The two most critical load cases and their corresponding boundary conditions (courtesy of SDC Trailers). . . . .	97

6.2	Displacement contour for the load case of resting on landing legs and trailer bogie (30 tonne UDL). $U_2$ = displacement in the y-direction in millimetres.	98
6.3	Stress plot for trailer main beam from the rear (0 m) to the front end (13.5 m) for the load case of resting on landing legs and trailer bogie (30 tonne UDL).	99
6.4	Displacement contour for the load case of running on fifth wheel and trailer bogie (30 tonnes UDL). $U_2$ = displacement in the y-direction in millimetres.	99
6.5	Stress plot for trailer main beam from the rear (0 m) to the front end (13.5 m) for the load case of running on fifth wheel and trailer bogie (30 tonne UDL).	100
6.6	Design methodology flowchart, adapted from Monroy Aceves <i>et al.</i> [31]. . .	101
6.7	Beam bending stiffness of the main longitudinal trailer I-beam from the rear (0 m) to the front end (13.5 m). . . . .	103
6.8	The geometry, loading and boundary conditions of the parametric FE model of the main longitudinal I-beam developed in Abaqus. The critical heights along the beam at the front, goose-neck and rear are all shown. Note that the x and z directions indicated correspond to the 1 and 2 material directions, respectively. . . . .	103
6.9	Displacement of the main longitudinal steel (YS355) I-beam at (a) the front end, (b) the rear end and (c) the maximum failure index (Eqn. 6.3) within the beam, all plotted against beam mass for a 15 tonne uniformly distributed line-load. The design envelope represented by the bottom left quadrant of each graph is established from the mechanical performance of the conventional 500 kg steel I-beam defined in Section 6.2.2. Model 'a' is found to be the lightest beam that fits within all three design envelopes. Key for markers in Tables 6.3 and 6.4. . . . .	106
6.10	Parameters of the FE model of the composite trailer. I-beams modelled with beam elements and deck modelled with a general shell section with a simplified stiffness matrix $[D]$ . A 30 tonne UDL was applied to the top surface of the deck. Note that the x, z and y directions indicated correspond to the 1, 2 and 3 material directions, respectively. . . . .	107
6.11	Meshing of the FE model in Abaqus, with a typical mesh size of 10 cm, corresponding to 135 beam elements per beam and 3,375 shell elements for the decking. . . . .	108

6.12	Displacement of the main longitudinal I-beams (of different materials indicated by different marker colours) at the front end for a 30 tonne UDL, plotted against total chassis mass (combined mass of the beams and decking). (a) Deck shell stiffness matrix $[D]_1$ : Pultruded GFRP decking (440 kg). (b) Deck shell stiffness matrix $[D]_2$ : CFRP-balsa sandwich panel decking (910 kg). Note that the total mass of the corresponding current typical steel chassis and hardwood decking is approximately 2,000 kg. . . . .	110
6.13	Performance plots of the composites chassis modelled in Abaqus with a 30 tonne UDL applied to the top surface of the decking. (a) Displacement of the main longitudinal beam at the front end. (b) Displacement of the main longitudinal beam at the rear end. (c) Maximum failure index within the beam. (d) Total raw material cost. Note that all models assume a deck defined by the shell stiffness matrix $[D]_1$ : pultruded GFRP decking (440 kg). Red markers indicate CFRP beams and blue markers indicate GFRP at the rear of beam and CFRP at the front end of the beam, as defined in Fig. 6.8. Details of models A, A1, B, and B1 are provided in Table 6.7. Current allowable displacement at the rear of the beam is 2 mm, this could potentially be relaxed to 4 mm to further increase weight savings. The total mass of the corresponding current typical steel chassis and hardwood decking is approximately 2,000 kg. . . . .	113
6.14	Trends in performance plots (Fig. 6.13) for the composites chassis with CFRP I-beams modelled in Abaqus. (a) Displacement of the main longitudinal beam at the front end. (b) Displacement of the main longitudinal beam at the rear end. Key see Tables 6.6 and 6.7. . . . .	114
B.1	Load-displacement curves of sandwich panels in three point bending compared to birch plywood decking. . . . .	130
C.1	Intermediate density end-grain balsa micro-structure. . . . .	131
C.2	High density end-grain balsa micro-structure. . . . .	132
D.1	Variations in (a) compressive strength and (b) compressive modulus, with density of end-grain balsa core used in sandwich panel construction. Properties are determined in accordance with ASTM C365/C365M. Dashed lines correspond to polynomial fits to experimental data. . . . .	133

# List of tables

2.1	The current amendments to the Road Vehicles (Construction and Use) Regulations 1986 (SI 1986/1078) relevant to articulated vehicles with a total of five or six axles. . . . .	21
2.2	Engineering constants used in the drive cycle analysis. . . . .	28
2.3	Lightweight marginal costs for the mass-cost trade-off for different transport systems. [32, 33] . . . . .	33
2.4	The component weight assumptions made in determining the relative benefit of lightweight trailer subcomponents. Note that * indicates estimated from CAD model supplied by SDC Trailers and material properties taken from CES EduPack 2013 [26]. . . . .	37
3.1	Stiffness and strength properties of WISA-Trans birch plywood subjected to a wheel loading over a contact area of 80 mm $\times$ 180 mm in accordance with ISO 1496 (note: no load factor has been applied) [24]. $P_{max}$ = ultimate wheel load and $\delta_{max}$ = deflection at $P_{max}$ . . . . .	44
3.2	Average moisture content by weight (with standard deviations) of pristine 30 mm thick (21 ply) phenolic coated Finnish birch plywood, over six different time intervals. . . . .	46
3.3	Summary of averaged results (with standard deviations) from three point bend testing of pristine 30 mm thick (21 ply) Finnish birch plywood. . . . .	52
4.1	Face sheet and structural core materials considered in the sandwich panel material selection process. . . . .	63
4.2	Minimum face sheet thickness and failure modes for various sandwich panels (28 mm total thickness) with either woven GFRP or aluminium face sheets. Symbols correspond to those shown in Fig. 4.6. Specific gravity of structural cores shown in brackets. . . . .	65

4.3	Material properties of selected face sheet materials. Flexural properties determined through flexural testing with span length = 120 mm, loading/support roller diameter = 19 mm, specimen length = 160 mm, specimen width = 25 mm and test speed = 5 mm/min. (Minimum of five specimens tested in every case and average values reported). Flexural stiffness determined from the initial slope in the load-displacement curve. . . . .	67
4.4	Material properties of end-grain balsa core [34]. . . . .	67
4.5	Comparison of weight characteristics of sandwich panel decking to birch plywood (WISA-Trans) decking. Total mass calculation assumes a deck area of 27 m <sup>2</sup> . . . . .	71
5.1	Comparison of weight characteristics of pultruded GFRP decking compared to birch plywood decking. Total mass calculation assumes a deck area of 27 m <sup>2</sup> . . . . .	83
5.2	Fibre reinforcement characteristics of the two pultrusions investigated. The characteristics of the GFRP laminates fabricated by wet hand lay-up in Chapter 4 are also shown for comparison. . . . .	86
5.3	Indentation testing of 'Pedestrian Plank' with a 40.0 mm diameter steel indenter. Note that * indicates localised fracturing around indentation. . . .	87
5.4	Comparison of the mechanical performance of two pultruded GFRP sections to the aluminium U-beams used in 'walking-floor' trailers. Eqns. 5.3 to 5.5 estimate the mechanical performance of the sections using average material properties taken from [26]. . . . .	91
6.1	Load range for the trailers tested in the FORWARD project [35]. . . . .	95
6.2	Material properties used in finite element modelling [26]. . . . .	101
6.3	Dimensions of the current typical steel main longitudinal beam and the 5,184 geometry variations analysed with the parametric model in Abaqus. . . . .	104
6.4	Critical dimensions of the shape-optimised steel (YS355) I-beam, as shown in Fig. 6.9. The height of the beam at the rear, goose-neck and front sections are defined in Fig. 6.8 and the web thickness was assumed to be two thirds of the flange thickness. Note that the total mass of the current typical 13.5 m steel I-beam is approximately 500 kg. . . . .	105
6.5	Dimensions of the beams (5,184 geometry variations total) investigated with the two different structural decks of stiffness $[D]_1$ and $[D]_2$ . Flange width and thickness remains uniform along the length of the beam. . . . .	107



---

6.6	Dimensions of the lightweight composite beams (5,184 total geometry variations) modelled in conjunction with the structural decking defined by the simplified stiffness matrix $[\mathbf{D}]_1$ . . . . .	111
6.7	Critical dimensions of selected composite beams. The height of the beam at the rear, goose-neck and front section are defined in Fig. 6.8 and the web thickness was assumed to be two thirds of the flange thickness. Note that total mass includes 440 kg for decking which could be achieved through either a GFRP pultrusion or sandwich panel. . . . .	112

# Nomenclature

## Roman Symbols

$A$  Cross-sectional area

$a$  ( $a_w$ ) Mass of sample in air (in water)

$b$  Specimen width

$C$  ( $C_a$ ,  $C_i$ ) Moisture concentration (ambient, initial)

$C_{DA}$  Areal coefficient of aerodynamic drag

$C_{RR}$  Coefficient of rolling resistance

$D$  Diameter of hole punch - Chapter 4

$D$  Diameter of indenter - Chapter 3

$D$  Flexural rigidity - Chapter 5

$D$  Stiffness matrix terms - Chapter 6

$d$  Diameter of indentation

$D_x$  Through thickness diffusivity

$E$  ( $E_c$ ,  $E_f$ ) Young's modulus (core, face sheet)

$E$  ( $E_{aero}$ ,  $E_{kinetic}$ ,  $E_{RR}$ ,  $E_{trac}$ ) Energy (aerodynamic, kinetic, rolling resistance, tractive) - Chapter 2

$EI_m$  Mass energy performance index

$F$  ( $F_{aero}$ ,  $F_{max}$ ,  $F_{RR}$ ,  $F_{trac}$ ,  $F_{weight}$ ) Force (aerodynamic, maximum, rolling resistance, tractive, weight)

---

$I$	Second moment of area about the neutral axis
$k$	Gradient of the initial linear portion of the load-deflection curve
$L$	Specimen length
$l$	Unsupported span length
$M$	Bending moment about the neutral axis - Chapter 5
$M$	Bending moments per unit length - Chapter 6
$m$ ( $m_{comp}$ , $m_{fib}$ )	Mass (composite, fibres)
$M_1$	Stiffness material selection index - Chapter 4
$M_2$	Strength material selection index - Chapter 4
$N$	Forces per unit length
$P$ ( $P_{max}$ )	Load (ultimate load)
$P_{trac}$	Tractive power
$Q$	Static moment of area
$q$	Uniform load per unit length
$s$	Distance traveled
$T$	Time
$t$ ( $t_c$ , $t_f$ , $t_{fr}$ , $t_r$ , $t_w$ )	Thickness (core, face sheet, front flange, rear flange, web)
$V$	Total shear force
$v$	Velocity
$v_{fib}$	Fibre volume fraction
$W$ ( $W_\infty$ )	Percentage total weight gain from moisture (at equilibrium)
$w$ ( $w_\infty$ , $w_i$ )	Total weight gain from moisture (at equilibrium, initial)
$x$	Thickness co-ordinate
$y$	Perpendicular distance to the neutral axis

$g$  Acceleration due to gravity

### Greek Symbols

$\delta$  ( $\delta_{max}$ ,  $\delta_{residual}$ ,  $\delta_{total}$ ) Deflection (maximum, residual, total)

$\sigma$  ( $\sigma_c$ ,  $\sigma_f$ ,  $\sigma_{ult}$ ) Flexural stress (core, face sheet, ultimate)

$\tau$  ( $\tau_c$ ,  $\tau_f$ ) Shear stress (core, face sheet)

$\varepsilon$  Engineering strain

$\eta$  ( $\eta_{eng}$ ,  $\eta_{trans}$ ) Efficiency (engine, transmission)

$\gamma_{12}$  Shear membrane strain

$\kappa$  Curvature

$\kappa_{12}$  Shear membrane twist

$\rho$  ( $\rho_{air}$ ,  $\rho_c$ ,  $\rho_{comp}$ ,  $\rho_f$ ,  $\rho_{fib}$ ,  $\rho_w$ ) Density (air, core, composite, face sheet, fibres, water)

### Acronyms / Abbreviations

ADR European Agreement concerning the International Carriage of Dangerous Goods by Road

Al Aluminium

ASTM American Society of the International Association for Testing and Materials

BH Brinell Hardness

BMC Bulk Moulding Compound

CAD Computer-Aided Design

CES Cambridge Engineering Selector

CFRP Carbon Fibre Reinforced Polymer

CS Core Shear

CSM Chopped Strand Mat

FE Finite Element

---

FI	Failure Index
FMCGs	Fast Moving Consumer Goods
FRP	Fibre Reinforced Polymer
FY	Face Yield
GFRP	Glass Fibre Reinforced Polymer
GHG	Green House Gas
GVW	Gross Vehicle Weight
HGV	Heavy Goods Vehicle
HSE	Health and Safety Executive
ID	Ductile Indentation
IE	Elastic Indentation
ISO	International Organization for Standardisation
LHV	Lower Heating Value of diesel
PC	Polycarbonate
PP	Polypropylene
PU	Polyurethane
PVC	Polyvinylchloride
RTM	Resin Transfer Moulding
SMC	Sheet Moulding Compound
UDL	Uniformly Distributed Load
UD	Unidirectional
VARTM	Vacuum Assisted Resin Transfer Moulding

Note: Other symbols and abbreviations not mentioned are defined in the text or figure when appearing.

# Chapter 1

## Introduction and review of the state-of-the-art

### 1.1 Introduction

Road haulage is without doubt the dominant medium for goods transportation throughout the United Kingdom (UK) and there are no indications of this changing in the foreseeable future. Moreover, predictions suggest that road freight activity will remain of underlying importance to society and the economy alike [36]. Road freight movement however is having an adverse effect on the environment as it accounts for approximately 4.7% of the UK's carbon foot print [37]. New aggressive targets established by the UK government aim to drastically reduce the emissions of greenhouse gases such as carbon dioxide (CO<sub>2</sub>) by 2050.

The fuel consumption of a vehicle and its emissions are directly related. The fuel consumption of a road freight vehicle is determined by many factors, such as engine efficiency, driving conditions and vehicle weight. Since empty vehicle weight contributes significantly to overall vehicle weight, it is a contributor to fuel consumption and CO<sub>2</sub> emissions. Therefore, applying lightweight materials in the design of these vehicles is one avenue that needs to be thoroughly explored in reducing the carbon foot print of the road freight industry.

The most common road freight trailer found in the UK is a 13.6 m long curtain side. A schematic overview of this type of trailer is shown in Fig. 1.1, along with the approximate weight of major subcomponents. There are very few regulations on the design of these typical road freight trailers. This provides a large scope for innovation within the design process. The exception to this are vehicles and trailers that carry dangerous goods (e.g. petroleum), as these are heavily regulated for safety purposes. The limitations on typical trailers are mostly concerned with outside dimensions, brake behaviour, tyre specifications and lighting

requirements, rather than structural performance. This means the structural design of the trailer is largely unconstrained creating a window of opportunity for a ‘clean-slate’ redesign with the aim of significantly reducing empty weight. Replacing smaller subcomponents within existing conventional trailer structures may also prove to be a cost effective way to achieve lightweighting.

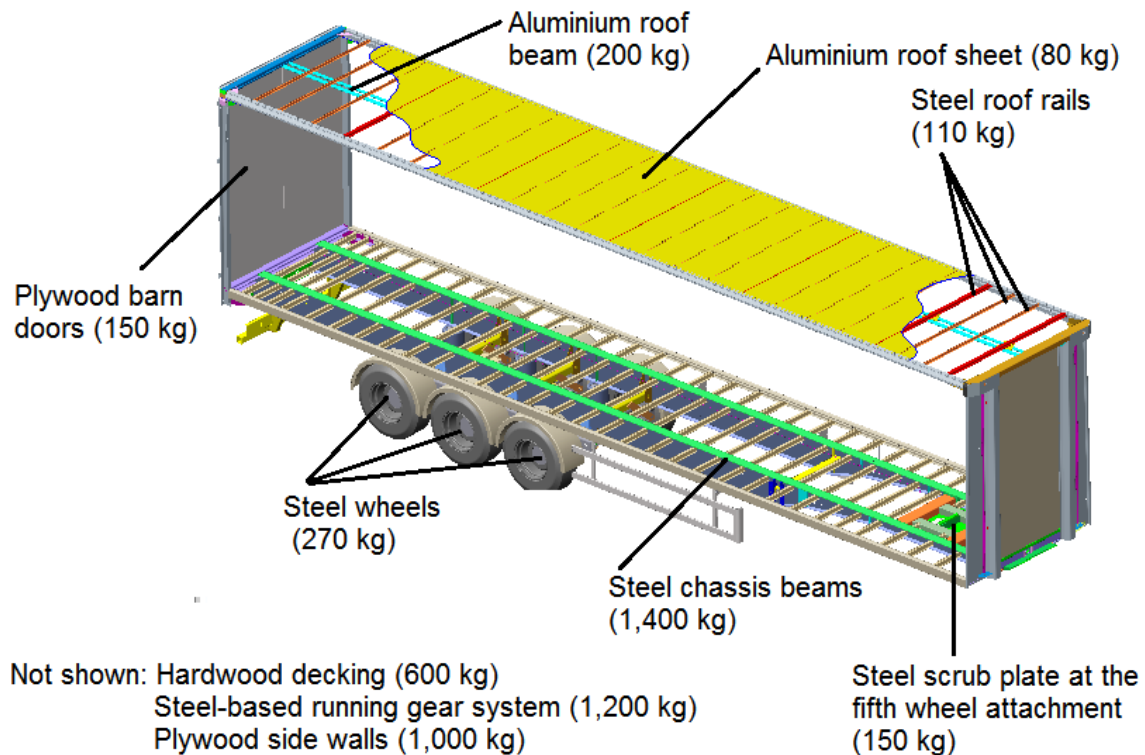


**Fig. 1.1** Structural design of a typical 13.6 m long curtain side trailer and the approximate weight of major subcomponents (courtesy of SDC Trailers). Note that the trailer connects to the truck tractor unit at the fifth wheel attachment point toward the front of the trailer.

Composite materials are a good candidate for use in both the ‘clean-slate’ redesign and subcomponent replacement approaches. In recent decades the realisation of the advantages of replacing metal alloys with composite materials has become prevalent across numerous industries including aerospace, energy, high performance automotive and sporting goods. The broad advantages of composite materials can include; reduced weight, increased corrosion resistance, greater fatigue life and reduced maintenance requirements. However, the increased material and production costs associated with composites often limit their application to high performance, weight critical applications. As such, the increased cost associated with a composite trailer should be carefully balanced alongside the economic benefits that such a trailer can bring.

## 1.2 Review of the state-of-the-art

The idea of applying lightweight materials in road freight trailer design is not a new one. Throughout the last two decades there has been a growing appreciation of the benefits brought from reducing the empty weight of road freight vehicles. This appreciation has ultimately led to a growing trend of applying lightweight composite materials in road freight vehicles and trailers. In assessing previous composite based lightweighting projects, this review has been split into three broad areas; holistic composite trailers, composite subcomponents and other related composite works including automotive, bridge and aerospace projects. The key works in each of these areas are reviewed here. It should be noted that small (passenger) vehicle automotive and rail lightweighting projects were considered to be out of the scope of this review. They were considered to be significantly different structurally to road freight trailers and face significantly different economic barriers. Also, while there has been much work done on the lightweighting of passenger vehicles, these are manufactured under different conditions and in far greater volume than road freight trailers.

The commercial nature of the majority of the previous road freight lightweighting projects dictates that the information found in the public domain is often vague and there is often a lack of technical detail on the materials and manufacturing processes used. It is also believed that the benefits of the lightweighting could be overestimated with the intention of increasing product marketability. Nevertheless, the shortage of academic publications on lightweighting heavy goods vehicles (HGVs) forces this review to rely primarily on information in the public domain, making it a state-of-the-art review rather than a conventional academic literature survey.

### 1.2.1 Holistic composite trailers

The Compositrailer (Fig. 1.2), commercialised in Belgium in 2000, represents one of the first significant attempts at the creation of a trailer wholly from composite materials. It is claimed that the 13.6 m glass fibre reinforced polyurethane chassis reduced the chassis weight from 3,500 kg to 2,800 kg, with the overall trailer weight thought to be around 5,850 kg. The design also employed 'walking-floors' as well as fireproof z-stitched composite sandwich panels (known as Acrosoma Panels) used in the trailer side walls. The project also attempted a staged integration of composites into a conventional trailer design; though this was deemed unsuccessful as premature failure of metal subcomponents would often result from dynamic loads and temperature fluctuations within the trailer. After the initial release of the trailer, Martin Marietta Composites based in the United States (US) attempted to adapt the concept for the North American market. While it is believed the Belgian company sold around 40



lightweight trailers, both the European and North American projects were in the end not commercially successful and eventually abandoned; presumably because of high production costs and lack of interest from their respective markets. [1]



**Fig. 1.2** The 13.6 m Belgian made Compositrailer [1].

The ROADLITE Trailer (Fig. 1.3a) developed by Nottingham University and EPL Composites is another stand out design that uses composites holistically [2]. The flat-bed trailer incorporates a 10 m long glass fibre reinforced thermoplastic chassis with an integrated decking, while the first prototype used a sandwich panel decking laid over the glass fibre chassis. The trailer was produced by a vacuum assisted resin transfer moulding (VARTM) process and is reported to be approximately 20% lighter and 18% stiffer than the conventional steel based design. Low cost composites and processing techniques were targeted throughout the design in order to try to achieve a competitive position within the trailer market. While it is claimed that the trailer can have an economic payback period of within two years, it is yet to be commercialised, again indicating the reluctance of the market to accept a wholly composite trailer.

Similar to the ROADLITE trailer is the 13.6 m flat-bed CleanMould trailer (Fig. 1.3b) developed by six collaborators, including EPL composites, as a follow-up to the ROADLITE project [3]. The program which concluded in 2010 developed a novel glass fibre reinforced thermoplastic material which combined a low viscosity resin and high fibre content continuous fibre reinforcement. The recyclability of this material features prominently in the marketing of the trailer, as this is often a drawback for many composite materials. It was reported that the design is approximately 10% lighter than its steel counterpart and more aerodynamic, giving rise to a reduction in fuel consumption by over 10%. However, the stated benefits of the CleanMould trailer, like other composite trailers, are difficult to validate.

German-based The Team Technology (TTT) Composite AG designed a carbon fibre reinforced epoxy monocoque tri-axle curtain side trailer known as Phoenixx (Fig. 1.4a) [4]. The trailer was designed and developed by German trailer manufacturer Kögel and was



**Fig. 1.3** (a) The 10 m ROADLITE trailer developed by Nottingham University and EPL composites [2]. (b) The 13.6 m CleanMould trailer developed by EPL composites and other collaborators continued on the work from the ROADLITE trailer project [3].



**Fig. 1.4** (a) The 13.6 m carbon fibre based Phoenixx trailer developed by TTT Composite AG for German trailer manufacturer Kögel [4]. (b) The carbon fibre based Walmart concept trailer developed by American trailer manufacturer Great Dane Trailers project [5].

produced with manufacturing support from CarboTech, based in Salzburg, Germany. It was reported that the unladen weight of the trailer is 3,700 kg, significantly lighter than a conventional design of the same size which would weigh in the vicinity of 6,000 kg. The design incorporates a carbon fibre reinforced epoxy monocoque chassis, an opening roof, a single side post and pneumatic legs. Its format is most suited to the haulage of palletised goods. Kögel has suggested that the production costs of the trailer are double that of a similar steel trailer and approximately 30% greater than an equivalent aluminium trailer.

Similarly, though more recently in 2014, American retailer Walmart collaborated with trailer manufacture Great Dane Trailers to create a prototype trailer (Fig. 1.4b) made wholly of carbon fibre composite. The trailer incorporates two 16 m long side panels that are made from a single sheet of carbon fibre. It was claimed that the trailer is 1,814 kg lighter than a comparable trailer made from conventional materials [5].



**Fig. 1.5** (a) The 13.6m carbon fibre based refrigerated trailer developed by TTT Composite AG for German retailer Aldi [6]. (b) The 13.6m refrigerated GIGA trailer which uses a carbon fibre monocoque structure developed by Dutch company Talson Transport Engineering [7].

Composites have also been applied holistically in the design of numerous refrigerated trailers. In 2010, TTT Composite AG released a 13.6 m refrigerated trailer (Fig. 1.5a) for use by German retail chain Aldi. The trailer had a monocoque design that was built around an epoxy based carbon fibre reinforced plastic (CFRP) chassis [6]. The design reduced the empty weight of trailer by around 33% in comparison to a conventional refrigerated trailer of the same size. This reportedly led to a 30% reduction in fuel consumption and a 15% reduction in CO<sub>2</sub> emissions. The production costs however were reported to be in the order of 30% more than the conventional trailer.

Similar to the Aldi trailer is the lightweight refrigerated GIGA trailer (Fig. 1.5b) manufactured by Dutch outfit Talson Transport Engineering. The GIGA trailer uses a self-supporting structure based on a ‘closed torsion free structure without a chassis’ and has been especially designed for carrying ‘cooled mega volume air freight’. The benefits of the GIGA trailer are reported to be similar to those reported by the Aldi trailer [7].

Apart from being used to lightweight dry and refrigerated trailers, composites have also been used by multiple companies to create lightweight tankers. The most notable of these is the Omni Tanker (Fig. 1.6a), designed and manufactured by Australian company Evolution Tankers Pty Ltd. The tanks are comprised of a foam sandwich construction with a high density structural foam separating inner and outer carbon fibre laminates. The tanks also have a polyethylene thermoplastic interior to increase chemical resistance and have an exterior gel coat finish to provide a smooth polished surface. The tanks are built for a wide number of tractor-trailer combinations including small rigid vehicles, triaxle trailers, B-doubles and road train configurations. Like more conventional steel or aluminium tankers, the Omni uses a compartment design with compartment capacities varying from 6,000 L to 8,500 L. These tankers have been designed and built to the Australian Dangerous Goods code ADG7, as well as Australian Standards AS2809 and AS2634 [8].



**Fig. 1.6** (a) The carbon fibre based Omni Tanker developed by Australian company Evolution Tankers Pty Ltd. [8]. (b) Tippable composite cylindrical tanker made by French company Spitzer-Eurovac [9].

A tippable composite cylindrical tanker (Fig. 1.6b) has been manufactured by French company Spitzer-Eurovac. This tanker uses numerous carbon fibre and glass fibre reinforced composites in the design of the tippable vessel. It was claimed that the tank is 400 kg lighter than comparable aluminium tankers and is able to carry the same materials. The tank has been granted French type approval, and five prototypes have been built, though it is believed that no significant sales breakthroughs have been made [4].

Prior to releasing the Phoenixx carbon fibre trailer mentioned earlier, TTT designed a carbon fibre based monocoque tipper (Fig. 1.7a) [4]. The tipper was manufactured with the help of German based bodybuilder Meierling. The tipper has a standard capacity of 25 m<sup>3</sup> and an unladen weight of 3,600 kg, significantly lighter than conventional steel and aluminium tippers. The tipper was launched at the 2004 Hanover show and has been tested over several years carrying sand and stone, showing no major issue with operational wear.

More recently than the TTT tipper, a collection of Dutch companies have developed a carbon fibre reinforced thermoplastic based composite tipper trailer known as Fiby tipper (Fig. 1.7b) [4]. It was reported to be up to 50% lighter than comparable steel loading bins. This is a large type tipper, with a capacity of around 32.5 m<sup>3</sup>, and like the TTT designed tipper, it has been designed to haul bulk products such as sand, gravel and agricultural products. The Fiby tipper is the first product from CompositTransport which aim to open an automated factory in the Netherlands in 2015 to produce a range of variety of thermoplastic based products including: tippers (articulated and rigid), trailer chassis, container tanks, truck wheels, tanks, inland waterway vessels and salt dispersers. CompositTransport believe they can reduce commercial risk by producing a variety of composite structures from the same factory and they estimate the demand for lightweight tippers alone to be at least 1,000 units [10].





**Fig. 1.7** (a) Carbon fibre monocoque tipper trailer developed by TTT Composite AG in collaboration with fellow German company Meierling [4]. (b) Thermoplastic based Fiby tipper developed by a collection of Dutch companies for ComposiTTTransport [10].

Examining the previous uses of composites in road freight trailers, it is evident that there is an apparent reluctance from the market to accept designs that are centred primarily on composite materials. This most likely arises from the lack of clarity or disbelief surrounding the exact long term benefits that a composite trailer can provide to recover the higher capital costs that result from the higher material and production costs of composite materials. There is undoubtedly some scepticism to invest in lightweight material technologies that are not as proven as and more expensive than existing materials. For the market to reach a greater acceptance of composite trailers, tankers and tippers, manufacturers need to find a way to reduce production costs and do more to substantiate the claims they make surrounding the benefits of lightweighting. Market research suggests that the increased capital costs associated with the composite trailer need to be recuperated through its benefits inside four years in an eight year lifetime for there to be interest from the marketplace. However, since composites have tailorable mechanical properties, it is believed that a composite trailer could have a significantly longer lifetime than a conventional trailer and this could also be factored into purchasing decisions.

### 1.2.2 Composite subcomponents

Aside from the afore-mentioned trailers, tankers and tippers that are designed around a majority of composite materials, numerous companies have incorporated composite sub-components into trailer designs, which are proving to be somewhat more successful in the marketplace. For example, composite sandwich panels are now a popular choice for the side walls of box type trailers and refrigerated trailers. These panels have been built with a wide variety of different materials in both the core and face sheets. Common face sheet materials

include: various grades of aluminium and glass fibre reinforced polymer (GFRP) laminates, as well as wood based sheets such as plywood and particle board. Common core materials include foams such as: polyurethane, polystyrene, phenolic and polyvinylchloride, as well as honeycombs such as aluminium, polycarbonate and polypropylene. These sandwich panels typically act to reduce weight, while increasing buckling resistance and insulation.

One panel of particular interest is the VersaMax panel manufactured by French company VersaPlast and launched in 2012. The panel consists of face sheets made from a woven combination of polypropylene and glass fibres, and a polypropylene honeycomb core. These lightweight panels are recyclable, impact-resistant and relatively low cost. The panels are sold in thicknesses from 5 mm to 100 mm and are significantly lighter than conventional panels though maintain comparable stiffness. For example, a 20 mm thick VersaMax panel weighs around  $3.6 \text{ kg/m}^2$  and has comparable stiffness to a conventional 17 mm thick GFRP coated plywood panel which weighs approximately  $12 \text{ kg/m}^2$ . The VersaMax panels can be manufactured to a height of 5 m and an unlimited length, meaning that they could be used as a one piece side wall to a double-deck trailer. VersaMax panels are similar to Omnia panels which have been available in the UK for some time. However, VersaPlast claims that their VersaMax panels are cheaper, making them more suitable for the cost driven trailer market. [38]

Companies throughout Europe and the United States that market their own variations of composite sandwich panels for use in trailers include, though are not limited to: Wabash Composites (USA) [39], Normanton Laminating Services (UK) [40], Omnia (UK) [41], Panelite Composite Solutions (UK) [38], VersaPlast (France) [38] and Acrosoma (Belgium) [41].

Some work has also been done to lightweight trailer decks through the application of composites. North American company Havco Products LLC produce laminated oak boards backed with glass fibre reinforced epoxy to increase panel stiffness (Fig. 1.8). Laminated oak flooring has been the mainstay material in dry-van trailers in North America for more than four decades. The composite stiffened oak panel was reported to be about 90% stronger than a monolithic oak panel and this extra strength allows for a reduction in thickness compared to conventional wood flooring. The product has been field tested and in trailers for more than ten years and has been commercially produced since 2000. [11]

Research has also been done on lightweighting the heavy oak trailer decking through the application of a sandwich panel composed of ribbed FRP face sheets and a core of extruded aluminium tubes (Fig. 1.9). Both GFRP face sheets (Fig. 1.9a) and CFRP face sheets (Fig. 1.9a) were considered. The CFRP face sheet sandwich panel was found to produce a 68% weight saving over monolithic oak decking and was also reported to be significantly stiffer. [12]

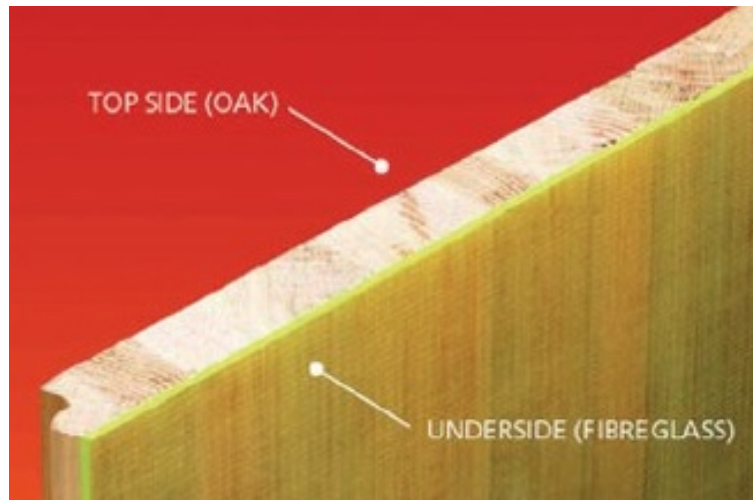


**Fig. 1.8** Oak wood trailer decking reinforced with glass fibre reinforced epoxy, developed by Havco Wood Products LLC [11].

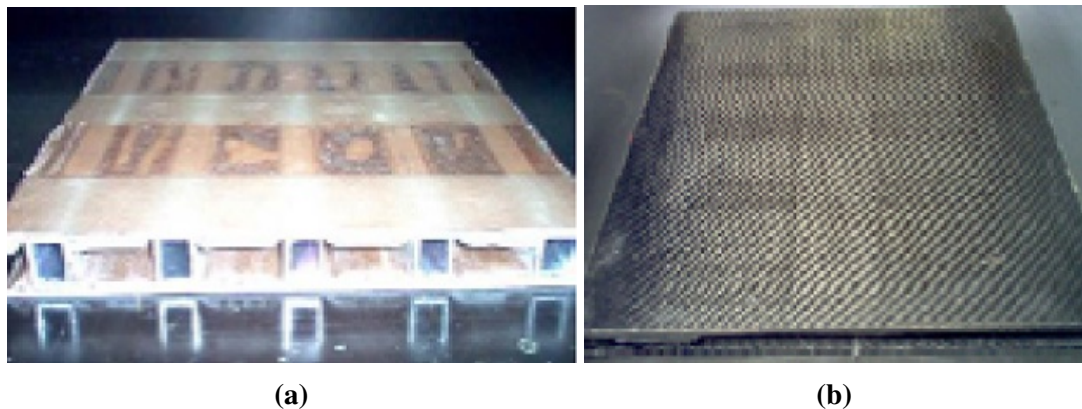


**Fig. 1.9** Prototype sandwich panel trailer decking with extruded aluminium tube cores and (a) GFRP face sheets and (b) CFRP face sheets [12].

Another recent advancement in the development of lighter subcomponents is the GFRP based air suspension running gear system, which was launched by The BPW Group in 2012. The system known as ECO Vision weighs approximately 320 kg per trailer axle compared to conventionally built air systems which weigh about 400 kg per axle. Therefore, for a tri-axle trailer this corresponds to a weight saving of 240 kg. While the concept is built to the same specifications for conventional air suspension systems, it is yet to enter mainstream production. [42]

The development of lightweight carbon fibre wheels for HGVs is another lightweighting technique that is yet to enter the mainstream. In 2003, Dutch company Prins Dokkum BV released a trailer wheel constructed entirely from carbon fibre reinforced epoxy (Fig. 1.10). Known as Dynawheel, the wheels have type approval in Europe and have undergone extensive laboratory and field tests. It was claimed that each wheel weighs 19 kg, compared to 25 kg aluminium wheels and 45 kg steel wheels. Hence, the Dynawheel could reduce the weight of a tri-axle trailer with steel wheels by approximately 156 kg. [13]



**Fig. 1.10** The Dynawheel developed by Prins Dokkum BV is the first wholly carbon fibre composite HGV wheel [13].

A growing trend that is closely linked to subcomponent lightweighting is the addition of composite sub components to enhance the aerodynamic profile of the trailer, such as; side skirts, tractor-trailer gap fairings and boat tail fairings. Some companies involved in the production and fitting of such fairings include Freight Wing (USA) [43] and ATDynamics (USA) [44]. This approach has typically been favoured by operators as they perceive the benefits from improving the aerodynamic profile to be more noticeable than lightweighting alone.





**Fig. 1.11** (a) The new London Wrightbus incorporates a large structural GFRP section at the rear developed by Gurit [14]. (b) The CompoBus used in Los Angeles boasts a wholly composite design [15].

### 1.2.3 Related lightweighting projects

#### Heavy vehicle automotive lightweighting

There are several other related heavy vehicle projects that have employed composite materials with varying degrees of success. American parcel delivery company UPS formed a ‘Plastic Trucks Project’ whereby the empty weight of their urban delivery vehicles was reduced by around 400 kg. This gave a reported maximum improvement in fuel efficiency of 40% when the vehicles were deployed on longer delivery routes [45]. The new London Wrightbus (Fig. 1.11a) is another similar example. Here five structural components in the rear end of the Wrightbus were replaced with glass fibre reinforced composites designed by Gurit and manufactured by Wrightbus to reduce the structural weight by several hundred kilograms. Gurit also investigated a composite bus chassis that demonstrated potential weight savings of around 3,000 kg [14].

In a similar scheme to the London Wrightbus, the Los Angeles public transport network introduced a wholly composite bus, known as CompoBus (Fig. 1.11b) that was aimed at reducing the operating costs of the public bus network through increased fuel savings. The CompoBus uses a novel floor structure (Fig. 1.12) which saves an estimated 40% in weight compared to standard wooden floors. The floor design uses a flat panel bonded to a sine wave rib structure, both of which are made from glass fibre reinforced polypropylene. It is thought that the lightweight deck would also bring material cost savings in excess of 50% and have an expected lifetime of 12 years, double that of conventional wooden floors [46].

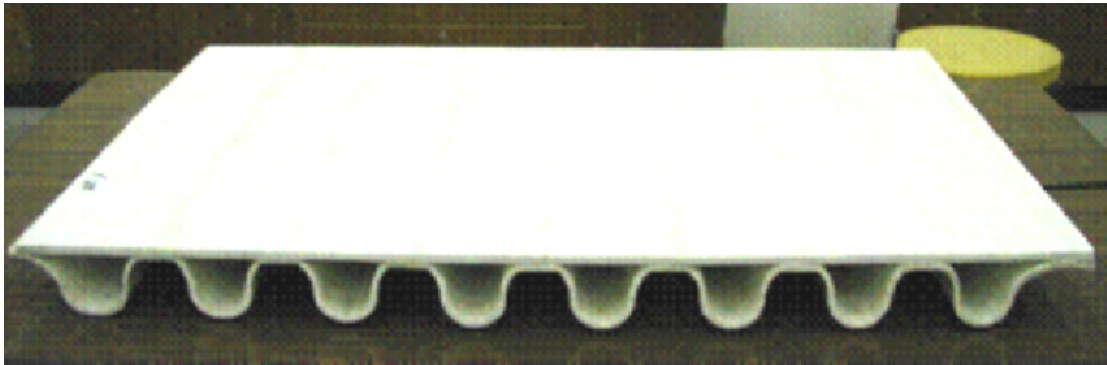


**Fig. 1.12** The glass fibre reinforced polypropylene floor structure used in the CompoBus [16].

### Composite bridges

The conventional ladder-type design of a HGV trailer chassis typically incorporates two large longitudinal I-beams, and several smaller transverse I-beams which support the trailer decking. The I-beams are typically made from steel, while the decking is typically composed of hardwood or similar type material. This basic structure resembles the structural design of many bridges, suggesting the use of composite materials to produce lightweight bridges should also be examined. Potyrala [17] has performed a state-of-the-art review on the use of FRP materials in bridge construction. The review notes that, since the inception of the first all composite bridge in 1982, FRP materials have been gaining an increasing level of acceptance in the bridge designing community. The use of these materials in bridges can be split into two broad categories; hybrid structures, which use a combination of traditional and FRP materials, and all composite bridges which have a superstructure of entirely FRP materials. A select few bridges from both categories are discussed below, however a detailed listing of hybrid and holistic composite bridges can be found in [17].

The Friedberg Bridge in Germany (Fig. 1.13) built in 2008 is a prime example of a hybrid composite bridge that has been designed with quick installation in mind. The bridge consists of two longitudinal steel I-beams and a cellular GFRP deck structure that is made by pultrusion manufacturer Fiberline Composites. The deck sections are kept free from cuts for mechanical fastenings holes and the panels are adhesively bonded to the steel members. The superstructure of the bridge is 21.45 m long, 5 m wide and can withstand a uniformly distributed load of 9 kN/m<sup>2</sup>. [17]

The Fiberline Bridge in Kolding (Denmark) was built by Fiberline Composites in 1997 to demonstrate the potential of a bridge with an all composite super structure. At 40 m long, the bridge is one of the world's largest GFRP bridges and has paved the way for the development of bridges composed primarily of pultruded GFRP components. The bridge has

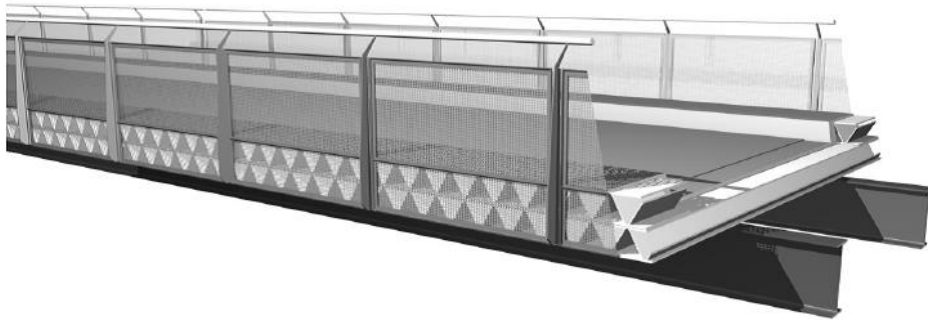


**Fig. 1.13** The Friedberg Bridge uses GFRP pultrusions over two steel I-beams [17].

also helped to demonstrate the durability of composite materials in structural applications, as it has not needed any significant maintenance since its inception in 1997. Also in 1997, Fiberline Composites produced a footbridge (Fig. 1.14) in Pontresina (Switzerland) from pultruded GFRP members. The bridge consists of two 12.5 m sections giving the bridge a total length of 25 m, a width of 3 m and a load capacity of 500 kg/m<sup>2</sup>. Once more the bridge utilises adhesive bonding to increase rigidity, decrease part count and help achieve a quick installation. The total weight of the bridge was reported to be 3,300 kg. [17]

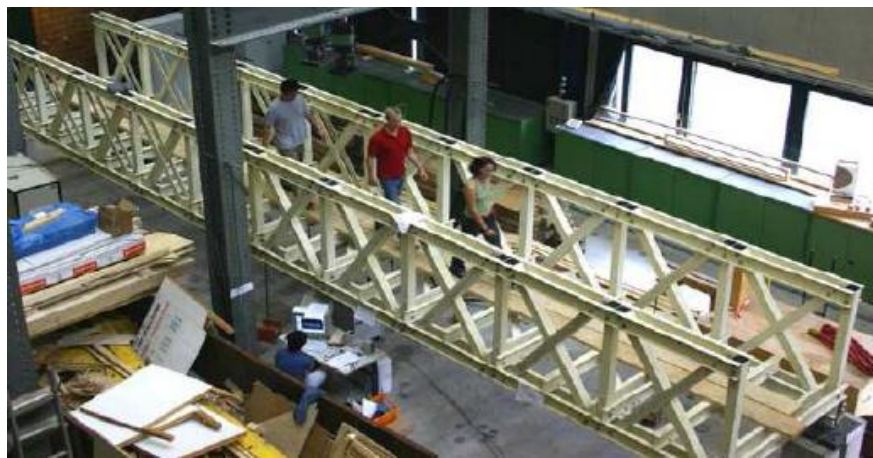


**Fig. 1.14** The Pontresina Bridge undergoing laboratory testing [17].

The West Mill Bridge (Fig. 1.15a) which was built in Oxfordshire in 2002 is another example of a road bridge with an all composite superstructure. It was designed and built by a consortium within the Advanced Structural Systems for Tomorrow's Infrastructure (ASSET) project. The bridge uses Fiberline GFRP pultrusions in the four main longitudinal members, the decking and the side panels. Each of the four main longitudinal members are comprised of four square profiles which are reinforced by both glass and carbon fibres. Like the previous



**Fig. 1.15** (a) Typical cross section of the West Mill Bridge [17]. (b) Standen Hey road bridge uses GFRP deck pultrusions laid span-wise [18].

examples, the longitudinal members and decking are adhesively bonded. The bridge has a span of 10 m, width of 6.8 m and a load carrying capacity for vehicles up to 46 tonnes. [17]

Fiberline GFRP road deck pultruded profiles have also been used longitudinally in the construction of a bonded FRP bridge at Standen Hey, UK (Fig. 1.15b). While pultruded deck profiles are typically laid transversely over span-wise longitudinal members, the profiles here have been laid in the span-wise direction. The bridge is being used to trial the performance of resin injected bolted joints which is proving promising in establishing a cost-effective, resilient and durable method for joining in FRP bridge engineering. [18]

Apart from pultruded GFRP sections in bridges, resin transfer moulded (RTM) GFRP pedestrian bridges have also been designed and fabricated successfully. For example, the 60 m long Pont y Ddraig lifting footbridge (Fig. 1.16a) uses two RTM GFRP sections that are stiffened by CFRP planks in critical areas (Fig. 1.16b). The size of these CFRP planks was optimised to minimise cost while increasing mechanical performance to the required level. Sections of the structural foam core used in the bridge are routed out so that the planks could be inserted. It has been noted that RTM fabrication technique is more popular in pedestrian bridges where the visual aesthetics are important. [18]

Research has also been performed on quantifying the social and economic impact of different bridge types over the course of their lifetime. An indicator set, known as PANTURA, has been developed to analyse and benchmark best practices in the life cycle sustainability of urban bridges. The indicator set includes the following attributes:

- Sustainability: price (life cycle cost, whole cost), disturbance, safety, environment
- Environment: emissions, recycling, materials
- Disturbance: dust, noise, delay, time

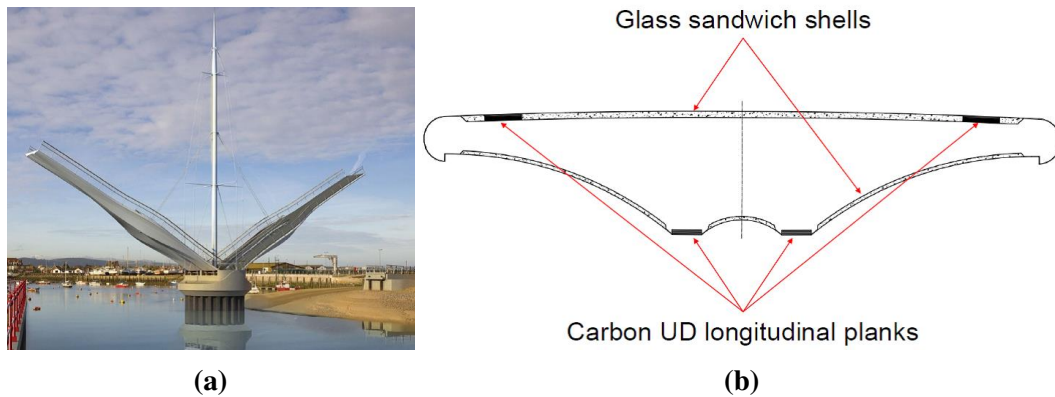


**Fig. 1.16** (a) Pont y Ddraig footbridge, Wales. (b) Typical cross section of the Pont y Ddraig footbridge. [18]

- Safety: worker safety, resident safety

With respect to these indicators, different bridge options were evaluated and the results showed that steel frame bridges with FRP decks fulfil the PANTURA goals in the best way. However, there are still a range of broad issues that hinder the application of composites to bridge construction. In particular, the following are active areas of research [18]:

- Durability and long term fatigue performance
- Compatibility between composites and traditional bridge construction materials
- Cure time and temperature requirements of adhesives on site
- Surface preparation and quality assurance of adhesively bonded joints
- Development of smart and effective systems for on-site assembly

### Air freight containers

Air freight containers (Fig. 1.17a) are another similar engineering structure to road freight trailers. These containers have had composite technologies applied to them in recent times with the aim of lightweighting the structure. IsoGrid Composites Canada Inc. has developed a CFRP isogrid structure (Fig. 1.17b) that is being used as a lightweight replacement to the aluminium structures typically used in air freight pallets. [19]



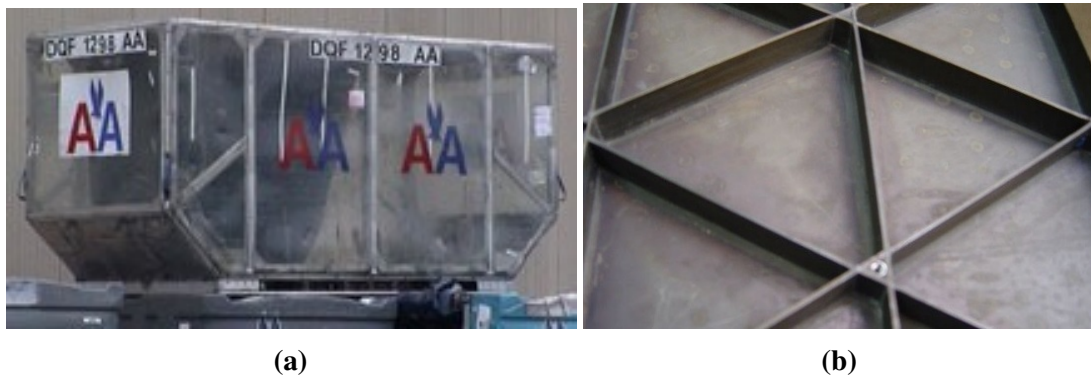


**Fig. 1.17** (a) Air freight container that incorporates an iso-grid floor. (b) CFRP iso-grid floor. [19]

### 1.3 Conclusions and scope of thesis

The state-of-the-art review has noted that prototype holistic composite trailers, such as the Compositrailer, have largely been rejected by the market. This is attributed to their higher initial investments costs compared to conventional steel chassis trailers, combined with a lack of evidence on fuel consumption reduction claims.

On the other hand, the subcomponent replacement approach to lightweighting has proven slightly more successful, arguably because investment costs are significantly less than those required for a trailer that is primarily built from composite materials. Hence, in terms of market acceptance, it seems lightweighting via the subcomponent replacement approach is the most prudent first step. Once new material technologies have been accepted and proven in numerous subcomponents, there will most likely be a greater willingness from both manufacturers and operators to accept designs that are centred on composite materials. Indeed, the industry could learn from the success of structural composites in the bridge construction industry.

There are multiple objectives that this project aims to satisfy. The first major aim is to construct a systematic framework for identifying road freight vehicles that are best suited to lightweighting. This seems to be lacking in the previous composite trailer projects discussed in this chapter. The second major aim of the project is to develop lightweight composite subcomponents for integration into exiting trailer chassis structures. The final aim of the project is to develop models to investigate the design space of a lightweight composite chassis and to clarify the weight reduction limits that could be achieved with composites. All of the major aims of the project are directed at the successful implementation of a lightweight composite trailer within a ten year time frame.

# Chapter 2

## Energy consumption, fleet logistics and strategies for lightweighting

### 2.1 Introduction

The main contributors to energy consumption of HGVs can be grouped into three broad categories [22]:

1. Vehicle design factors; such as vehicle dimensions, mass, volume, engine efficiency, rolling resistance, aerodynamic profile and material selection.
2. Logistical factors; such as vehicle utilisation, vehicle speed, vehicle routing and supply chain structure.
3. External factors; such as the drive cycle, the traffic conditions, driver behaviour and weather conditions.

It has also been noted that we can expect around a 6.5% reduction in fuel consumption from reducing trailer unladen mass by 25% [22]. This may seem to be a modest reduction relative to improving logistical factors such as running full by mass or running full by volume, which the analysis suggests can reduce fuel consumption by over 40% through reducing the total number of vehicles in a fleet. However, the estimated reduction of 6.5% in fuel consumption from lightweighting is still significant enough to pursue and may be more readily implemented compared to other measures. In fact, it has been suggested that reducing the unladen mass of the trailer is probably the easiest of the vehicle design changes to implement [22].

It should be noted however, in order to achieve the ambitious 2050 Green House Gas (GHG) reduction target a portfolio of measures will be required. Such measures could

include: trailer lightweighting, improved trailer aerodynamics, the adoption of alternative fuels and initiatives to improve vehicle utilisation, like those suggested by Léonardi and Baumgartner [47]. Driver training and reward schemes have been shown to have merit in reducing fuel consumption [48]. The need for a portfolio of solutions to achieve ambitious long-term GHG emission reductions is well noted in literature [49].

One major obstacle that is thought to be hindering the uptake of lightweight materials in HGV trailers is the difficulty in quantifying the energy consumption benefits that lighter trailers can bring. This is because in most developed economies such as the UK, operations are typically limited by volume rather than Gross Vehicle Weight (GVW) or weight over axle. This is highlighted by Fig. 2.1 which shows data for the UK. This is largely attributed to the fact that the majority of vehicles move low density fast moving consumer goods (FMCGs). The average density of products that are commonly moved by HGVs are shown in Fig. 2.2.

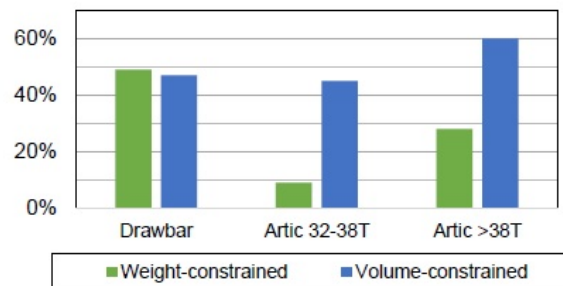


**Fig. 2.1** Percentage of weight and volume constrained HGVs operating in the UK, adapted from [20].

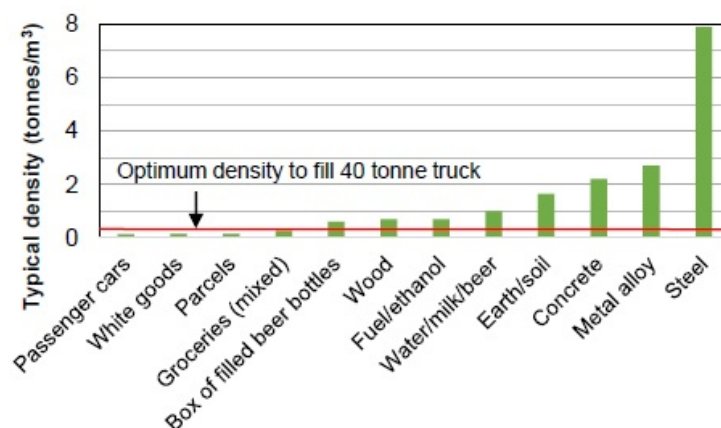


**Fig. 2.2** Approximate densities for a range of common road freight payloads, adapted from [21].

The economic and environmental gains from lightweighting will only become relevant in weight-limited applications, as the relative benefits will diminish and become far less



quantifiable in operations that are limited by volume. As such, it is proposed that the success of a lightweight trailer will depend heavily on identifying appropriate sectors of the road freight industry which frequently weight-out, that is, operate close to their legal maximum GVW. While there are statistics released by the Department for Transport about GVW and fill-rate, the data lacks important details, such as tractor-trailer combination type and weight over axle, which can be found by examining individual HGV fleets in greater detail.

The aim of this chapter is to identify specific logistic operations and corresponding HGV trailers that are prone to weighting-out and to use this information to deduce what energy savings could be realised through reducing empty trailer weight. This will assist fleet operators and trailer manufacturers alike in assessing which trailers stand the most to gain from lightweighting. Specific trailers are identified through a statistical study of the weight characteristics of two commercial HGV fleets operating in the UK (Section 2.2). The first fleet (Section 2.2.1) primarily distributes FMCGs while the second fleet (Section 2.2.2) is concerned with bulk haulage. The distribution of FMCGs and bulk haulage generate a significant amount of road freight movements in the UK in terms of both tonnes lifted and tonne-kilometres. Both fleets examined here are owned by large companies within these sectors, so they can give a good insight into these sectors as a whole within the UK. The weight data obtained from these case studies is then used in an idealised drive cycle analysis (Section 2.3) to predict reductions in energy consumption that result from reducing the mass of trailers by 30%. The potential economic effect of lightweighting is then addressed in Section 2.4.3 and strategies to apply composites are introduced in Section 2.5.

## **2.2 Statistical weight analysis of two different road freight fleets**

### **2.2.1 Heavy goods vehicle fleet used in grocery distribution**

The aim of the first statistical case study is to investigate the tractor-trailer combinations that tend to be limited by weight in a HGV fleet used to transport non-refrigerated groceries from a distribution centre in the UK. At the distribution centre there are two main types of operation; trunking operations to other distribution centres and store delivery. Trunking operations are typically performed with an articulated combination of a three axle 13.6 m double-deck trailer with box side-walls (Fig. 2.3a) combined with a three axle tractor. A three axle 13.6 m single deck curtain side trailer (Fig. 2.3b) combined with either a two or three axle tractor are the two other less common types of tractor-trailer combination that operate from the distribution centre. All tractor-trailer combinations used in distribution are



**Fig. 2.3** (a) A three axle 13.6 m double-deck trailer with box side-walls. (b) A three axle 13.6 m single deck curtain side trailer.

**Table 2.1** The current amendments to the Road Vehicles (Construction and Use) Regulations 1986 (SI 1986/1078) relevant to articulated vehicles with a total of five or six axles.

No. of axles	Max. GVW	Max. weight over axle	Comments
6	44* tonnes or 41 tonnes	10.5 tonne limit on on drive axle.  24.0 tonne limit on trailer bogie (this equates to 8.0 tonnes per trailer axle).	* indicates that the tractor must be fitted with a low pollution (at least Euro 2 compliant) engine. Tractor and trailer must both have three axles.
5	40 tonnes	11.5 tonnes over all axles.	Two axle tractor and three axle trailer or three axle tractor and two axle trailer.

required to adhere to UK regulations on maximum GVW and maximum weight over axle as shown in Table 2.1. In addition to weight regulations, volume constraints dictate that double-deck trailers are limited to carrying 75 grocery cages, while single deck trailers are limited to 45 cages.

Based on weighbridge ticket data collected over a typical week of operations, probability distributions have been created for weight over tractor axle, weight over trailer axle, GVW and number of cages carried for the three most common articulated combinations operated out of the distribution centre (Figs. 2.4, 2.5, 2.6). Each distribution was created from a kernel smoothing function estimate calculated with the 'kdensity' function in MATLAB. To show the consistency of the smoothing function, a histogram of raw weight data was plotted alongside the smoothed distribution for each of the GVW plots. Note that only histogram

plots are shown for the number of cages, as they are more appropriate given the discretised nature of this data. In the few cases where trailers are used to carry a small number of pallets in addition to cages, the distribution of number of cages has been simplified by assuming that one pallet is equivalent to two cages.

Plotted over each of the distributions are the maximum allowable values as described previously, which help to identify the limiting factor in operation for each of the different combination types. It was assumed that combinations using a three axle tractor are fitted with at least a Euro 2 compliant engine so that the maximum legal GVW will be 44 tonnes. Note that median values rather than mean values were reported as they provide the best indicator of an average value since there are outliers in the distributions and the data is not symmetrically distributed.

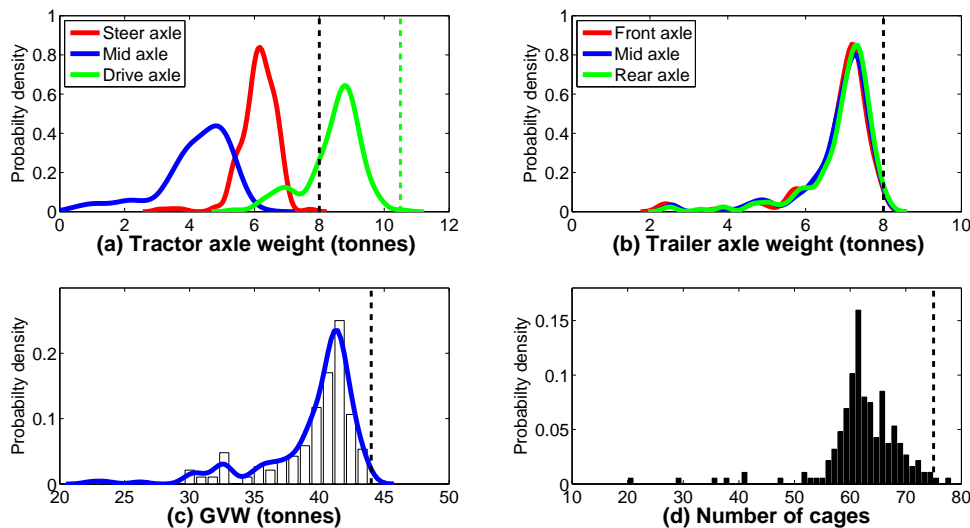


**Fig. 2.4** Probability distributions (with kernel smoothing function applied) for: (a) tractor axle weight, (b) trailer axle weight, (c) GVW and (d) a histogram of number of cages for 13.6 m double-deck box trailers combined with three axle tractors used in non-refrigerated grocery distribution. Dashed lines indicate maximum allowable values. Sample size = 188.

Fig. 2.4 indicates that weight, rather than number of cages, is more likely to be the limiting factor in the operation of the double-deck trailers. In particular, the average GVW (Fig. 2.4c) of the double-deck trailers is 40.8 tonnes, which is 93% of the maximum allowable value of 44 tonnes. Similarly, the weight over trailer axle (Fig. 2.4b), which was found to have an average value of 7.1 tonnes, which is 89% of maximum allowable value of 8.0 tonnes. However, the average number of grocery cages (Fig. 2.4d) carried for double-deck trailer operations was found to be 62, which is only 83% of the maximum allowable value of 75 cages. This is to be expected, as numerous fleet operators report that double-deck trailers

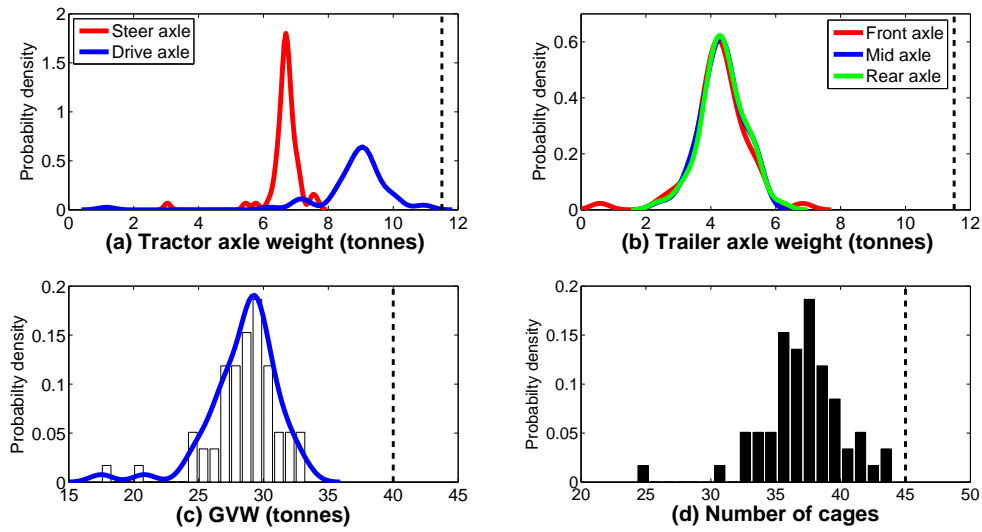


**Fig. 2.5** Probability distributions (with kernel smoothing function applied) for: (a) tractor axle weight, (b) trailer axle weight, (c) GVW and (d) a histogram of number of cages for 13.6 m single deck curtain side trailers combined with two axle tractors used in non-refrigerated grocery distribution. Dashed lines indicate maximum allowable values. Sample size = 59.

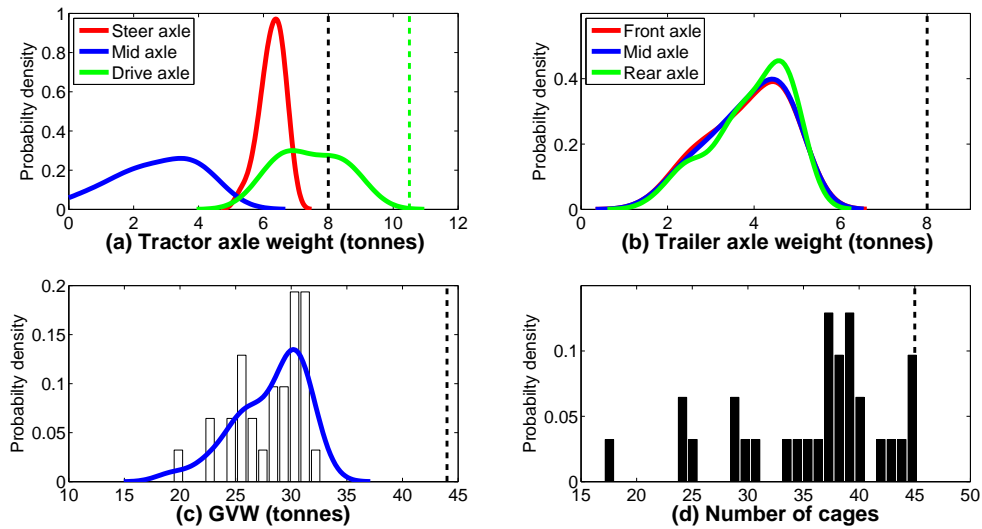


**Fig. 2.6** Probability distributions (with kernel smoothing function applied) for: (a) tractor axle weight, (b) trailer axle weight, (c) GVW and (d) a histogram of number of cages for 13.6 m single deck curtain side trailers combined with three axle tractors used in non-refrigerated grocery distribution. Dashed lines indicate maximum allowable values. Sample size = 31.



**Fig. 2.7** (a) Rigid '8 wheeler tipper' used in bulk haulage. (b) Steel tipping bin articulated combination with a total of six axles used in bulk haulage.

tend to reach their maximum allowable weights before they can be completely filled, owing to their increased size and volume.

In contrast to double-deck trailer operation, Figs. 2.5 and 2.6 show that both types of single deck trailer combinations operate far from their maximum allowable axle weight and GVW. For example, the average GVW for both types of single deck trailer operations is 29 tonnes, which is far short of the maximum allowable limit of both combinations. On the other hand, the number of cages carried by single deck trailers is closer to the maximum allowable limit, though it is still somewhat far from it. For both types of single deck trailer operations, the average number of grocery cages carried was found to be 37, which is 82% the maximum allowable value of 45 cages.

### 2.2.2 Heavy goods vehicle fleet used in bulk haulage

The aim of the second statistical case study is to investigate the HGVs that tend to be limited by weight in a commercial bulk haulage fleet operating in the UK. Within the fleet there are two categories of vehicles; rigid '8 wheeler tippers' (Fig. 2.7a), which have a maximum legal GVW of 32 tonnes and articulated combinations with a total of six axles which have a maximum legal GVW of 44 tonnes. The rigid tipping vehicles are typically comprised of aluminium tipping bins, whilst the 44 tonne vehicles are articulated combinations with three axle tractor units and three axle trailer units with either an aluminium 'walking-floor' or a steel tipping bin (Fig. 2.7b).

As in the previous case study, weighbridge ticket data was collected to create probability distributions for GVW for both 32 and 44 tonne vehicles (Fig. 2.8a). To examine the effect of payload type on GVW, the weight data was broken down further to show average GVW

by payload type for both weight categories of vehicles (Fig. 2.8b and c). Note that for the same reasons as in the previous case study, median values were used to average.

Fig. 2.8 shows that the 44 tonne capacity vehicles operate close to their maximum allowable weight with an average GVW of 43.0 tonnes. This is in contrast to the rigid 32 tonne capacity tipping vehicles which operate far from their maximum allowable weight with an average value of 22.9 tonnes. The analysis also shows while the two different weight class of vehicles are carrying similar payload types, the 44 tonne vehicles are much more frequently operating near their maximum legal GVW. This is attributed to the fact that the 32 tonne vehicles are deployed more flexibly in operations; for example, they are frequently used in jobs that are paid by trip rather than payload weight.

## 2.3 Energy consumption estimation through an idealised drive cycle analysis

This section attempts to quantify the energy consumption reductions that can be brought from lightweighting the trailers (in articulated combinations) presented in the previous case studies by applying an idealised drive cycle analysis.

As vehicles become lighter it is prudent from an operations perspective to use the extra weight saved to increase the payload weight of the vehicle. However, this can act to mask the energy benefits from lightweighting as the GVW will be roughly the same as before the trailer weight reduction. Hence, in this case we will observe that a similar amount of fuel has been consumed. To overcome this issue, Odhams *et al.* [22] quantified energy consumption through an energy performance index. They define mass energy performance index  $EI_m$  with units of kJ/tonne.km, for vehicles that are mass-limited (Eqn. 2.1):

$$EI_m = \frac{\text{Total energy used}}{\text{Payload mass} \times \text{Distance travelled}} \quad (2.1)$$

Here the total energy used equates to the tractive energy  $E_{trac}$  of the vehicle required to overcome the energy associated with aerodynamics  $E_{aero}$ , rolling resistance  $E_{RR}$  and kinetic energy. These energies can be determined by first considering a simple force balance on a vehicle travelling on a straight and level road as shown in Fig. 2.9.

A force balance determined from the free body diagram yields a formula for tractive force  $F_{trac}$  (Eqn. 2.2), in terms of aerodynamic force  $F_{aero}$ , rolling resistance force  $F_{RR}$  and linear momentum. This equation can then be expanded (Eqn. 2.3). Tractive power (Eqn. 2.4) was then determined by multiplying tractive force (Eqn. 2.3) by the vehicle velocity  $v$ . Integration of the positive values of tractive power over an idealised drive cycle (Fig. 2.10) yields the

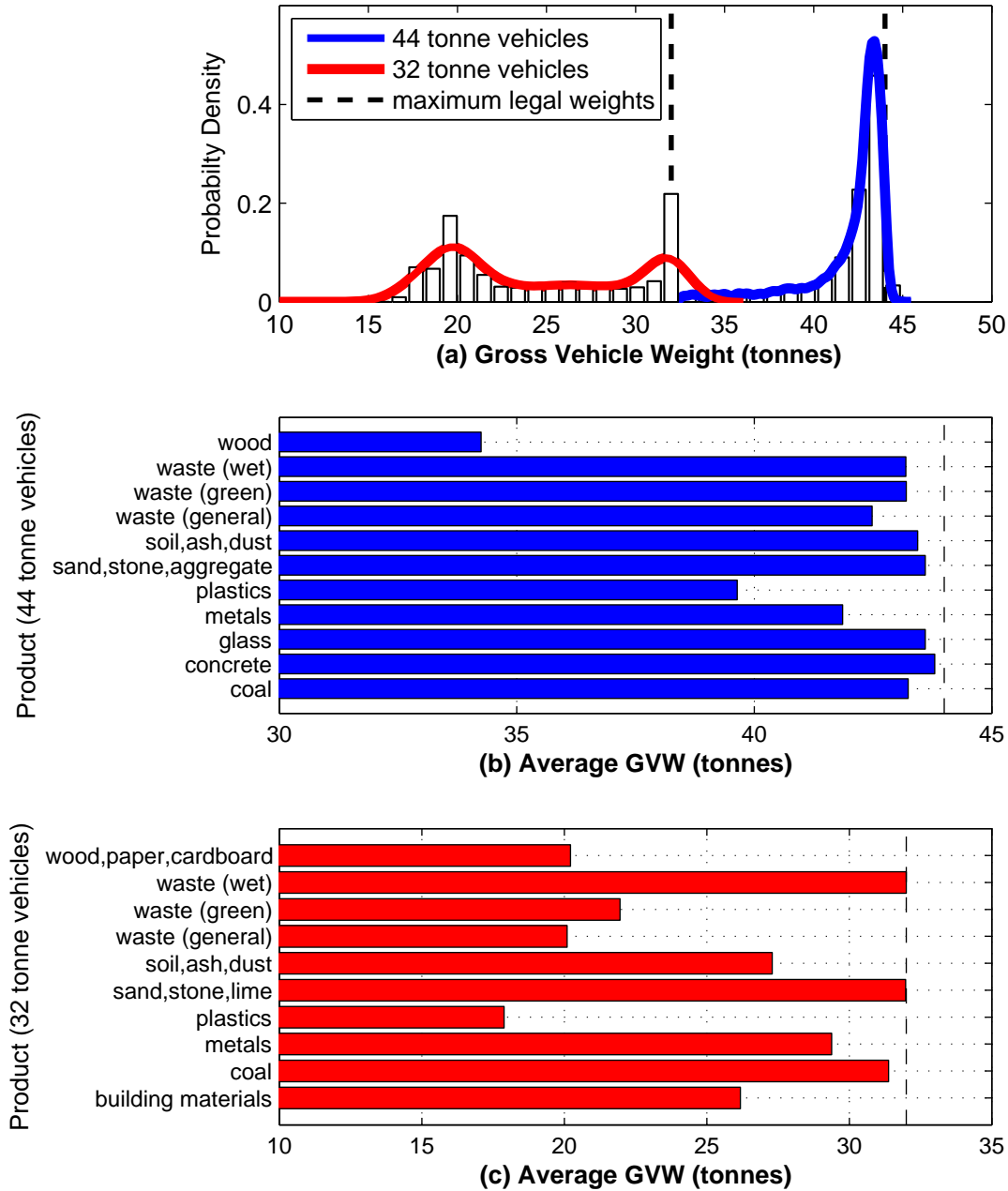


**Fig. 2.8** (a) Probability distribution (with kernel smoothing function applied) for GVW for 44 tonne vehicles (sample size = 5,773) and 32 tonne vehicles (sample size = 3,572) used in bulk haulage. (b) Average GVW by payload type for 44 tonne articulated combinations (sample size = 4,719). (c) Average GVW by payload type for rigid tippers with a maximum legal GVW of 32 tonnes (sample size = 2,855).

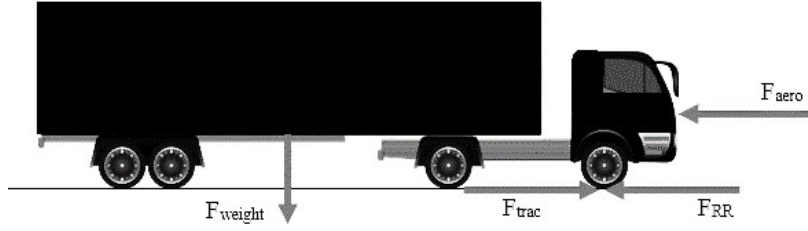


**Fig. 2.9** Free body diagram of a lorry travelling along a straight level road.

tractive energy required to travel a certain distance  $s$  in that time  $T$  (Eqns. 2.5 and 2.6). To simplify the analysis, only positive tractive energy was accounted for. Because tractive force is negative throughout the entire braking period at the end of the drive cycle, the tractive energy here is negative, hence the fuel consumed during this period is neglected. The engineering constants used throughout the drive cycle analysis are defined in Table 2.2 and the vehicle mass  $m$  in the equations refers to GVW.

$$F_{trac} = F_{aero} + F_{RR} + m \frac{dv}{dT} \quad (2.2)$$

$$F_{trac} = \frac{1}{2} C_D A \rho_{air} v^2 + C_{RR} m g + m \frac{dv}{dT} \quad (2.3)$$

$$P_{trac} = \frac{1}{2} C_D A \rho_{air} v^3 + C_{RR} m g v + m v \frac{dv}{dT} \quad (2.4)$$

$$E_{trac} = E_{aero} + E_{RR} + E_{kinetic} \quad (2.5)$$

$$E_{trac} = \frac{1}{2} C_D A \rho_{air} \int_{T_0}^{T_1} v^3 dT + C_{RR} m g s + \frac{1}{2} m (v_2^2 - v_1^2) \quad (2.6)$$

The corresponding volume of fuel burnt for the journey can then be estimated by multiplying the tractive energy by the inverse of the lower heating value of diesel, with the engine and transmission efficiencies also being accounted for (Eqn. 2.7). The effect of vehicle accessories and gear ratios on fuel consumption have both been neglected for this simple



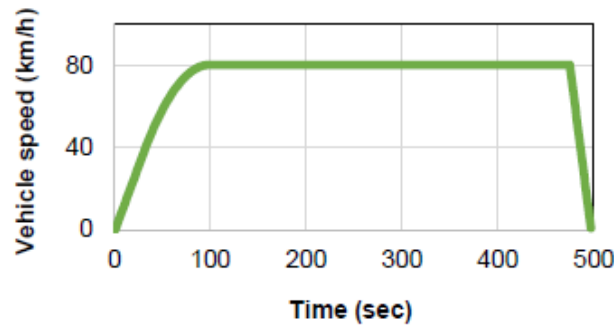
**Table 2.2** Engineering constants used in the drive cycle analysis.

Property	Value
Coefficient of aerodynamic drag ( $C_{DA}$ )	6.62 m <sup>2</sup> [50]
Coefficient of rolling resistance ( $C_{RR}$ )	0.0066 [22]
Density of air at sea level ( $\rho_{air}$ )	1.225 kg/m <sup>3</sup> [50]
Acceleration due to gravity ( $g$ )	9.81 m/sec <sup>2</sup>
Lower heating value of diesel (LHV)	35,500,000 J/L [50]
Efficiency of engine ( $\eta_{eng}$ )	0.4 [50]
Efficiency of transmission ( $\eta_{trans}$ )	0.9 [50]

comparative analysis.

$$Fuel\ consumed = \frac{1}{\eta_{eng}\eta_{trans}LHV}E_{trac} \quad (2.7)$$

All the vehicles in both case studies are typically being operated outside of urban areas on long haul journeys over highways. With this in mind, an idealised drive cycle to reflect this kind of journey was chosen for use in the tractive energy analysis. The drive cycle used is shown in Fig. 2.10 and has been adapted from [22].

**Fig. 2.10** Idealised long haul drive cycle over a distance of 10km, adapted from [22].

This procedure was then used to evaluate the potential reductions in mass energy performance index for the articulated vehicle combinations from the two case studies presented in Section 2.2. The average values of GVW found in the case studies were used to establish the reference case. The following three scenarios were examined (Fig. 2.11):

1. Reducing trailer weight by 30% and maintaining payload weight at its current level. In this scenario the reduction in mass energy performance index is directly related to the reduction in fuel consumption.

2. Reducing trailer weight by 30% and increasing payload weight by the amount of weight saved in trailer lightweighting. In this scenario fuel consumption will reflect current levels though payload weight will increase, thus resulting in an overall reduction in mass energy performance index.
3. Reducing trailer weight by 30% and increasing payload weight until the vehicle weights-out (reaches its maximum legal GVW). Here fuel consumption will increase slightly and payload weight will increase markedly producing an overall reduction in mass energy performance index.

There is also a fourth possible scenario of maintaining trailer weight at its present level while increasing payload weight until the vehicle weights-outs. This scenario represents operational improvements only. This was not considered in the analysis. However, the reduction in mass energy performance index for this case will be less than third scenario considered.

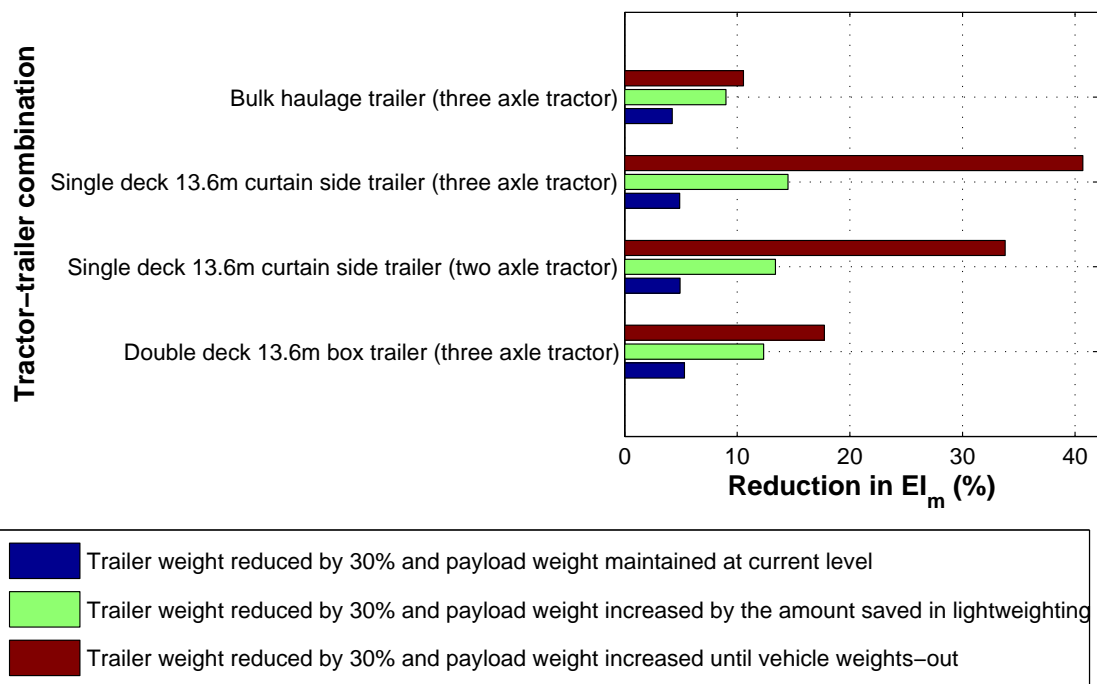


**Fig. 2.11** Estimates of energy consumption reductions that can be achieved through three scenarios involving lightweighting. The average values of GVW found in the case studies (Section 2.2) were used to establish the reference case. Note that the third scenario, which involves reducing trailer weight by 30% and increasing the payload until the vehicle reaches its maximum legal GVW (weights-out), will be difficult to achieve for single deck trailers used in grocery distribution because of their volume restrictions. However, this scenario should be achievable in bulk haulage trailers and double-deck trailers used in grocery distribution.

Note that 30% weight reduction assumed in the scenarios reflects the weight saving achieved by lightweight prototype trailers outlined in Chapter 1. The different levels of mass fill rates in each of the scenarios correlates to different levels of improvement to the logistics side of operations.

## 2.4 Discussion

### 2.4.1 Weight and energy consumption analysis

The statistical analysis in Section 2.2 has identified the articulated combination of 13.6 m double-deck box trailers with a three axle tractors as being the tractor-trailer combination that operates closest to its maximum allowable weight limits. This seems reasonable as these trailers have a larger volume and empty weight compared to that of single deck trailers. This suggests that the double-deck trailers in this fleet in particular are good candidates for weight reduction, subject to logistics constraints such as time. This notion is supported by the fact that the analysis in Section 2.3 suggests that we can expect a reduction of up to 18% in mass energy performance index by reducing the weight of the double-deck trailers by 30% and increasing their payload until the vehicle reaches its maximum legal GVW. The analysis in Section 2.3 also suggests that we could potentially reduce the mass energy performance index of single deck trailers by up to 41% through the same scenario. However, this scenario is significantly more difficult to achieve in practice largely because of the limited volume of single deck trailers.

The increase in average payload weight that is assumed by two of the three scenarios in Section 2.3 will most likely require significant improvement to the logistics side of fleet operations. Such improvements could include (but are not limited to); more accurate knowledge of individual cage weight data through refinement of the warehouse management system, refinement of route planning and improving vehicle utilisation. The need to improve vehicle utilisation is not only indicated by the two fleet case studies in Section 2.2 but also national statistics. For example in the UK in 2010, up to 29% of the tonne-kilometres moved by road freight were not limited by either weight or volume [51]. This suggests that there is a large scope for improvement in vehicle utilisation across many HGV fleets.

One way of improving vehicle utilisation is through the application of double-deck trailers. Indeed, these trailers are growing in popularity and both market research and case studies show that they can provide noteworthy improvements to vehicle utilisation [52]. Moreover, market research suggests that investment in double-deck trailers may rise particular within the retail, road haulage and grocery store sectors [52]. These factors all reiterate that double-deck

trailers are a prime candidate for lightweighting by greater investment in lightweight designs and technologies. It should be noted however, while double-deck trailers are particularly appropriate for the UK where there are high bridge and tunnel clearances, the lesser height clearances that feature in many other European countries means their application are limited in mainland Europe. Indeed, previous lightweight prototype trailers have been built primarily with the mainland European market primarily in mind, which would suggest that the concept of a lightweight double-deck trailer has been largely neglected to-date.

Another way of improving vehicle utilisation is through the application of longer trailers, which have started a 10 year trial in the UK in January 2012 [53]. These longer trailers, like double-deck trailers, have a typically high empty weight which also makes them a good candidate for lightweighting, especially if they are to be permitted for use beyond the trial period.

While the grocery fleet analysed in Section 2.2.1 has not taken into consideration refrigerated trailers, it can be expected that these trailers will be operating even closer to their maximum legal GVW, as the trailers carry the additional weight of the refrigeration system.

The analysis of the bulk haulage fleet in Section 2.2.2 has shown that the articulated vehicles with a maximum legal GVW of 44 tonnes are much more likely to be limited in operation by weight compared to the rigid tippers that have a maximum operating weight of 32 tonnes.

Section 2.3 showed that up to an 11% reduction in mass energy performance index of 44 tonne bulk haulage vehicles is achievable by reducing empty trailer weight by 30% and increasing payload weight until the vehicle reaches its maximum legal GVW. This significant energy saving combined with the fact these vehicles operate close to their maximum allowable GVW make them another good candidate for lightweighting. Moreover, it is thought that ‘walking-floor’ trailers used in the 44 tonne articulated combinations pose a strong candidate for lightweighting as they are commonly used to haul general waste and green waste materials that are not as dense and damaging as the materials carried by steel tipping bins. Because 44 tonne steel tipping bins are often used to carry heavy bulk products such as stone and scrap metal they need to be extremely robust in construction, meaning that they are potentially a poor candidate for lightweighting. While employing a lightweight 44 tonne articulated tipper only on jobs with less damaging payloads could overcome this issue, this is unlikely in practice since the trailer will become significantly less flexible in its operation, which is often of prime importance to fleet operators.

The analysis of reduction in mass energy performance index carried out in Section 2.3 relies on the fact that empty trailer mass for all the articulated combinations can be reduced by 30%. This weight reduction could be achieved through other means apart from the

application of lightweight composite materials. For example, implementing a steerable wheel trailer, like that developed by Jujnovich [54], which would allow for larger spacing between trailer axles and hence a reduction in chassis size and weight. Also removing the lifting deck on double-deck trailers where they are not needed would significantly reduce trailer weight.

### 2.4.2 Fuel tankers

The historical trend of replacing existing aluminium structures with newly designed composite structures suggests that aluminium fuel tankers are a good candidate for composite redesign. Aluminium tankers in the UK are currently designed to meet strict design rules laid out by the European Agreement concerning the International Carriage of Dangerous Goods by Road (ADR) [53]. The ADR makes recommendations for design limits for both fibre reinforced and metal alloy tankers. However, the requirements for fibre reinforced tankers are notably more conservative, restricting the potential gains that could be made by the application of composites. In particular, section 6.9.2.5 of the ADR stipulates that for tankers made from fibre reinforced plastics require a safety factor of at least four, while section 6.8.1.16 of the ADR stipulates that metal alloy tankers require a safety factor of two [53].

Section 1.2.1 described two composite tankers that have been built previously; most notably the Omni tanker in Australia. However this has not been built to the ADR standard, rather the Australian Dangerous Goods code ADG7 and Australian Standards AS2809 and AS2634. This standard is perhaps more lenient with the application of new material technologies. Section 6.1 of the standard outlines the requirements for the construction and testing of packagings (including tank vehicles) and in particular, section 6.1.1.2 states [55]:

"The requirements for packagings in 6.1.4 are based on packagings currently used. In order to take into account progress in science and technology, there is no objection to the use of packagings having specifications different from those in 6.1.4, provided that they are equally effective, acceptable to the competent authority and able successfully to withstand the tests described in 6.1.1.3 and 6.1.5. Methods of testing other than those described in this Code are acceptable, provided they are equivalent."

Similarly, the French built Spitzer-Eurovac tanker has won French type approval only and is yet to be used in the UK. The risk of rollover is undoubtedly one key factor that drives the conservative nature of the ADR which is serving to limit the application of composites in tankers for the UK market. In 1996, Frazer-Nash Consultancy Ltd. performed research

**Table 2.3** Lightweight marginal costs for the mass-cost trade-off for different transport systems. [32, 33]

Transport sector	Basis of estimate	Marginal costs (£/kg)
Automotive (family car)	Fuel saving	Up to 1.5
Automotive (high performance)	Performance	Up to 8
Automotive (road freight)	Payload	Up to 14
Civil aviation	Payload	Up to 350
Spacecraft	Payload	Up to 10,000

for the Health and Safety Executive (HSE) on the generation of internal pressure in tanker rollover [56]. One of the key findings of the simulations performed in this research was that a typical Australian designed Hockney type tanker produced between 4 and 5 bar gauge pressure near the tank lids during rollover, while a typical UK tanker produced between 1.5 and 2.0 bar gauge pressure during the same rollover. The simulations also showed that the higher the lateral stiffness of a tanker, the higher the internal pressure that is generated during a rollover. A composite tanker would likely have higher stiffness than conventional tankers and this being the case would lead to higher internal pressures being generated during rollover. Further simulations in conjunction with experimental data would help to prove that composites are safe for use in tankers despite their extra stiffness, and as such, that the European ADR should be adjusted to be more lenient for the application of FRPs.

### 2.4.3 The economics of trailer lightweighting

With the growth of composite materials in the transport sector, there has been much speculation about the real economic value of applying these lightweight material systems across different transport sectors. Indeed the economic value of lightweighting varies greatly depending on the transport sector, as can be seen in Table 2.3.

Market research indicates that investors expect the additional capital investment cost associated with the acquisition of a lightweight trailer to be made back within four years, though a shorter period is more desirable. If this is not possible, the market would likely be reluctant to accept lightweight technologies. With this in mind, the following calculations are presented to show that under the right circumstances, the additional capital investment cost of a lightweight double-deck trailer can be recuperated in around two years through fuel savings alone.

#### **Assumptions:**

Tractor weight = 6,700 kg

Trailer weight = 10,900 kg

Total combination empty weight = 17,600 kg

Lightweight trailer = 8,700 kg (20% lighter)

Typical cage capacity = 62 cages

Average haul length = 120 km (240 km round trip)

Number of cages moved per year = 26,000

Vehicle fuel efficiency from drive cycle analysis (Section 2.3) = 7.3 MPG (= 2.58 km/L)

Capital cost of existing double-deck trailer = £20,000

### **Calculations:**

Average weight of cages = (maximum GVW – total combination weight) / typical capacity =  
 $(40,800 - 17,600) / 62 = 374$  kg

Additional cages by lightweight trailer =  $(10,900 - 8,700) / 374 = 5$

Movements per year for standard trailer =  $26,000 / 62 = 419$

Movements per year for lightweight trailer =  $26,000 / 67 = 388$

Reduction in yearly kilometres for lightweight trailer =  $(419 - 388) * 240 = 7,440$  km

Fuel savings for lightweight trailer =  $7,440 * (2.58)^{-1} = 2,900$  L (= 7.5% total reduction)

### **Results:**

Assuming that the price of fuel is £1.40 per litre, the total savings per year gained from the operation of a 20% lightweight trailer is equal to £4,000. If the capital investment cost of the 20% lighter trailer is 40% more than a standard trailer, i.e. £8,000 more, then the payback period on the investment of additional capital is approximately two years. If diesel fuel prices rise, the actual payback period would become even less. Note that the 7.5% total reduction in fuel consumption corresponds to a 1.5% improvement per roll cage.

Retrofitting of structural components is most likely not economically viable. However, retrofitting of easily interchangeable sub components, such as side walls and decking, might be viable should the financial gains be immediate. For example; installing lightweight Omnia panels to trailer side walls can reduce empty trailer weight by over one tonne, though this has still come under scrutiny from trailer operators for having a payback period that is too long. These lightweight polypropylene honeycomb panels cost approximately £65/m<sup>2</sup> compared to conventional GFRP-faced plywood panels which cost approximately £28/m<sup>2</sup>. This means that for a typical double-deck trailer, the lightweight Omnia panels will increase the trailer cost by around £3,900, though they will reduce the empty weight of the trailer by approximately 1,020 kg. If the vehicle travels 120,000 km per year and the price of diesel is £1.40, then applying the drive cycle analysis method used in Section 2.3, the payback period for these lightweight panels was found to be approximately 3 years and four months

for double-deck trailers, and approximately four years for single deck trailers. While these payback periods are not favourable for large hauliers who dispose of their trailers after five years, they can be more attractive to operators who own their own fleets and see trailer lifetimes in excess of eight years.

## **2.5 Potential strategies for the application of composites to trailers**

Strategies for applying composites to the HGV trailers can be split into two broad categories; composite solutions for specific subcomponents and adopting a ‘clean-slate’ design approach for the whole trailer. For these strategies to reach the point where they can be implemented in industry, they need to be largely driven by cost. One trailer manufacturer reports that material costs alone represent approximately 60% of the total production costs of a trailer. It is believed that the most successful composite solutions will strike a balance between cost, mechanical performance and weight reduction.

### **2.5.1 Staged integration of composite subcomponents**

The integration of composites subcomponents into conventional designs to-date has been restricted by numerous factors. Firstly, a mismatch in stiffness between composites and steel leads to high stress zones developing under torsion loads. High stress areas include areas around the kingpin and neck toward the front end of the trailer, as well as areas around the suspension toward the rear of the trailer that see high loadings from tyre scrubbing. Adhesive bonding of GFRP pultruded roof rails is a lightweighting technique that has previously been explored by SDC Trailers Ltd. However, difficulties with bonding to metal railings, temperature requirements of the adhesives during cure, as well as the repairability of bonded joints, all led to the technology being abandoned. End-of-life considerations are also of utmost importance as trailers have to be returned to the manufacturer for recycling. Steel and wood are more desirable than composites from a recyclability stand point.

Examining the current structural design of a typical 13.6 m curtain side trailer (Fig. 1.1), it is immediately obvious there are many opportunities for composite subcomponent replacement. In particular, the subcomponents that are good candidates for lightweighting include: side walls, running gear, wheels, chassis members, suspension bracing, barn doors, decking and the roof structure. Operators generally like to have steel rubbing plates as these can sustain significant wear and tear during connection to a tractor’s fifth wheel. Hence, steel rubbing plates are a poor candidate for composite substitution.



To determine the relative benefits of lightweighting each of these components, Fig. 2.12 was created. It indicates estimated potential weight savings that can be realised through numerous subcomponent replacements. The main assumptions made in generating this plot are detailed in Table 2.4, where lightweight replacement components are required to have approximately the same strength and stiffness of conventional components. It should be noted that the data used in creating this plot has been provided by industrial partners, manufacturers and also material selection software CES EduPack 2013 [26]. While Fig. 2.12 provides only rough estimates of weight saving benefits, it indicates that the greatest benefits can be expected from subcomponent replacement of the side walls, decking and the chassis structure.

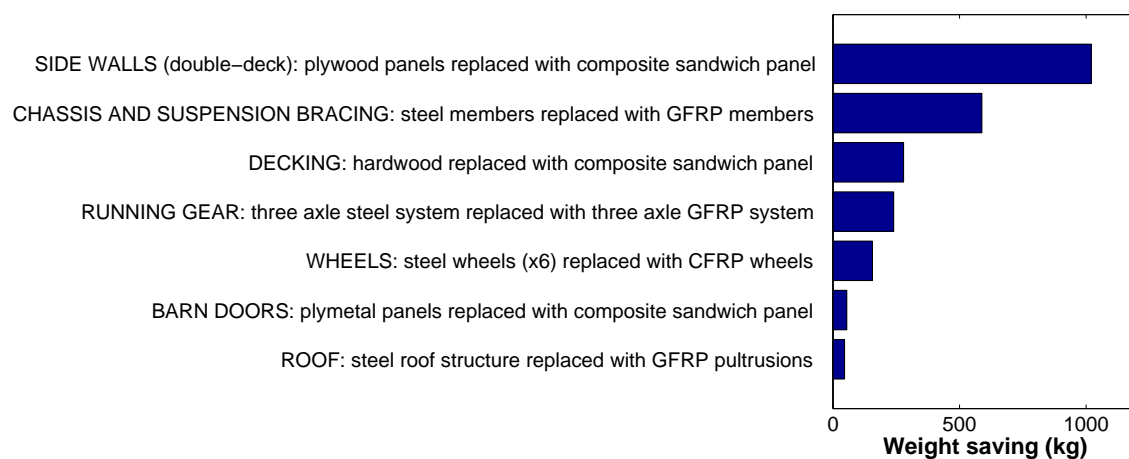


**Fig. 2.12** Estimates of potential weight saving opportunities from various subcomponent replacement strategies.



**Fig. 2.13** Hardwood flooring laid over steel chassis beams (view from underside of a 13.6 m flat-bed trailer at the goose-neck).

**Table 2.4** The component weight assumptions made in determining the relative benefit of lightweight trailer subcomponents. Note that \* indicates estimated from CAD model supplied by SDC Trailers and material properties taken from CES EduPack 2013 [26].

Subcomponent	Description of conventional material and weight estimate	Description of lightweight material and weight estimate
Side walls	GFRP coated plywood panels = 14 kg/m <sup>2</sup>	Polypropylene honeycomb sandwich panels = 4.8 kg/m <sup>2</sup>
Running gear (×3)	Steel based air suspension system = 400 kg per axle	GFRP based air suspension system = 320 kg per axle
Wheels (×6)	Steel wheels = 45 kg per wheel	CFRP wheels = 19 kg per wheel
Chassis* (longitudinal beams ×2)	Steel sections = 980 kg	Pultruded GFRP sections = 570 kg
Chassis* (transverse beams ×31)	Steel sections = 380 kg	Pultruded GFRP sections = 220 kg
Suspension bracing*	Steel sections = 121 kg	Pultruded GFRP sections = 100 kg
Barn doors	Galvanised steel coated plywood = 23 kg/m <sup>2</sup>	Sandwich panel = 9 kg/m <sup>2</sup> (estimate only)
Decking	Half lapped keruing hardwood = 26 kg/m <sup>2</sup> 30 mm thick birch plywood = 21 kg/m <sup>2</sup>	Sandwich panel = 15 kg/m <sup>2</sup> Pultruded GFRP decking = 17 kg/m <sup>2</sup>
Roof	Steel roof structure = 110 kg Aluminium roof sheet = 79 kg Aluminium rails (×2) = 190 kg	Pultruded GFRP roof structure = 64 kg GFRP (SMC) sheet = 100 kg Pultruded GFRP rails (×2) = 200 kg

Fig. 2.12 clearly shows that replacing the plywood side walls of a double-deck trailer with a composite sandwich panel will save approximately one tonne of weight, which is the greatest weight saving that can be achieved through this approach. Chapter 1 identified numerous commercially available sandwich panels that are capable of bringing this weight saving. The figure also shows that the next greatest weight saving that could be achieved is through applying composites in the trailer chassis and this will be explored in greater detail in Chapter 6. The next greatest benefit is achieved through replacing hardwood decking (Fig. 2.13) with a lightweight composite panel, which is thought to provide up to 250 kg of weight saving. Indeed, there are no commercially available lightweight trailer floors available in the marketplace, indicating that this is an interesting topic for further research. A lightweight trailer floor could also be universally applicable to many different trailer types, making it an attractive option from a commercial viewpoint. For these reasons, trailer decking becomes the focus of Chapters 3 and 4, as well as part of Chapter 5.

Fig. 2.12 also indicates that lightweighting the steel running gear and the steel wheels with the prototypes described in Chapter 1 could also provide significant weight savings (240 kg and 150 kg, respectively). Lightweighting the barn doors and the roof structure is thought to bring minimal benefits only.

### 2.5.2 ‘Clean-slate’ composite re-design of trailer

Adopting a ‘clean-slate’ design approach will allow for the full benefits of composite materials to be realised. This approach can help allow for the integration of aerodynamic and structural functions, which can help achieve weight reduction and aerodynamic improvement simultaneously. Moreover, the directional nature of composites can be exploited to increase structural reinforcement at areas of high stress concentration, such as the goose-neck, and remove mass in parts of the structure are not significantly loaded.

The previous composite trailers that have adopted a ‘clean-slate’ design approach (outlined in Section 1.2.1) suggest that the major drawback in this approach is increased material and production costs associated with composites. In particular, the resin transfer moulding (RTM) process (used to manufacture the Compositrailer, ROADLITE trailer and Clean-Mould trailer) is very unlikely to be adopted by existing trailer manufacturers. Adopting this process would require significant investment in new equipment and facilities, as well as extensive operator training. Likewise with the carbon fibre based Phoenixx and Walmart trailers which require an autoclave to cure carbon fibre components. Perhaps the most financially viable way of achieving a composite redesign is to outsource the manufacture of composite components and then integrate these components in existing trailer assembly lines. This would involve minimum investment in equipment, facilities and operator retraining.

The ‘clean-slate’ approach will also allow for the integration of composite materials with other emerging HGV technologies such as active steering of trailer wheels which has been shown to reduce lateral design loads [54].

## 2.6 Conclusions

Reducing the empty weight of HGV trailers used in mass-limited operations can bring significant energy consumption savings which will lead to a reduction in both operation costs and carbon footprint. The mass energy performance index defined by Odhams *et al.* [22] is a useful way to quantify the energy consumption of mass-limited heavy goods vehicles. By using this index in conjunction with fleet weight statistics and a simplified drive cycle analysis, it is possible to quantify the reductions in energy consumption caused by hypothetical reductions in empty trailer mass. Using this approach, trailers that will benefit the most from weight reduction can be identified systematically, allowing for lightweighting strategies to be implemented more effectively.

The statistical analysis of two HGV fleets that are operated in the UK identifies double-deck trailers used in grocery distribution and ‘walking-floor’ trailers used in bulk haulage as two examples of HGV trailers that are good candidates for lightweighting, as they operate relatively close to their legal weight limits. While the analysis here was limited to two HGV fleet case studies, these fleets are owned by large companies that represent a significant proportion of road freight tonne-kilometres within their respective sectors.

To reduce empty trailer mass in practice, applying lightweight composite materials to trailer subcomponents such as decking and side walls seems a logical way to begin the process as this can be implemented in short time frames and for a minimal increase in cost. However, for a long-term solution more radical design changes will be needed to drastically reduce empty trailer weight. Despite the fact that holistic lightweight composite trailers have failed to gain any significant market acceptance, these trailers will become increasingly viable as greater emphasis is placed on reducing the energy consumption of the road freight industry. An in-depth understanding of fleet operations gained by examining representative fleet data, like that presented here, will aid the development and application of lightweight trailers that are economically viable.

## Chapter 3

# Mechanical characterisation of hardwood trailer decking

### 3.1 Introduction

Hardwood of various varieties has been the mainstay of road freight trailer decking for decades. Indeed, there is research that suggests it is the most sustainable kind of trailer deck material, as it is renewable, recyclable and creates lower carbon emissions in manufacture compared to steel, aluminium and plastics [57]. However, this past research has neglected to take into consideration the potential energy savings that can be realised by using lightweight materials (such as FRPs) in trailers, as discussed in Chapter 2. In order to develop a successful lightweight trailer deck that can challenge the dominance of hardwood, it is first essential to develop a detailed understanding and mechanical characterisation of conventional hardwood trailer decking, and this is the focus of this chapter.

Because of the different availabilities of hardwood varieties throughout the world, the wood used in trailer decking varies depending on geographic location. In Europe and the UK, the most common form of hardwood used in trailer decking is Finnish birch plywood, originating in North and North Eastern Europe. The raw material of this birch plywood is composed of both *Betula pendula* and *Betula pubescens*. In North America on the other hand, oak wood decking is more common in road freight trailers. As this research took place in the UK, birch plywood is the subject of this investigation and this is also generally considered to be the cheapest form of trailer decking.

The experience of UK road freight trailer operators indicates that water damage and indentation damage are the two most prevalent forms of in-service damage caused to hardwood trailer decking. Wear from repeated loading and unloading of grocery cages is also

of concern to operators. Damaged decks are often repaired or replaced depending on the severity of damage, typically assessed through a visual inspection. There is minimal published literature that attempts to characterise the effects of these common types of in-service damage to Finnish birch plywood, and trailer operators are typically reliant on manufacturer guidelines. A better understanding of the effects of in-service damage is crucial in helping to understand if damaged decking should be replaced. A full mechanical characterisation of Finnish birch plywood trailer decking will also create a useful benchmark for comparing new trailer decking systems against.

The mechanical characterisation of wood-based flooring is a relatively mature subject. The Forests Products Laboratory in the United States has developed a number of accelerated test procedures designed to characterise the performance of wood floorings [58]. These test procedures have since been published by the American Society of the International Association for Testing and Materials (ASTM) and can be found in ASTM D 2394-05: 'Standard methods for simulated service testing of wood and wood-base finish flooring' [59]. Within the standard there are test procedures for measuring resistance to concentrated loading, floor surface indentation from small area loads, and damage from rolling loads. Methods for measuring the abrasion resistance, coefficient of friction and the effects of surface wetting are also outlined in this standard.

The mechanical performance of hardwood, including Finnish birch and Finnish birch plywood has been thoroughly addressed in literature. Heräjärvi [60] has investigated the modulus of elasticity and the modulus of rupture of Finnish birch and the relationship of these flexural properties to specific gravity. There are also industry handbooks which quantify how flexural properties of Finnish birch plywood are affected by moisture damage [61]. Swaczyna *et al.* [62] tested the Brinell hardness and abrasive wear resistance of eight wood species commonly used in flooring panels and found that hardness is closely related to wood density, while wear resistance has a high variance. Karshenas and Feely [63] investigated the flexural properties and interlaminar shear strength of used plywood that had been re-used in concrete slab formwork. The experimental data was used to correlate the bending strength and bending stiffness of the used plywood. Knapic *et al.* [64] investigated the performance of cork oak wood as a solid wood flooring. Dimensional stability to air humidity and liquid water, hardness and wear resistance were all investigated.

The published literature and the recommendations made in ASTM D 2394-05 both give a good insight into the tests that can be used to characterise in-service damage to wood based flooring. However, a detailed investigation into the damage types most common to hardwood road freight trailer decking will be beneficial in properly characterising trailer deck performance. The experience of industrial partners operating large fleets of road freight trailer

indicates that water damage, indentation damage and abrasive wear need to be thoroughly examined.

The aim of this chapter is to determine the effect of the most common forms of in-service damage on the flexural properties of Finnish birch plywood used in road freight trailers. A particular focus of this study is to quantify the effect of indentation damage on flexural properties and to compare this to the effect of moisture damage, which is already well understood in the literature. This will provide a deeper insight into whether damaged trailer decking can still be considered fit for service, as well as provide a benchmark for the performance of novel deck systems, such as composite sandwich panels and pultrusions.

## 3.2 Materials and damage study methods

### 3.2.1 Materials

Finnish birch (*Betula pendula* and *Betula pubescens*) plywood, tradename WISA-Trans, manufactured by UPM-Kymmene Corporation was the focus of this investigation. This is the most common material used in road freight trailer decking in Europe and the UK. It is also used extensively in other industries, such as in formwork panels in the construction industry. Stewart [65] provides a description of the process used to fabricate these plywood panels. First, birch logs are cut and debarked and then softened in warm water, before being peeled away in a lathe. After peeling, the wood veneers are trimmed, dried and graded depending on how many defects they contain. Different grades of veneers are then used in the back, face and core of the plywood laminate. The veneers are coated with a phenolic resin adhesive (Fig. 3.1) which cures when the veneers are stacked and hot pressed, to give the finished plywood laminate (Fig. 3.2). The phenolic coating that is applied to the exposed surfaces and exposed edges of the laminate helps to minimise moisture uptake during service life.

Samples were cut from 30 mm nominal thickness (21 ply) panels for each of the test types. Typically five samples were tested in each of the different tests described below. Cutting the samples from a larger plywood panel resulted in the edges of the specimens being exposed with no phenolic coating. In practice, the edges will always be coated with phenolic adhesive to minimise the moisture uptake of the wood.

The plywood has two principal material directions which correspond to the orientation of the outer veneers, indicated by the direction of an arrow (printed on by the manufacturer) on the back face of the material (Fig. 3.3). Parallel to the direction of the arrow was defined to be the 0° direction and perpendicular to the arrow was defined to be the 90° direction. Because of its directionality, Finnish birch plywood is generally laid over trailer chassis beams so

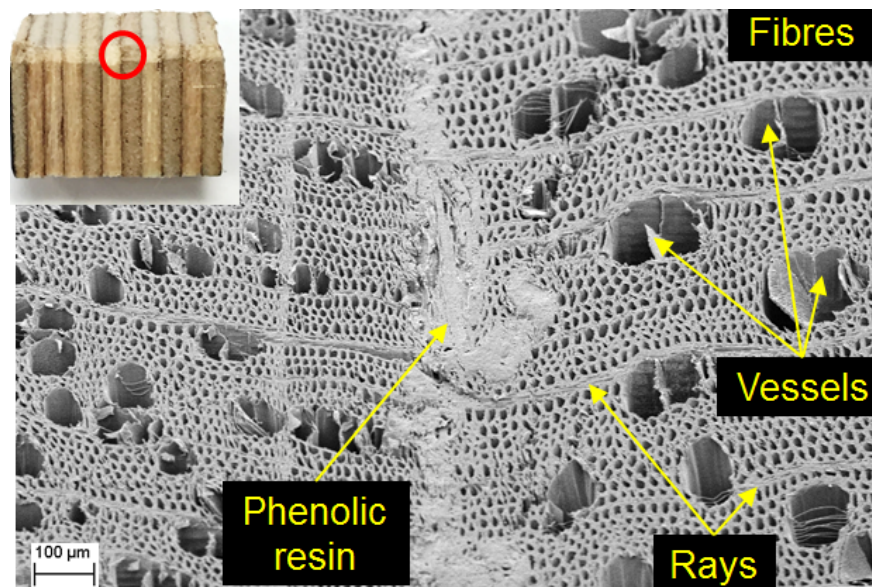


**Fig. 3.1** Micrograph of the cell structure of Finnish birch plywood, with phenolic resin adhesive used to join veneers.

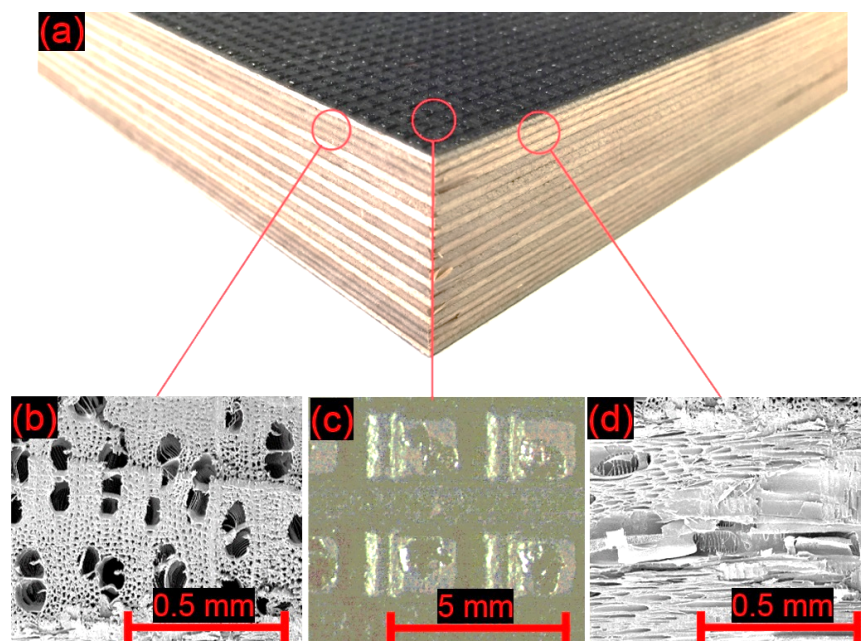


**Fig. 3.2** (a) Phenolic resin coated 30 mm thick Finnish birch plywood, trade name WISA-Trans.  
 (b) Cell structure transverse to the grain direction.  
 (c) Hot pressed non-slip phenolic coating.  
 (d) Cell structure parallel to the grain direction.



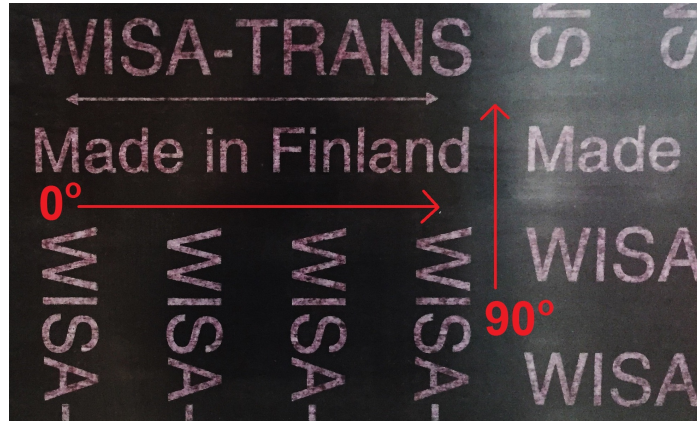


**Fig. 3.3** The underside of WISA-Trans birch plywood with a black phenolic resin coating and the two principal material directions defined relative to the printed arrow.

**Table 3.1** Stiffness and strength properties of WISA-Trans birch plywood subjected to a wheel loading over a contact area of 80 mm × 180 mm in accordance with ISO 1496 (note: no load factor has been applied) [24].  $P_{max}$  = ultimate wheel load and  $\delta_{max}$  = deflection at  $P_{max}$ .

	Span = 400 mm		Span = 500 mm	
Thickness (mm)	$P_{max}$ (kg)	$\delta_{max}$ (mm)	$P_{max}$ (kg)	$\delta_{max}$ (mm)
27	2,800	8.4	2,400	11.1
28	3,000	7.7	2,700	10.7
30	3,300	7.5	2,900	10.1

that the 0° orientation is in three point bending, as this direction is considerably stiffer and stronger than the 90° direction.

WISA-Trans decking is designed to conform to ISO 1496: ‘The specification and testing of general cargo containers for general purposes’ [66]. The manufacturer provides data (Table 3.1) on the maximum load  $P_{max}$  and corresponding maximum deflection  $\delta_{max}$  resulting from the wheel load of a forklift, as recommended by the standard. Data for the most common thicknesses and span lengths used in road freight trailer decking are provided in Table 3.1.

### 3.2.2 Flexural testing

Three point bending tests were performed to determine the flexural stiffness and strength of both pristine and damaged specimens. In all scenarios, at least five specimens were tested and results averaged. Pristine specimens were tested in both the 0° and 90° orientations, while the damaged specimens were only tested in the 0° orientation as this is the typical

in-service load orientation. The reproduction of moisture damage and indentation damage in flexural test specimens is explained in more detail in the following two sections.

The three point bending method was chosen since this is the loading configuration commonly applied in-service from forklift and grocery cage wheels. However, it has been observed that 10-15% lower values for flexural properties have been found using the three point bending method compared to the four point bending method for wood products, including cross-grain laminates of plywood [67]. In spite of this, the flexural properties obtained from this testing regime were used to compare the effects of different types of damage, and for this purpose the three point method is appropriate.

The three point bend test set up and specimen parameters are shown in Fig. 3.4. A span to thickness ratio of approximately 15/1 is used to ensure that the specimens will fail in bending. The span length of 428 mm used in testing was the maximum allowable span length given the fixture and test machine used. This is close to the 450 mm span length that is typically used in a standard 13.6 m UK road freight trailer. All three point bend tests were performed on an Instron tensile test machine using a test speed of 5 mm/min. A laser displacement sensor is used to capture displacement at the mid-span.

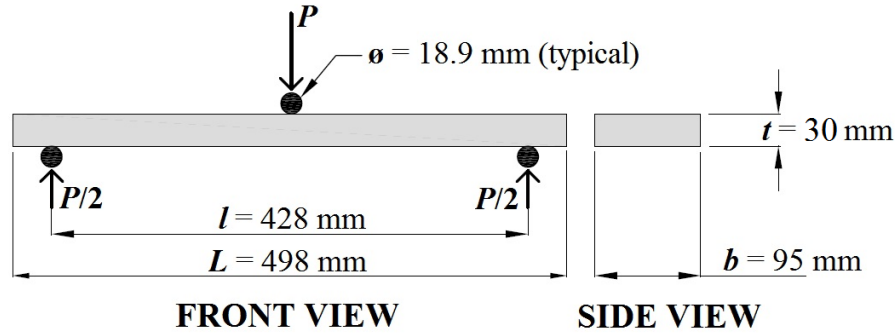


**Fig. 3.4** Specimen dimensions and test parameters used in three point bend testing.

The ultimate flexural stress  $\sigma_{ult}$  was calculated (Eqn. 3.1) using the maximum load  $P_{max}$  observed at failure, the unsupported span length  $l$ , the specimen width  $b$  and the specimen thickness  $t$ .

$$\sigma_{ult} = \frac{3lP_{max}}{2bt} \quad (3.1)$$

The flexural modulus  $E$  was calculated (Eqn. 3.2) using the gradient  $k$  of the initial linear portion of the load-deflection curve obtained during testing.

$$E = \frac{l^3k}{4bt^3} \quad (3.2)$$

**Table 3.2** Average moisture content by weight (with standard deviations) of pristine 30 mm thick (21 ply) phenolic coated Finnish birch plywood, over six different time intervals.

Duration of soaking (Hours)	Moisture content by weight (%)
1.3	6.2 ± 0.8
22	16 ± 1.3
48	19 ± 1.4
331	31 ± 1.8
616	44 ± 1.3
834	44 ± 0.8

### 3.2.3 Moisture damage

Specimens for flexural testing were subjected to varying levels of moisture damage through immersion in a water tank at room temperature, over six differing time intervals as defined in Table 3.2. At each time interval examined, five specimens were removed from the water tank and excess water was towel dried from the surface of the specimens. The moisture content of each specimen was then determined by the percentage of weight gained (averaged results for each time interval shown in Table 3.2). The specimens were subjected to the flexural testing regime described in Section 3.2.2 and results from the five specimens were averaged.

The soaking of specimens within the water tank represents an extreme case of moisture damage that is very unlikely to occur in-service, but was used to produce accelerated moisture damage. However, this approach allows for an analytical model of diffusivity to be applied with more confidence via the use of Fickian diffusion theory as outlined by Crank [68]. This assertion is supported by the fact that moisture has a tendency to travel parallel to the grain through vessels (visible in Fig. 3.1) in individual veneers, as observed when food red dye was left soaking within a hole drilled halfway through the thickness (Fig. 3.5). The diffusivity of the adhesive bond line between veneers will also have an influence on the distribution of moisture [69]. However, this effect was neglected to simplify the analysis.

By assuming that the specimens can be approximated by a one-dimensional infinite plate, the moisture concentration  $C$  with respect to time  $T$  in a plate with a thickness co-ordinate  $x$  (shown in Fig. 3.5) can be described by Fickian theory for steady state diffusion Eqns. 3.3 to 3.5 [70].

$$\frac{\partial C}{\partial T} = D_x \frac{\partial^2 C}{\partial x^2} \quad (3.3)$$

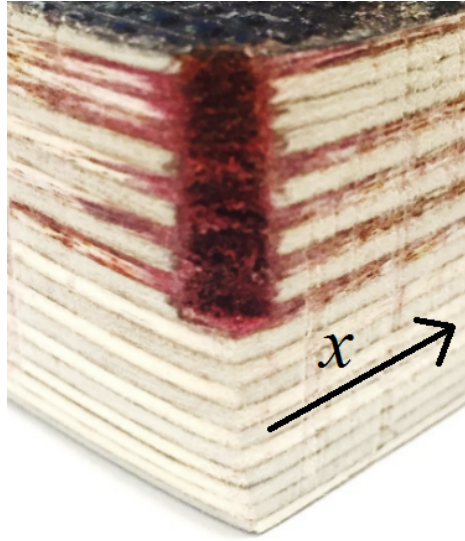


**Fig. 3.5** Diffusion of red dye outward from a central hole indicates that moisture has a tendency to travel parallel to the grain through vessels (visible in Figs. 3.1 and 3.2) in individual veneers.

$$C(x, 0) = C_i \quad (3.4)$$

$$C(0, T) = C(b, T) = C_a \quad (3.5)$$

where  $C_a$  is ambient moisture concentration,  $C_i$  is initial moisture concentration in the material, and  $D_x$  is through-thickness diffusivity. The solution to Eqns. 3.3 to 3.5 at plate thickness  $t$  is given by Eqn. 3.6 [70].

$$\frac{C - C_i}{C_a - C_i} = 1 - \frac{4}{\pi} \sum_{n=0}^{\infty} (2n+1) \sin \left[ \frac{(2n+1)\pi x}{t} \right] \exp \left[ \frac{-(2n+1)^2 \pi^2 D_x T}{t^2} \right] \quad (3.6)$$

The total weight gain  $w$  from moisture absorption was then determined by integrating the moisture concentration over the plate thickness (Eqn. 3.7) which yields Eqn. 3.8

$$w = \int_0^t C dx \quad (3.7)$$

$$G = \frac{w - w_i}{w_\infty - w_i} = 1 - \frac{8}{\pi^2} \sum_{n=1}^{\infty} \frac{\exp\left[-(2n+1)\pi^2\left(\frac{D_x T}{t^2}\right)\right]}{(2n+1)^2} \quad (3.8)$$

where  $w_\infty$  is the moisture weight gain in the material when equilibrium has been reached with the ambient humidity. Assuming an initial dry state, the moisture weight gain can be described as a percentage  $W$  (Eqn. 3.9), which is a product of  $G$  (Eqn. 3.8) and the percentage weight gain in the material when in equilibrium with its environment  $W_\infty$ . Eqn. 3.8 has been shown to have an approximate numerical solution of Eqn. 3.10 [70].

$$W(\%) = GW_\infty \quad (3.9)$$

$$G = 1 - \exp\left[-7.3\left(\frac{D_x T}{t^2}\right)^{0.75}\right] \quad (3.10)$$

For small values of  $t$ , Eqn. 3.10 can be expressed as

$$G = 4\sqrt{\frac{D_x T}{\pi t^2}} \quad (3.11)$$

Using Eqn. 3.8, through-thickness diffusivity  $D_x$  can then be expressed as Eqn. 3.12. Through-thickness diffusivity can also be determined from the initial slope of the curve of the moisture gain as a function of square root of time.

$$D_x = \frac{\pi}{16} t^2 \left[ \frac{w}{w_\infty \sqrt{T}} \right]^2 \quad (3.12)$$

### 3.2.4 Indentation damage

Indented birch plywood specimens for flexural testing were prepared with either three or six indentations across the width at the centre of each specimen as shown in Fig. 3.6. These specimens were of the same dimensions as those shown in Fig. 3.4. Indentations were created with a 25.5 mm diameter hardened steel spherical indenter with an applied load of 10 kN. Multiple indentations across the central width represents the most severe form of indentation damage likely to occur during the service lifetime of trailer decking. This damage is analogous to a forklift driving over foreign object debris on the surface of the trailer decking, which is a relatively common occurrence in everyday road freight operations.

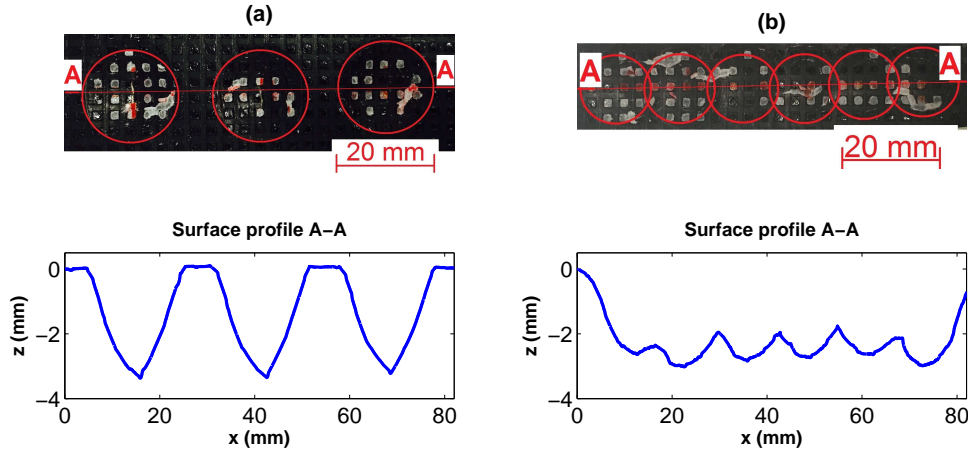


**Fig. 3.6** Top views and surface profiles of flexural test specimens with indentation damage. (a) Three indentations and (b) six indentations across the centre of the specimen. Indentations were created with a 25.5 mm diameter hardened steel spherical indenter at an applied load of 10 kN.

When Finnish birch plywood is permanently indented, a load cycle plot like that shown in Fig. 3.7 can be created. This plot reflects the interaction between the test specimen material properties (Young's modulus, Poisson's ratio, initial flow stress and strain hardening) and the elastic material properties of the indenter (Young's modulus and Poisson's ratio). The shape of the load cycle curve here indicates that elastic/plastic indentation takes place, whereby the material is indented to a total depth of  $\delta_{total}$  at a maximum indenting force of  $F_{max}$ , before relaxing during unloading to leave a residual dent of depth  $\delta_{residual}$ . The area within the hysteresis loop of the load cycle plot represents the plastic work of indentation and is a useful quantity in characterising indentation damage. This type of indentation has been successfully modelled and is well understood in literature [71, 72].

In addition to the specimens described above that were indented and subsequently tested in three point bending, other full-thickness birch plywood specimens were only tested by indentation. In particular, hardened steel spherical indenters of diameters 25.5 mm and 40.0 mm, as well as a nylon castor wheel (typical of that used in the road freight industry) of diameter 125 mm, have all been used to indent 30 mm thick birch plywood specimens. A loading rate of 2.0 mm/min was used in all cases and specimens loaded from 2 to 12 kN at increments of 2 kN. The samples were supported from the underside to prevent the introduction of bending effects. Contact profilometry was performed using a Taylor Hobson Form Talysurf 120 to measure the residual dent depths  $\delta_{residual}$ . Multiple measurements were taken at each indent location to minimise the chance of missing the point of maximum dent depth. The correlations between the maximum indentation force  $F_{max}$ , the residual dent depth  $\delta_{residual}$  and the plastic work of indentation were then examined.

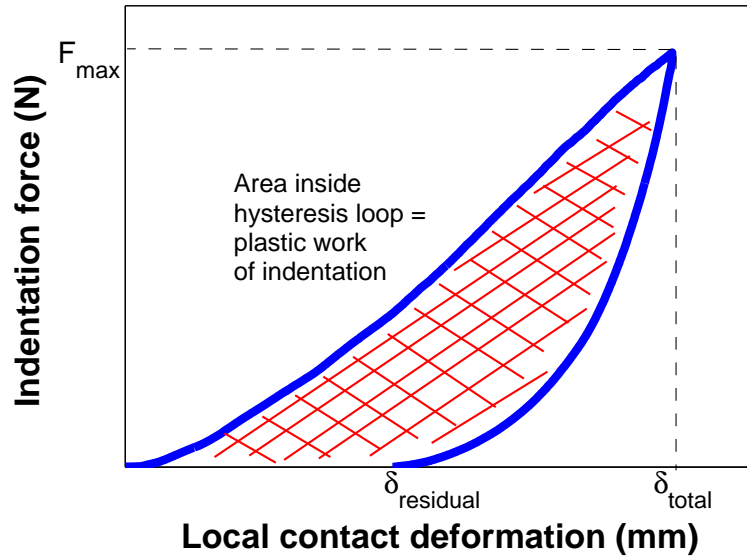


**Fig. 3.7** Load cycle plot of an elastic/plastic indentation, where the area inside the hysteresis loop is defined as the plastic work of indentation.

Brinell hardness can also be used to characterise indentation resistance and was calculated from the applied load  $P$ , the diameter of the indenter  $D$  and the diameter of the residual indentation  $d$ , as shown in Eqn. 3.13.

$$BH = \frac{2P}{\pi D(D - \sqrt{D^2 - d^2})} \quad (3.13)$$

### 3.2.5 Wear testing

Road freight trailer decking is often subjected to rolling loads from grocery cage wheels, which can cause a significant amount of wear to the exposed surface. It is therefore important to characterise the wear performance and the effect of the non-slip phenolic coating. An accelerated wear test machine to determine the abrasive resistance of wood was first developed at the US Forest Products Laboratory soon after World War Two [73]. The machine provided a comparative and reproducible test method for determining wear performance for wood floor materials. The original machine has been refined and a commercialised version was used here to analyse the wear performance of both phenolic coated and uncoated birch plywood. A schematic of the test set up used in all tests is shown in Fig. 3.8. All tests were performed at room temperature using H18 Taber abrasion wheels composed of a vitrified binder and aluminium oxide abrasive particles, which deliver a medium coarse abrasive action.

The Archard wear equation (Eqn. 3.14) defines wear rate as the volume lost from the wearing surface divided by the sliding distance. Wear rate typically depends on the normal

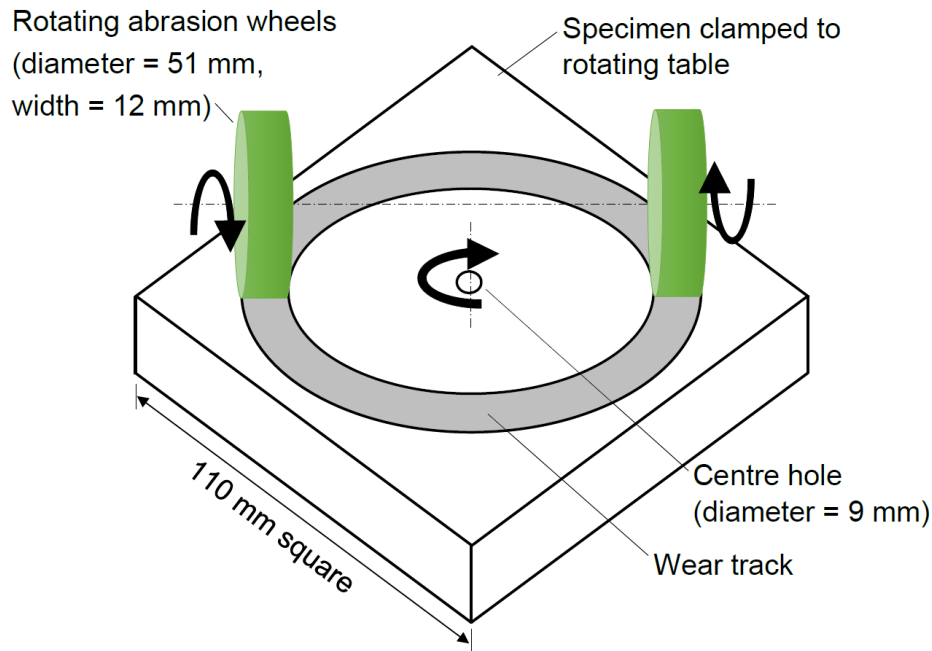


**Fig. 3.8** Rotary abrasion test set up for accelerated wear testing. Test speed = 72 RPM, applied load = 1 kg per wheel. Not to scale.

load being applied, the relative sliding speed, the initial temperature, as well as the thermal and mechanical properties of the materials in contact. [74]

$$\text{Wear rate} = \frac{\text{Volume lost from wearing surface}}{\text{Sliding distance}} \quad (3.14)$$

In wear testing of floor materials, the mass loss during testing is often measured and related back to the volume lost from the wearing surface by knowing the density of the material being tested. However, because the phenolic coating has a different density from plywood itself, the average wear depth is the strongest candidate to characterise wear volume in this case. Hence, contact profilometry was performed using a Taylor Hobson Form Talysurf 120 to measure the wear depth at numerous locations of the wear track and average values were reported.

### 3.3 Results and discussion

#### 3.3.1 Flexural testing

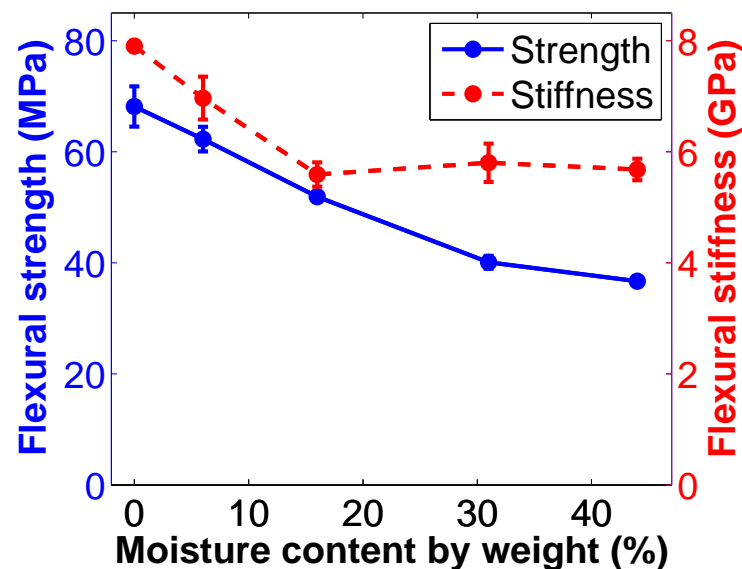
A summary of results obtained from the three point bend tests of undamaged specimens is provided in Table 3.3. It should be noted that the values of flexural properties may be slightly



**Table 3.3** Summary of averaged results (with standard deviations) from three point bend testing of pristine 30 mm thick (21 ply) Finnish birch plywood.

Orientation	No. of specimens	$P_{max}$ (kN)	$\delta_{max}$ (mm)	$\sigma_{ult}$ (MPa)	$E$ (GPa)
Longitudinal ( $0^\circ$ )	5	$8.8 \pm 0.5$	$13 \pm 1.0$	$68 \pm 3.2$	$7.9 \pm 0.08$
Transverse ( $90^\circ$ )	5	$5.8 \pm 0.9$	$11 \pm 0.9$	$45 \pm 5.0$	$5.3 \pm 0.18$

underestimated because of the three point bending method [67]. For the specimens with water damage, the flexural strength and flexural stiffness is plotted against the percentage of moisture by weight, see Fig. 3.9. The residual flexural strength of specimens with indentation damage and water damage are compared in Fig. 3.10. Both indentation damage and water damage were characterised through the loss in flexural stiffness compared to the stiffness of pristine specimens. It is evident from Fig. 3.10 that indentation damage can have a significant impact on the flexural properties of Finnish birch plywood. However, while indentation damage can look severe upon visual inspection, testing has shown that water damage, which can look far less severe, can have a greater effect on residual strength and stiffness. Increased levels of variance in flexural stiffness was also observed for all damaged specimens. However, the variance in flexural strength was not significantly affected by damage.

**Fig. 3.9** Flexural strength and stiffness (determined by three point bend tests) of Finnish birch plywood plotted against moisture content by weight. Error bars plotted correspond to standard deviation.

Representative load-displacement curves with corresponding failure mechanisms for both undamaged and moisture damaged specimens are shown in Figs. 3.11 and Fig. 3.12,

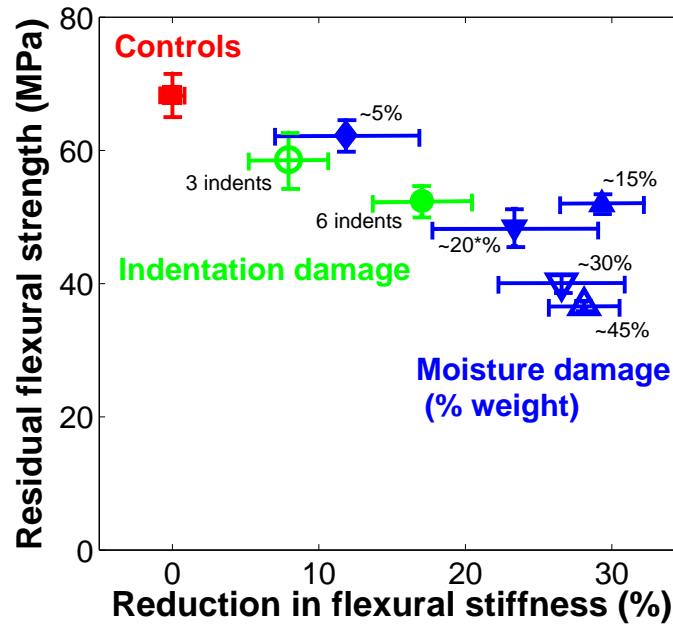


**Fig. 3.10** Residual flexural strength (determined through three point bend tests) of Finnish birch plywood decking with varying levels of damage, plotted against the reduction in flexural stiffness. Error bars plotted correspond to standard deviation. Note that \* indicates dried from 20% to 10% moisture.

respectively. Failure in dry specimens (both pristine and indented) was generally initiated at the tension side (lower side in three point bend tests) of the specimens (Figs. 3.11(1) and Figs. 3.11(1a)). The tensile fracture propagates through the bottom core veneers as they subsequently carry additional load (Fig. 3.11(2)). Finally a delamination initiates at a central veneer and propagates along the length of the specimen (Fig. 3.11(3)), while the top veneers remain intact carrying the residual load. Specimens with indentation damage undergo the same failure mechanisms as pristine specimens, the only difference being a cross-section reduction at the loading roller.

Failure in specimens with moisture damage was found to be dominated by interlaminar delamination between core veneers, which could be attributed to moisture accumulating at the adhesive layers between veneers [69]. Ruponen *et al.* suggested that this tendency of birch plywood with moisture damage to delaminate can be reduced or eliminated through binderless bonding of veneers and a post-manufacture thermal modification [75].

### 3.3.2 Moisture damage

The through thickness diffusivity  $D_x$  was found to be  $9.9 \text{ mm}^2/\text{day}$  from the initial slope of the curve of the moisture gain as a function of square root of time (Fig. 3.13). This has the

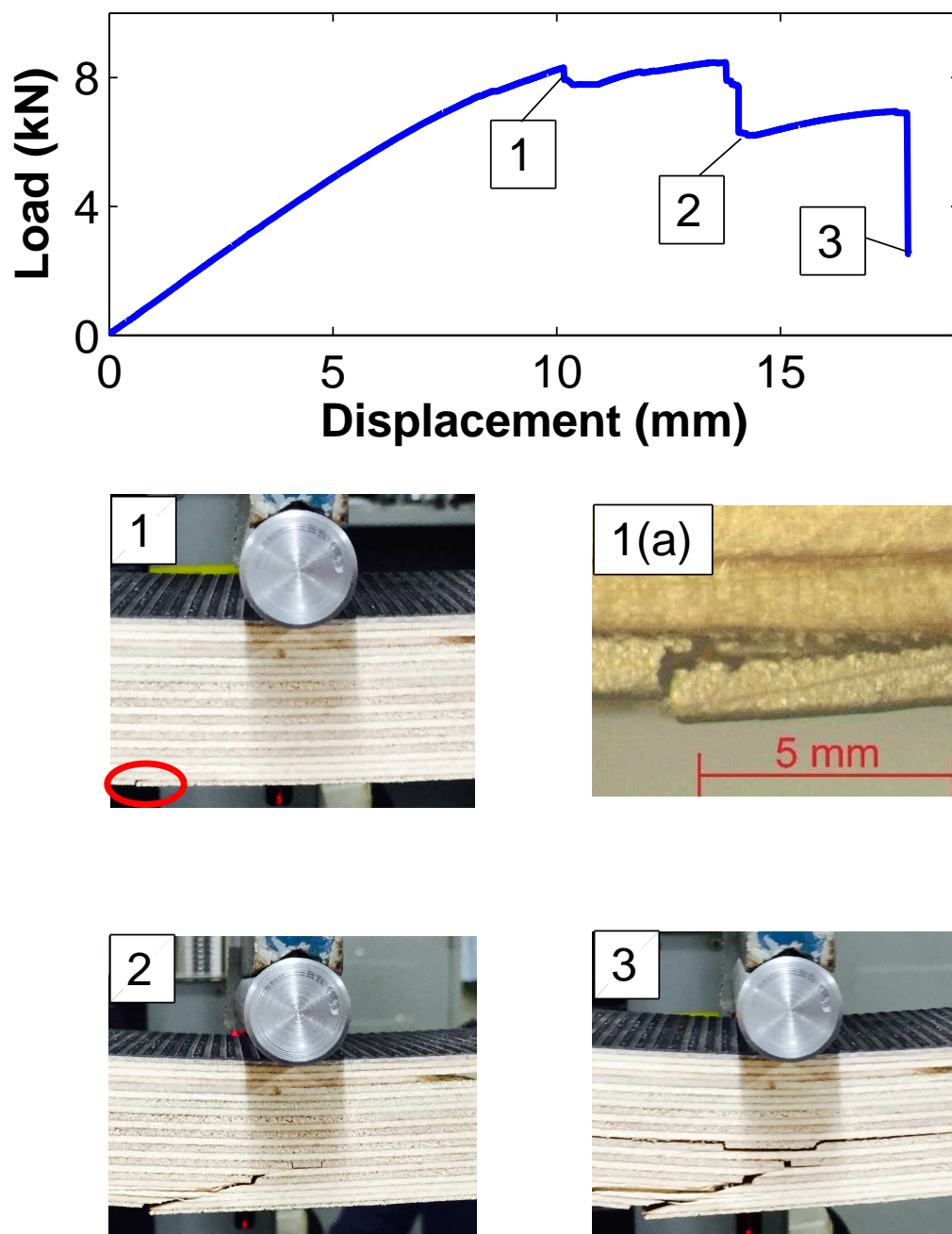


**Fig. 3.11** Typical load-displacement curve and corresponding failure mechanisms for pristine Finnish birch plywood (30 mm nominal thickness) in three point bending. Inset photos correspond to the positions indicated on the load-displacement curve.

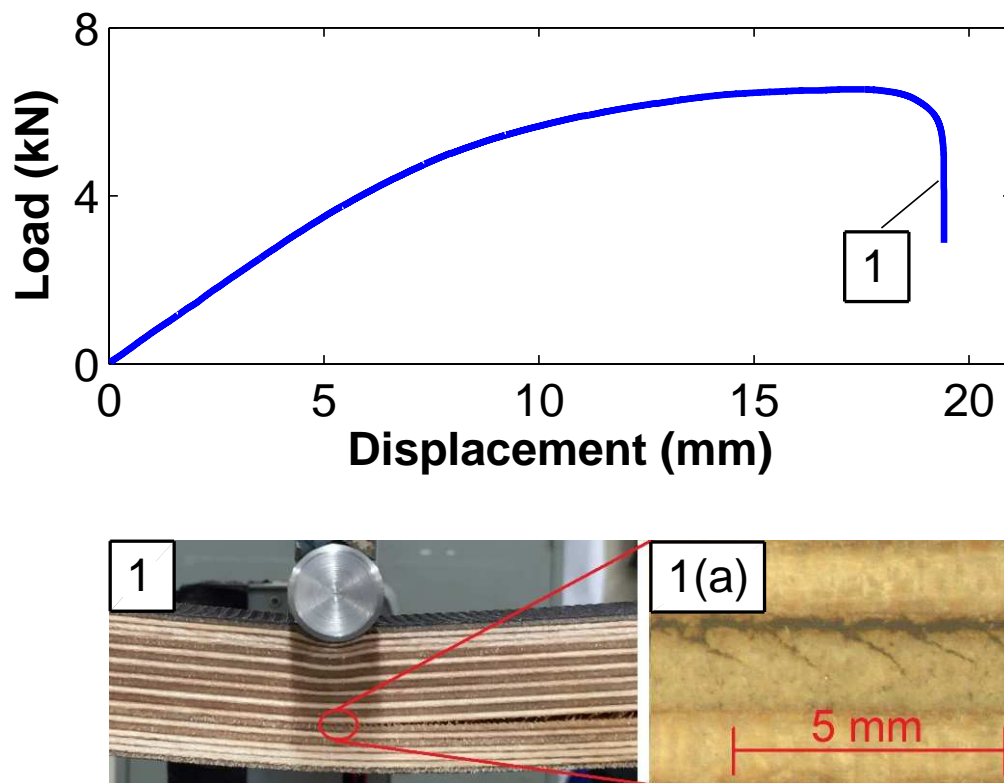


**Fig. 3.12** Typical load-displacement curve and corresponding failure mechanism for Finnish birch plywood (30 mm nominal thickness) with moisture damage in three point bending. Inset photo and micrograph correspond to the position indicated on the load-displacement curve.

same order of magnitude as other plywood materials [76, 77]. It can be seen in Fig. 3.13 that experimental data points for moisture increase with soaking time closely follow Fickian diffusion theory. It is evident from both the experimental data and analytical model that the maximum moisture content likely to be attained in Finnish birch plywood when fully immersed in water is approximately 45% by weight. The small differences between the experimental data points and the Fickian prediction is attributed to the assumptions that the diffusion is steady state and that specimens have an initial dry state, when in reality there is a small amount of moisture present at atmospheric conditions. The different moisture diffusivity of the adhesive layer may also be causing moisture to accumulate at the bond lines [69].

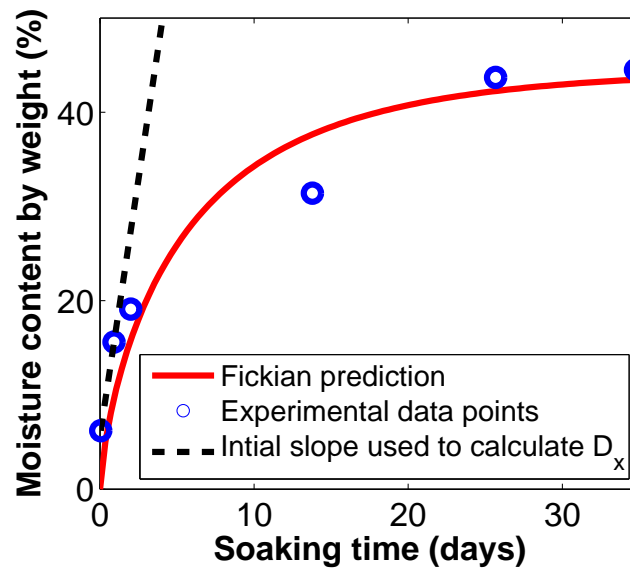


**Fig. 3.13** Moisture content by weight plotted against specimen soaking time. Experimental data points are a reasonable fit with Fickian diffusion theory calculated from the through thickness diffusivity  $D_x$  determined from the slope given by the first two experimental data points.

### 3.3.3 Indentation damage

The maximum indentation force  $F_{max}$  and residual dent depth  $\delta_{residual}$  are plotted against the plastic work of indentation (Fig. 3.14). The residual dent depth was found to vary linearly with plastic work of indentation, whilst the maximum indentation force exhibits a square root correlation with the plastic work of indentation, which is to be expected for this type of quasi-static load arrangement [78].

The Brinell hardness was determined at various loads (8, 10 and 12 kN) with an indenter diameter of 25.5 mm and the average value was found to be 27 MPa. This is in good

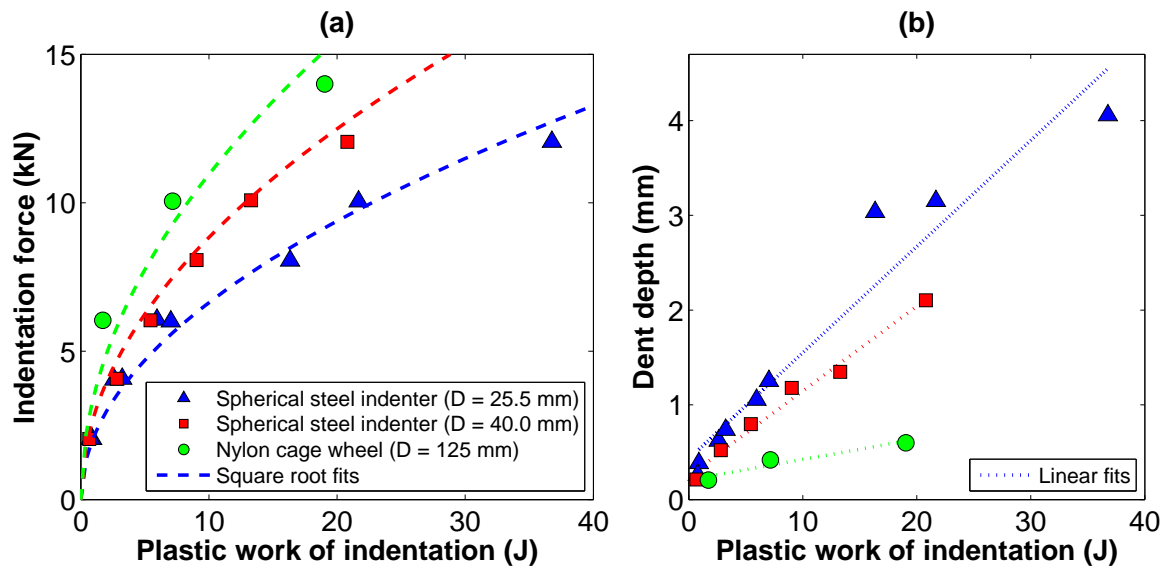


**Fig. 3.14** (a) Maximum indentation force and (b) residual dent depth plotted against plastic work of indentation.

agreement with the Brinell hardness of Finnish birch reported by Heräjärvi [79], who found the Brinell hardness of *B. pendula* and *B. pubescens* to be 23.5 MPa and 20.5 MPa, respectively. The results are also comparable to those reported for similar kinds of hardwood varieties used in flooring panels [62].

### 3.3.4 Wear testing

A summary of results of the accelerated wear testing of both phenolic coated and uncoated specimens is shown in Fig. 3.15. While phenolic coating is not commonly used in other types of wood flooring, it can be seen that the presence of the phenolic coating generally greatly improves the wear resistance of the birch plywood. The wear testing results of the uncoated birch plywood specimens support the notion that a high level of variance is to be expected in the wear resistance of uncoated wood floor materials [62].

It is evident that the phenolic coated specimens progress through three distinct stages of wear as labelled in Fig. 3.15:

- i. Initial period of running-in where the tips of the phenolic coating are worn off to leave a wear track surface like that shown in Fig. 3.16a.
- ii. Steady low-wear regime where the bulk of the phenolic coating is slowly worn down.
- iii. Final high-wear period where the phenolic coating is removed exposing the birch plywood, leaving a wear track like that shown in Fig. 3.16b).



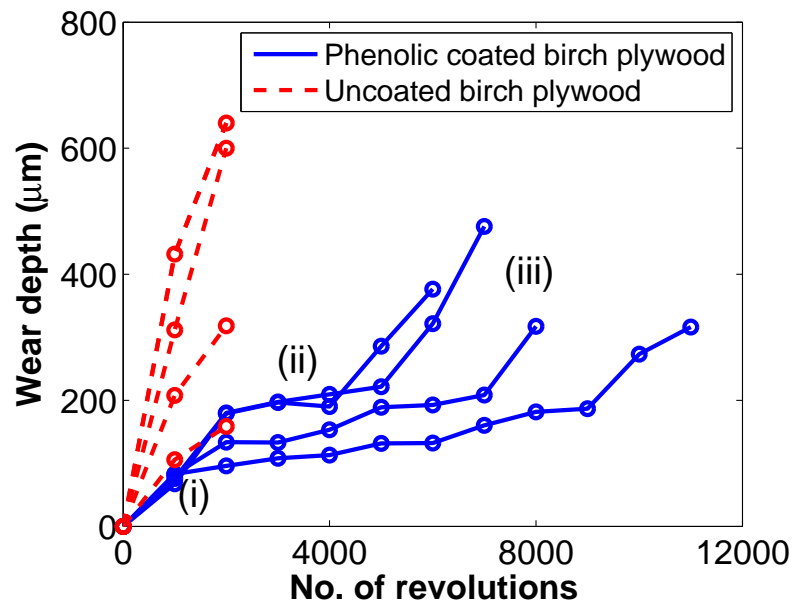


**Fig. 3.15** Maximum wear depth of coated and uncoated Finnish birch plywood plotted against the number of revolutions of the rotary abrasion machine for four repeated tests. Three distinct stages of wear observed in the phenolic coated specimens indicated.

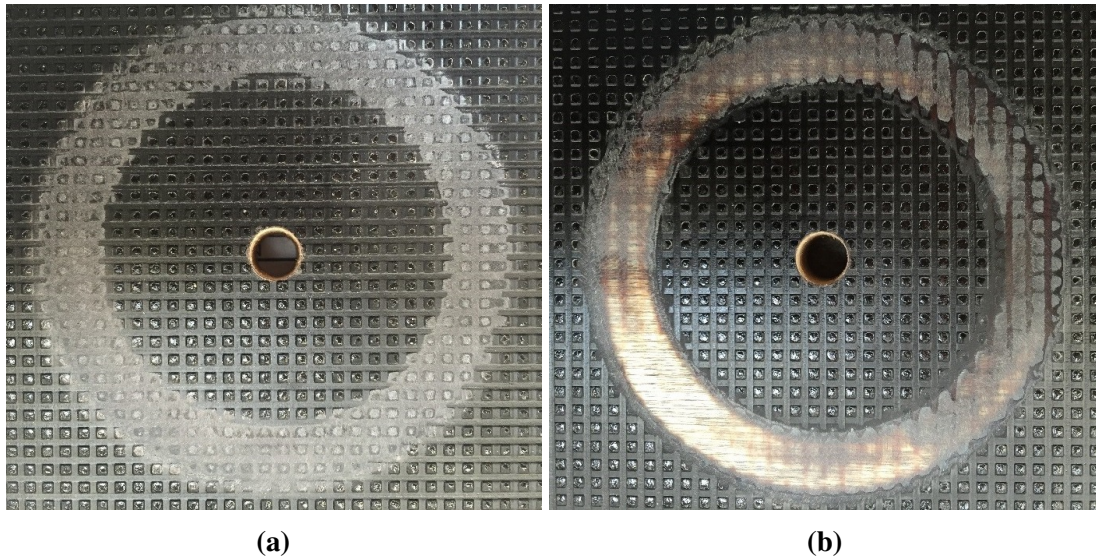


**Fig. 3.16** Wear of phenolic coated Finnish birch plywood after testing on rotary abrasion machine for (a) 1,000 revolutions as the tops of the non-slip phenolic coating are worn off and (b) 7,000 revolutions as the birch plywood becomes exposed.

## 3.4 Conclusions

From the mechanical testing regime used to characterise the performance of phenolic coated Finnish birch (*Betula pendula* and *Betula pubescens*) plywood, commonly used in HGV trailer decking, the following conclusions can be drawn:

- Indentation damage can have a significant impact on residual flexural properties.
- Moisture damage considerably reduces flexural strength and stiffness, whilst significantly increasing variance in flexural stiffness.
- While indentation damage can look severe during a visual inspection, it generally has a lesser effect on flexural stiffness and strength compared to moisture damage. However, indentation damage does also increase the variance in flexural stiffness.
- Moisture damage changes the failure mode of Finnish birch plywood in three point bending. A tensile fracture of the bottom veneer is likely to occur in pristine and indented specimens, whilst delamination of central veneers becomes the typical failure mode for specimens with moisture damage.
- Fickian theory of steady state diffusion provides a reasonable approximation of the water diffusion process in Finnish birch plywood when it is completely immersed in water.
- The hot pressed non-slip phenolic coating typically applied to this material greatly improves the wear performance. However significant levels of variance were observed during wear testing.
- The testing regime here has provided useful data that helps to quantify the extent to which damaged road freight trailer decking can still withstand in-service loadings. It also provides a benchmark for the performance of novel deck systems such as composite sandwich panels and pultrusions.



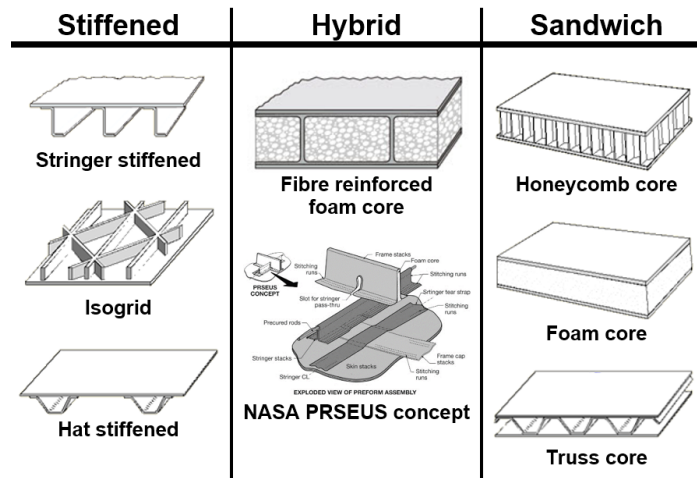
# Chapter 4

## Lightweight sandwich panel trailer decking

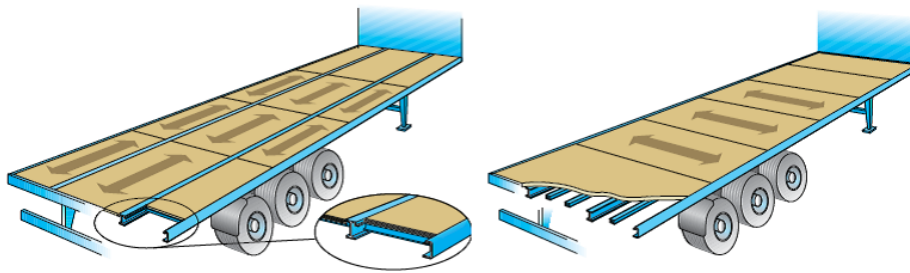
### 4.1 Introduction

The structural configuration of a lightweight deck can take many potential forms (Fig. 4.1), including: monolithic panels, stiffened panels, sandwich panels and hybrid panels (e.g. fibre reinforced foam core sandwich panels). The manufacture of hybrid panels is time consuming and costly, making them inappropriate for use here. The construction of monolithic panels is typically less intensive than the construction of sandwich panels. However, the use of a sandwich or stiffened panel can significantly increase flexural rigidity and flexural strength without significantly increasing weight. Hence, sandwich panels and stiffened panels (in the form of pultrusions in Chapter 5) are selected for further investigation and considered to be the best candidates for lightweight deck replacements.

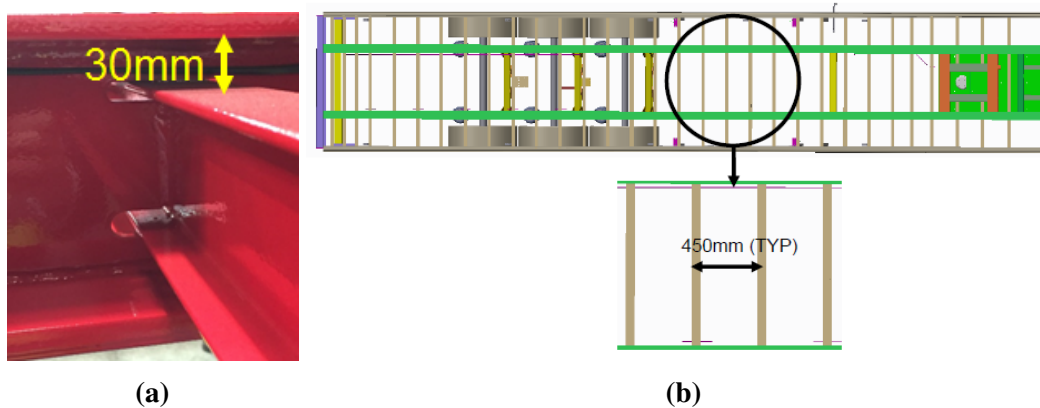
It is desirable that lightweight decking is designed so that it can be fitted or retrofitted to existing trailer chassis designs, so that existing chassis beams do not need to be modified. Matching the dimensions of the replacement deck with the hardwood based materials will help to achieve this. Conventional hardwood based decks are typically inserted between the transverse beams and top flange of the main longitudinal beams of the chassis, though they may also be laid directly over the longitudinal beams (Fig. 4.2). Hence, the nominal thickness of the deck should be approximately 28 - 30 mm (Fig. 4.3a) and it should have comparable flexural properties to hardwood based decking, particularly a span length of 450 mm, which is the maximum typical spacing between transverse members in a standard 13.6 m trailer (Fig. 4.3b).



**Fig. 4.1** Various lightweight panels can be split into three broad categories, adapted from [23].






**Fig. 4.2** Two installation techniques commonly used with hardwood decking [24].



**Fig. 4.3** (a) Spacing between the transverse and longitudinal beam members in a 13.6 m flatbed chassis determines the required sandwich panel thickness. (b) Plan view of the typical (TYP) spacing between the transverse members in a 13.6 m flatbed chassis, which determines the required span length  $L$  subjected to three point bending. Images courtesy of SDC Trailers.

In addition to loading and geometry requirements, the extremely cost-driven nature of the construction of road freight trailers dictates that above all, lightweight trailer decking must be cost competitive against conventional hardwood based decking. Discussions with industrial partners indicate that the industry is willing to trial new decking systems should the relative material cost be less than two times that of existing hardwood decking and the weight saving be significant (greater than 20%).

The use of a sandwich configuration to significantly increase flexural rigidity and flexural strength without significantly increasing weight, is shown in Fig. 4.4 [25]. These benefits are thought to outweigh the disadvantage of a slight increase manufacturing costs compared to a monolithic panel. The success of sandwich panels in the side walls of box trailers is also encouraging for their application to trailer decking. The sandwich panel investigation presented in the following section examines in detail two different sandwich panels in terms of material selection, detailed design, fabrication and testing.

	Weight	Flexural rigidity	Bending strength
	1	1	1
	~1	12	6
	~1	48	12

**Fig. 4.4** The sandwich effect: comparison between homogeneous and sandwich cross-sections, adapted from [25].

It should be noted that much recent work has been done on the design, optimisation, analysis and testing of sandwich panels [80–85]. However, the novelty of this study lies within tailoring a sandwich panel specifically for use in this application.

## 4.2 Material selection and detailed design

### 4.2.1 Material selection indices

The first step in sandwich panel design is to develop a material selection process for both the face sheets and core. To help achieve this, material selection software CES EduPack 2013 [26] was used to identify potential material combinations of the core and face sheets

**Table 4.1** Face sheet and structural core materials considered in the sandwich panel material selection process.

Face sheet materials	Structural core materials
Woven GFRP	End-grain balsa wood
GFRP laminate	Polypropylene (PP) honeycomb
CFRP laminate	Aluminium honeycomb
Hardwood	Aluminium foam
Aluminium (Al)	Polycarbonate (PC) honeycomb
	Polyvinylchloride (PVC) foam
	Phenolic foam
	Polyurethane (PU) foam
	Nomex honeycomb
	PP foam

that will allow the sandwich panel to be lighter than hardwood. Many different material combinations typically used in sandwich panel construction were considered, along with other common monolithic materials for comparison. A simple rule of mixtures was used to estimate equivalent sandwich panel material properties, based on the volume fraction of the core and face sheet materials within each of the panels. A list of the different material combinations considered for use in the sandwich panel is provided in Table 4.1. All possible combinations of face sheet and core materials were considered. The resulting material selection plot (Fig. 4.5) was created based on a beam in three point bending. By using performance indices  $M_1$  and  $M_2$  (Eqns. 4.1 and 4.2), the plot identifies sandwich panels that are lighter than birch plywood, while placing constraints on the maximum deflection and maximum stress, respectively [32]. Mass was selected for the objective function since it is the prime focus of this investigation. It is believed that conventional hardwood-based materials have been selected using a cost objective function.

$$M_1 = \frac{E^{1/2}}{\rho} \quad (4.1)$$

$$M_2 = \frac{\sigma^{2/3}}{\rho} \quad (4.2)$$

During the material selection process it was assumed that the sandwich panel face sheet thickness varied from 1 mm (with a 26 mm core) to 4 mm (with a 20 mm core). This was done to ensure that the sandwich panel has a nominal thickness of 28 mm to allow enough

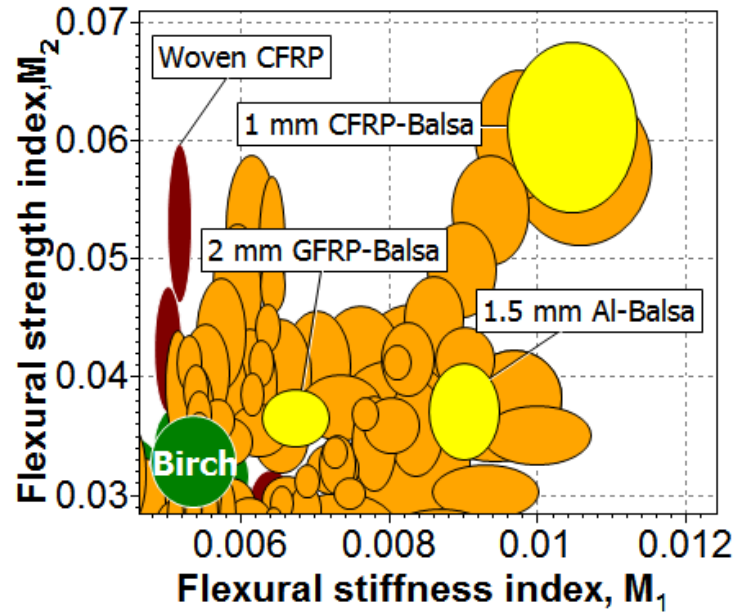


**Fig. 4.5** Material selection plot for a beam in three point bending developed in CES [26]. Orange and yellow markers indicate sandwich panels which match or exceed the performance of birch hardwood (shown in green) in three point bending.

room for a non-slip surface coating to be applied and hence have a total nominal thickness of around 30 mm to match birch plywood decking.

#### 4.2.2 Detailed design

Because material selection here is largely driven by cost, many of the sandwich panel material combinations that are common in other industries, such as aerospace, are far less feasible for use here, despite their superior mechanical properties. The materials identified as being acceptable from the material selection plot (Fig. 4.5) were analysed in terms of their relative cost and relative mass, and the cheapest and lightest material combinations are shown in Table 4.2. The sandwich panel material combinations not shown in Table 4.2 were considered to be unsuitable for use here since they do not meet the weight and mechanical performance requirements. The exact minimum face sheet thicknesses  $t_{min}$  required to match the stiffness and strength of birch plywood were found by considering the minimum collapse load and flexural rigidity of each of the sandwich panels, using average material properties provided in CES Edupack 2013 [26]. The minimum collapse load was determined by considering competing collapse modes (Appendix A). The results of this procedure are summarised in Table 4.2.

**Table 4.2** Minimum face sheet thickness and failure modes for various sandwich panels (28 mm total thickness) with either woven GFRP or aluminium face sheets. Symbols correspond to those shown in Fig. 4.6. Specific gravity of structural cores shown in brackets.

Symbol	Face sheet - core	$t_f$ (mm)	Design driver	Collapse mode
○	GFRP - end-grain balsa (0.2)	2.4	Stiffness	Core shear
△	GFRP - PP foam (0.6)	2.3	Stiffness	Elastic indentation
□	GFRP - PVC foam (0.3)	2.3	Stiffness	Elastic indentation
▽	GFRP - PU foam (0.3)	2.5	Strength	Elastic indentation
●	Aluminium - end-grain balsa (0.2)	1.2	Strength	Face yield
▲	Aluminium - PP foam (0.6)	1.2	Strength	Face yield
■	Aluminium - PVC foam (0.3)	1.2	Strength	Face yield
▼	Aluminium - PU foam (0.3)	1.7	Strength	Elastic indentation

It can be seen in Fig. 4.6 that sandwich panels comprised of an end-grain balsa core with either woven GFRP or aluminium face sheets are the most advantageous in terms of cost and mass. Thus these were selected for further investigation. These panels can significantly reduce mass, while keeping the increase in raw material cost within the upper bound that has been estimated from discussions with industrial partners.

### 4.2.3 Choice of raw materials

Bi-axial plain weave E-glass fibre fabric (areal weight 290 g/m<sup>2</sup>) and high quality general purpose (orthophthalic) polyester laminating resin, were selected for use in the GFRP face sheets owing to their low cost. Methyl ethyl ketone peroxide (MEKP) catalyst was used as the catalyst for the polyester resin. The raw materials used in these face sheets were supplied by Easycomposites Ltd, UK.

A 1.5 mm thick aluminium (5052 H32) tread plate was chosen for use in the top face sheet of the aluminium sandwich panels and a 1.2 mm thick high strength aluminium (6082 T6) sheet was used in the bottom face sheet. The selected tread plate is the thinnest available. These face sheets were supplied by Switchblade Metals Ltd, UK. The benefits of using aluminium tread plate as the top face sheet of sandwich panels in mass transport applications have been well documented [86].

Rigid end-grain balsa core sheets (Fig. 4.7), comprised of many constituent blocks of balsa bonded together with polyvinyl acetate (PVA) adhesive, were used in all sandwich panels and were supplied by Gaugler & Lutz oHG, Germany. Material properties of the chosen face sheet materials and end-grain balsa core are shown in Tables 6.2 and 4.4, respectively.

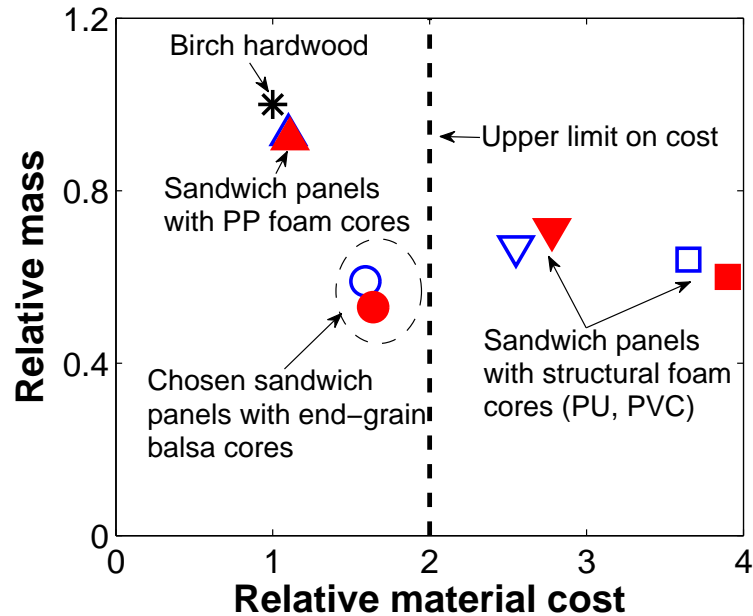


**Fig. 4.6** Plot of relative mass against relative cost for the eight cheapest acceptable sandwich material combinations identified from the three point bending material selection plot. Unfilled markers: sandwich panels with woven GFRP face sheets. Solid markers: sandwich panels with aluminium face sheets. Key see Table 4.2.

Table 4.4 shows the relevant material properties of three commercially available end-grain balsa cores taken from the manufacturer data sheet [34]. Both the intermediate density core (tradename Baltek SB.100) and the higher density core (tradename Baltek SB.150) were selected for investigation. Micrographs of the intermediate and the higher density cores are provided in Appendix C.

#### 4.2.4 Failure mode maps

Failure mode maps (Figs. 4.8 and 4.9) were constructed following the methods outlined by Gibson and Ashby [87] using the material properties in Tables 6.2 and 4.4. Minimum mass trajectories are plotted onto the maps using the procedure outlined by Steeves and Fleck [88] (details in Appendix A). Note that the current designs are slightly thicker than the original proposed nominal thickness of 28 mm, using to the closest suitable thickness of off-the-shelf raw materials. The total thickness of both panels is under 30 mm, which is still acceptable for this application.

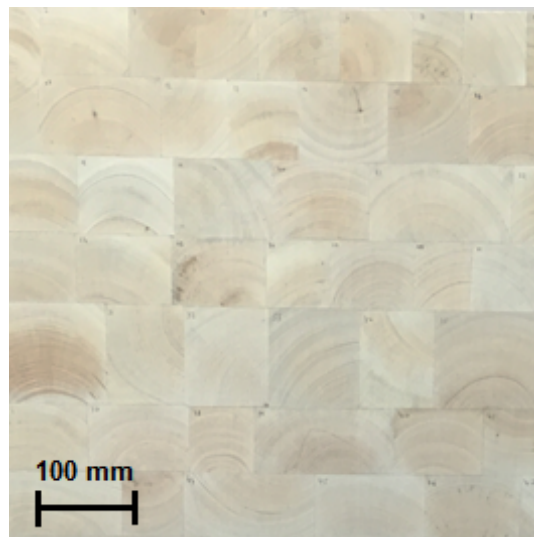


**Fig. 4.7** Baltek SB.100 rigid end-grain balsa core sheet comprised of many constituent blocks bonded together with PVA adhesive.

**Table 4.3** Material properties of selected face sheet materials. Flexural properties determined through flexural testing with span length = 120 mm, loading/support roller diameter = 19 mm, specimen length = 160 mm, specimen width = 25 mm and test speed = 5 mm/min. (Minimum of five specimens tested in every case and average values reported). Flexural stiffness determined from the initial slope in the load-displacement curve.

Face sheet material	Nominal thickness (mm)	Measured density (kg/m <sup>3</sup> )	Ultimate flexural strength (MPa)	Flexural stiffness (GPa)
Seven ply bi-axial weave GFRP	2.1	1,900	370	22
Aluminium tread plate (5052 H32)	1.5	2,700	360	65
Aluminium sheet (6082 T6)	1.2	2,700	490	77

**Table 4.4** Material properties of end-grain balsa core [34].

Tradename	Nominal density (kg/m <sup>3</sup> )	Shear strength (MPa)	Shear modulus (MPa)	Compressive strength (MPa)	Compressive modulus (MPa)
Baltek SB.50	109	1.8	136	22	1,616
Baltek SB.100	148	2.6	187	65	2,526
Baltek SB.150	285	5.2	362	77	4,428



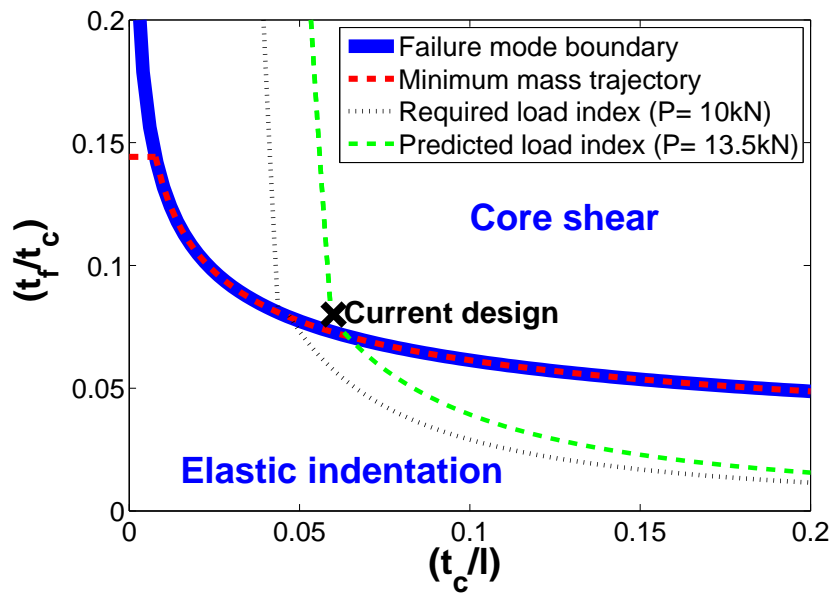


**Fig. 4.8** Failure mode map for sandwich panels with a woven GFRP face sheets of thickness  $t_f$ , an end-grain balsa core of thickness  $t_c$  and an unsupported span length  $l$ . Current design: 2.1 mm thick face sheets and 25.4 mm thick core.

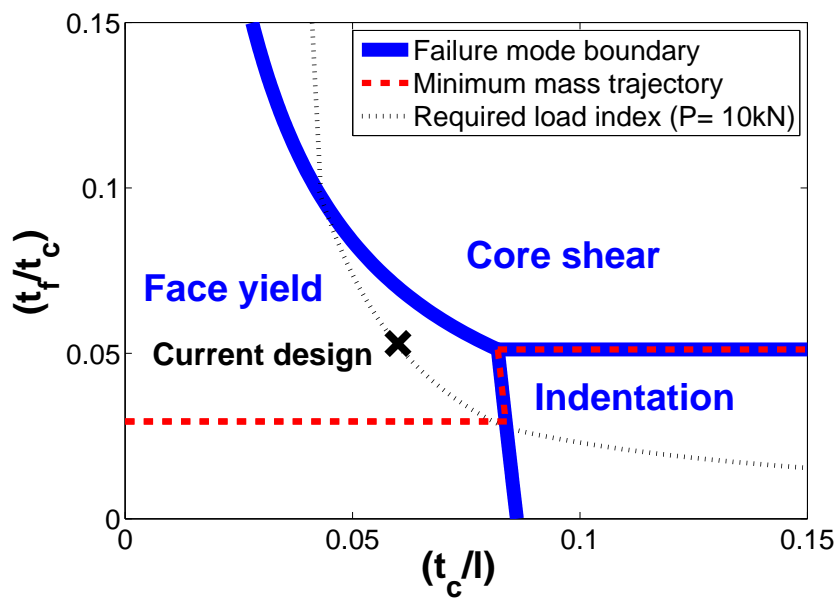


**Fig. 4.9** Failure mode map for sandwich panels with aluminium face sheets of thickness  $t_f$ , an end-grain balsa core of thickness  $t_c$  and an unsupported span length  $l$ . Current design: 1.5 mm thick top face sheet (tread plate), 1.2 mm bottom face sheet and 25.4 mm thick core.

### 4.3 Panel fabrication

There are several potential strategies that could be used to fabricate the two selected sandwich panels, particularly with respect to the woven GFRP sandwich panel. This panel can be manufactured with a single shot process where the face sheets are cured and bonded to the balsa core simultaneously, or they could be manufactured by a multi-stage process by which the face sheets are cured then bonded to the core, or indeed a combination of these strategies known as a co-bonding process could be used. Both the multi-stage process and the single shot process were chosen for further investigation as they are the most likely to be implemented practically. However, should these sandwich panels be mass produced for commercial use, a single shot manufacturing process would most likely be more desirable as it removes the need for costly structural adhesives, helping to keep material costs to a minimum.

Woven GFRP panels were fabricated using a wet hand lay-up process and left to cure under heat lamps. It was found that seven layers of 290 g/m<sup>2</sup> woven glass fibre fabric produced a desirable average thickness of 2.1 mm. Care was taken during the wet hand lay-up process to thoroughly roll the polyester resin into the dry fabric to minimise the number of voids, though the inherent lack of pressure in the process results in voids being present in the final laminate (Fig. 4.10b). Whilst a vacuum infusion process would likely significantly reduce the void volume fraction, the increased costs associated with this process make it less desirable for use here. The panels made with the single shot process are shown in Fig. 4.10.

During the single shot fabrication process, the end-grain balsa core was laid directly over the bottom face sheet before the resin cures and the top face sheet is subsequently laid up over the core. In the multi-stage fabrication process, on the other hand, cured GFRP panels were bonded to the end-grain balsa core using methacrylate adhesive (VuduGlu VM100), which typically has good bond strength with GFRP (Fig. 4.11a). The surface of the GFRP to be bonded was cleaned with distilled water to help improve the adhesion of the face sheet to the core.

Due to long lead times associated with acquiring 25.4 mm thick rigid SB.100 end-grain balsa core, two pieces of 12.7 mm thick core were used in replacement of the 25.4 mm thick core. The two 12.7 mm thick cores were bonded together with a structural epoxy adhesive (Permabond ET515). The superior mechanical properties of the adhesive compared to the core helps to ensure that this has minimal impact on overall panel performance. Panels that were constructed with the denser SB.150 core all used a 25.4 mm thick rigid core that did not require this additional fabrication step.

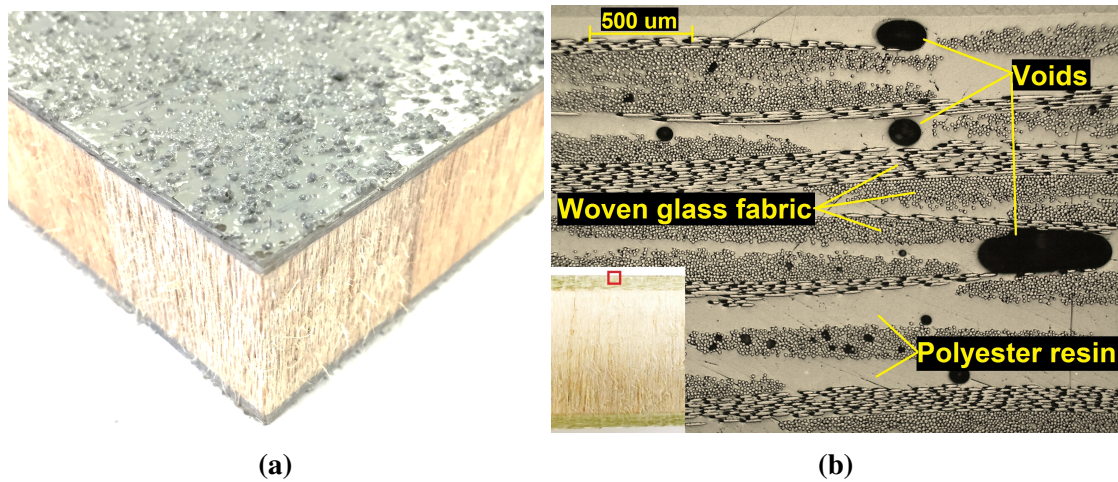


**Fig. 4.10** (a) Woven GFRP-balsa (SB.150) sandwich panel manufactured with a single shot process (2.1 mm thick face sheets and 25.4 mm thick core) and with a non-slip polyamine epoxy coating applied. (b) Micrograph of GFRP face sheet used in sandwich panel construction, showing the presence of numerous voids introduced during the wet hand lay-up of the face sheets (typical cross section inset).

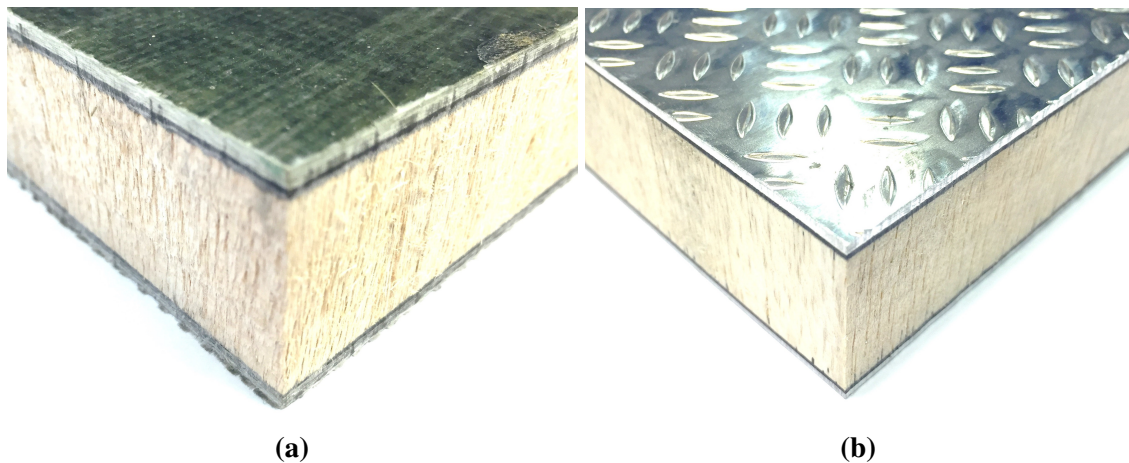


**Fig. 4.11** (a) Woven GFRP-balsa (SB.150) sandwich panel (2.1 mm thick face sheets and 25.4 mm thick core). (b) Aluminium-balsa (SB.150) sandwich panel (1.5 mm thick 5052 H32 tread plate top face sheet, 1.2 mm thick 6082 T6 bottom face sheet and 25.4 mm thick SB.150 core). Panels were constructed by bonding the face sheets to the core with methacrylate adhesive.

**Table 4.5** Comparison of weight characteristics of sandwich panel decking to birch plywood (WISA-Trans) decking. Total mass calculation assumes a deck area of 27 m<sup>2</sup>.

Deck type	Density (kg/m <sup>3</sup> )	Nominal thickness (mm)	Areal mass (kg/m <sup>2</sup> )	Total mass (kg)	Weight saving (%)
Birch plywood (WISA-Trans)	700	30	21.0	567	-
GFRP - balsa SB.150 (methacrylate)	515	31	16.0	431	24
GFRP - balsa SB.150 (single shot)	498	30	14.9	403	29
Al - balsa SB.150 (methacrylate)	529	30	15.9	428	24

The sandwich panels with aluminium face sheets (Fig. 4.11b) were fabricated by bonding the face sheets to the core using either methacrylate adhesive (VuduGlu VM100) or structural epoxy adhesive (Permabond ET515). Prior to bonding, the surface of the aluminium to be bonded was roughened with grit paper then degreased with acetone to help improve adhesion of the face sheet to the core. The weight characteristics of all SB.150 sandwich panels are compared to birch plywood in Table 4.5, and it can be seen that the single shot GFRP panel provides the greatest weight saving benefit.

## 4.4 Mechanical testing

Three point bending tests were performed to determine the flexural stiffness and strength of the fabricated sandwich panels, as well as conventional birch plywood. The test set up and specimen parameters are shown in Fig. 4.12. A span to thickness ratio of approximately 15/1 was used to help ensure that the specimens will fail in bending. The span length of 428 mm used in testing was the maximum allowable span length given the fixture and test machine used. This is close to the 450 mm span length that is typically used in a standard 13.6 m UK road freight trailer. All three point bend tests were performed on an Instron 5500R Universal Test Machine using a test speed of 5 mm/min. A laser displacement sensor was used to capture displacement at the mid-span of the bottom face sheet.

Panel testing on larger demonstrator panels was also performed to simulate loading from a forklift wheel that is commonly seen in-service. Large panels with dimensions of 550 × 400 × 30 mm were simply supported between two rollers (diameter 76 mm), providing an unsupported span length of 500 mm as shown in Fig. 4.13 The panels were loaded through a rubber pad in the centre of the mid-span over a contact area of 180 x 80 mm. The contact patch area of the rubber pad simulates a forklift wheel and was chosen as per the recommendations in ISO 1496: The specification and testing of general cargo containers for

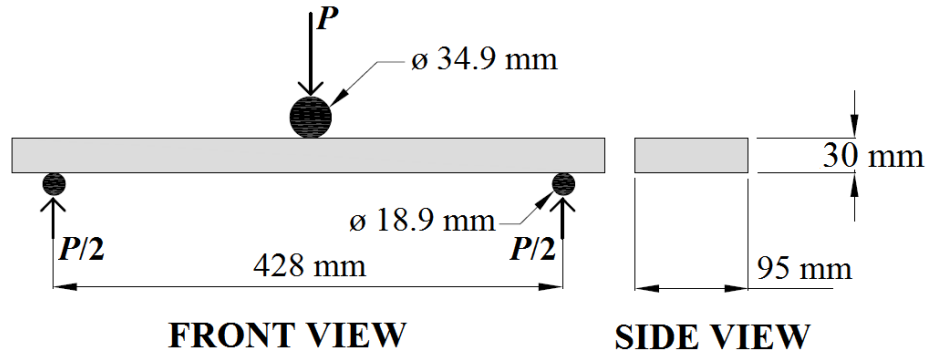


**Fig. 4.12** Nominal specimen dimensions and test parameters used in flexural testing, with an applied load  $P$ . Test speed = 5 mm/min.

general purposes [66]. A laser displacement sensor was also used in this test to determine the displacement at the centre underside of the panel.

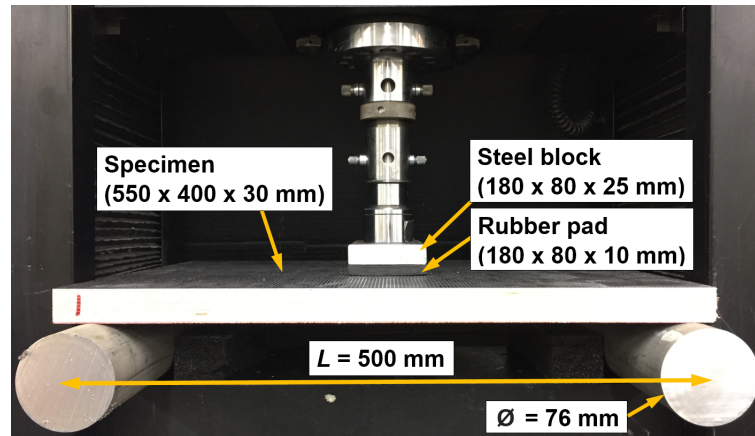


**Fig. 4.13** Panel testing setup with simulated forklift wheel contact. Test speed = 5 mm/min.

In order to determine the shear properties of the end-grain balsa used in sandwich panel construction, a novel 'hole-punch' style of test was used, a schematic of which is shown in Fig. 4.14. Here the shear strength  $\tau$  was calculated by  $\tau = P/A$ , where  $A$  is the specimen thickness multiplied by the circumference of the cylindrical punch. Since the cylindrical punch pushes an almost perfectly circular piece of balsa out of the test specimen, this is considered to be a reasonable way of determining the shear strength of balsa. The test method also allows for a comparative study of balsa shear modulus. A nominal shear modulus was determined from the initial slope in the load-displacement curve produced during the testing. However, since the elastic shear strain zone is not well defined here, the resultant value of shear modulus was taken to be nominal, rather than absolute. The nominal shear modulus  $G_{nominal}$  was found with the initial slope  $k$  in the load-displacement curve, the hole punch

diameter  $D$  and  $A$  (Eqn. 4.3).

$$G_{nominal} = \frac{kD}{A} \quad (4.3)$$

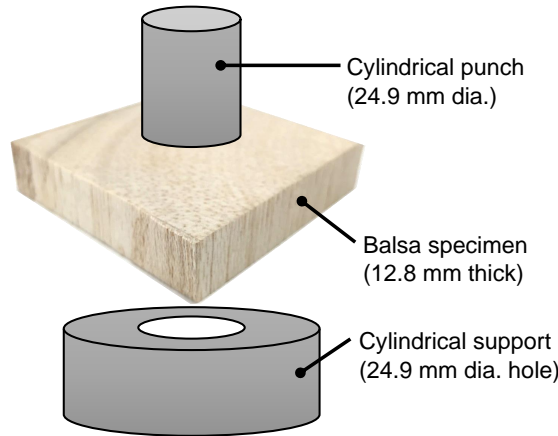


**Fig. 4.14** Schematic of ‘hole-punch’ test used to determine the apparent properties of constituent end-grain balsa blocks.

## 4.5 Results and discussion

Typical load-displacement curves for the sandwich panels with SB.150 end-grain balsa cores tested in three point bending are shown in Fig. 4.15, along with load displacement curves of conventional birch plywood decking of the same nominal dimensions. Fig. 4.16 plots the mean ultimate load and mean flexural modulus for all of the sandwich panel specimens tested. The flexural modulus was calculated from the gradient of the initial linear portion of the load-displacement curve obtained during testing. It can be seen in Fig. 4.15 that sandwich panels with SB.100 grade cores (Al-balsa (epoxy)) have significantly lower stiffness than those with SB.150 grade cores (Al-balsa (methacrylate)), even though they have identical face sheets. The increase in stiffness from GFRP-balsa SB.150 (single shot) panels to GFRP-balsa SB.150 (methacrylate) panels, as seen in Fig. 4.15, is attributed to the increased panel thickness from adhesive layers and thicker face sheets from the lack of pressure in the manufacturing process of the bonded panels.

It is evident from Figs. 4.15 and 4.16 that the sandwich panels with high density (SB.150) cores generally have superior flexural strength and comparable flexural stiffness in compar-

ison to birch plywood. The majority of the sandwich panel specimens with SB.100 grade cores failed prematurely in core shear and did not exhibit the desired flexural properties. The sandwich panel specimens with GFRP face sheets typically failed in core shear (Fig. 4.17a), while the methacrylate bonded aluminium sandwich panels typically failed through face sheet yielding, followed by core shear failure (Fig. 4.17b), as predicted by the failure mode maps (Figs. 4.8 and 4.9). On the other hand, the aluminium sandwich panel specimens bonded with epoxy adhesive exhibited premature debonding of the face sheets from the core.

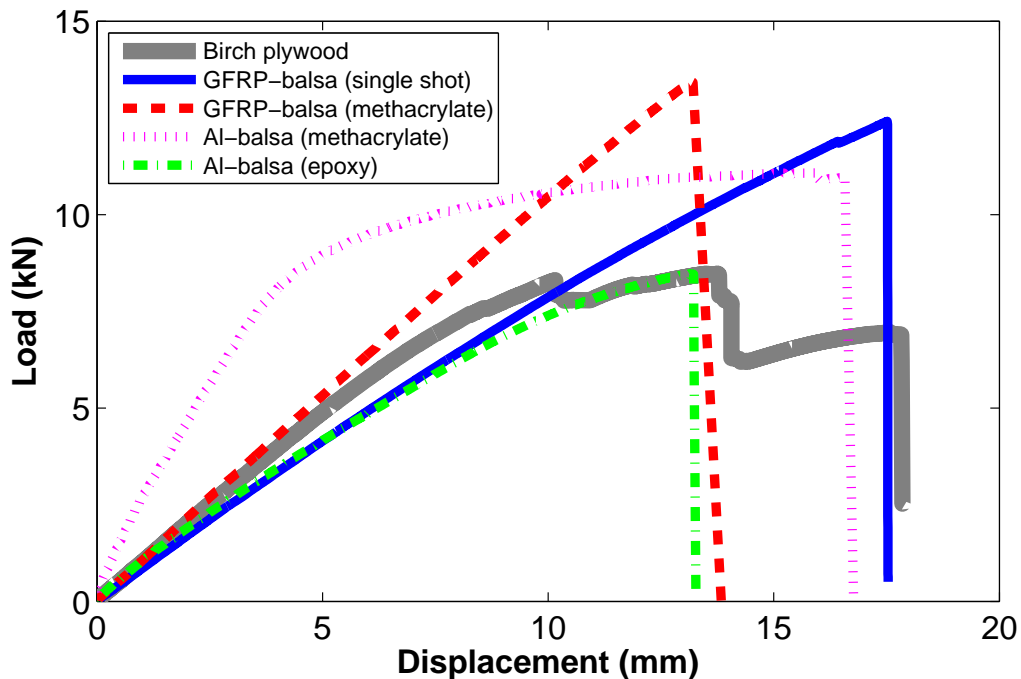


**Fig. 4.15** Typical load-displacement curves of the sandwich panels with SB.150 end-grain balsa cores in three point bending, compared to birch plywood. A full set of load-displacement curves is provided in Appendix B.

Representative load-displacement curves obtained from large panel testing of demonstrator sandwich panels and birch plywood of the same dimensions are shown in Fig.4.18, and a full set of curves is provided in Appendix B. It is evident that the GFRP-balsa (SB.150) panel once again had superior strength and comparable stiffness in comparison to birch plywood. This result is encouraging since this application is more strength than stiffness limited. It is also apparent from Fig.4.18 that the GFRP-balsa (SB.150) sandwich panel can withstand approximately four times the forklift wheel load of 12.25 kN that is commonly seen in-service. This panel ultimately failed at the top face sheet (Fig. 4.19), which is in compression, at a load of approximately in 45 kN. In contrast to this, the methacrylate bonded



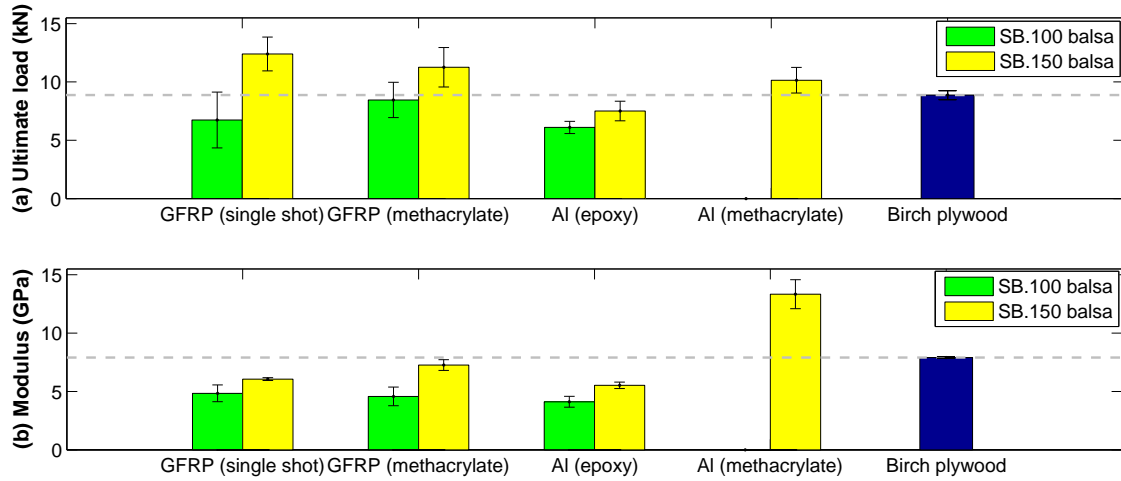


**Fig. 4.16** (a) Mean ultimate load and (b) mean flexural modulus of the sandwich panels in three point bending, compared to birch plywood. Error bars indicate standard deviation.

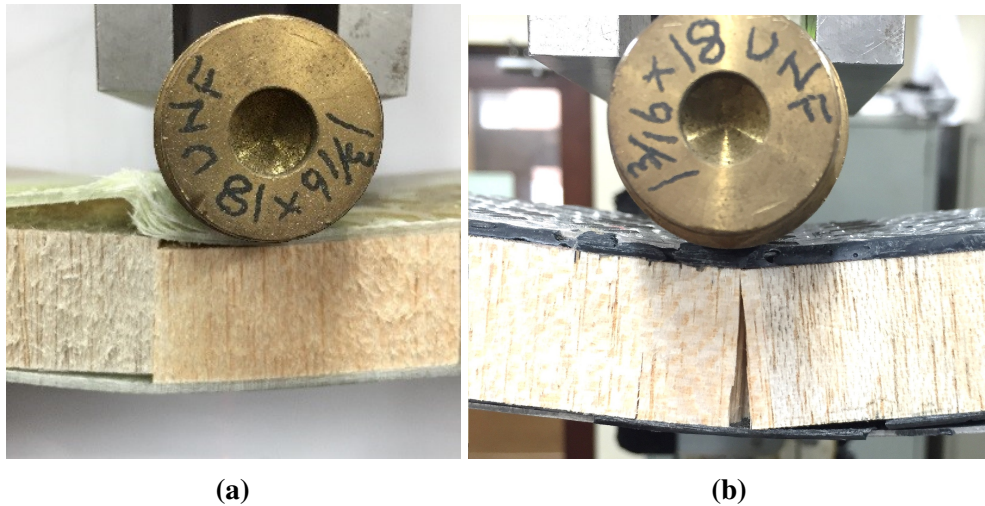


**Fig. 4.17** (a) Core shear failure observed in GFRP-balsa (SB.150) sandwich panels. (b) Face sheet yielding, followed by core shear failure observed in methacrylate bonded aluminium-balsa (SB.150) sandwich panels.



aluminium-balsa (SB.150) sandwich panel failed prematurely at approximately 12 kN as a result of face sheet debonding.

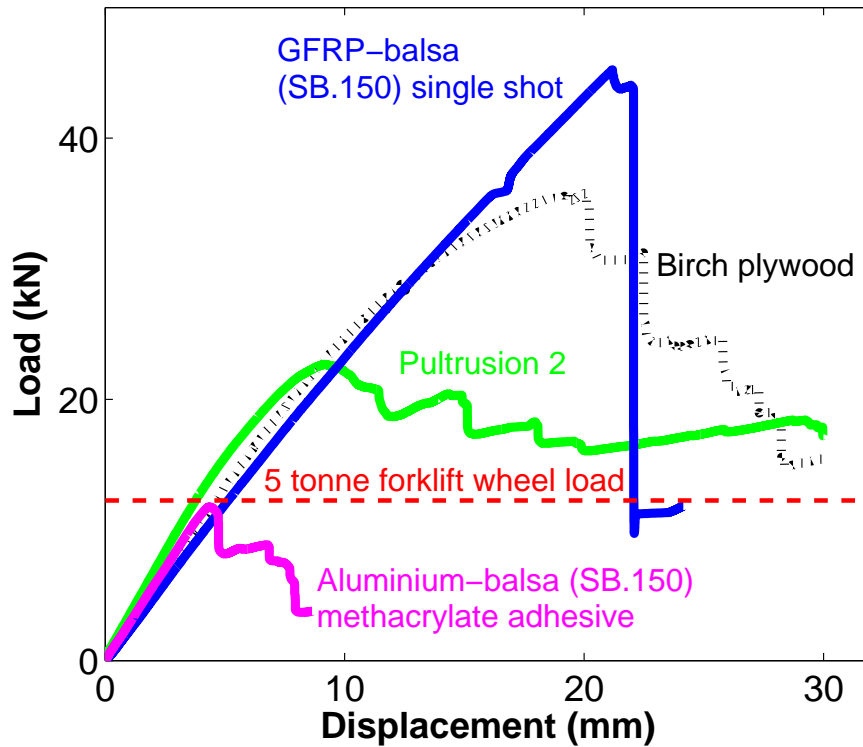


**Fig. 4.18** Load-displacement curves obtained from the large panel ( $550 \times 400 \times 30$  mm) testing with loading through a simulated forklift wheel ( $180 \times 80$  mm).

The premature core shear failures in the sandwich panels can be attributed to the presence of lower density constituent pieces of end-grain balsa that are found within a single sheet of rigid core (Fig. 4.20). It is well known that the mechanical properties of balsa vary with density [89–91]. This was confirmed by determining the shear properties of the end-grain core using the novel ‘hole-punch’ test. Results of the shear testing (Fig. 4.21) show the significantly reduced shear strength and stiffness of the lower density constituent blocks present within a single sheet of core material. This is most likely to be the cause of the adverse flexural properties observed in many of the SB.100 sandwich panel specimens. This problem was overcome by using the higher density SB.150 end-grain balsa core, which has been shown to have superior shear properties here and by Osei-Antwi *et al.* [91]. Similar trends for compressive properties with density of the balsa parallel to the end-grain were also identified (Appendix D).



**Fig. 4.19** Top face sheet failure observed during large panel testing of 30 mm thick woven GFRP-balsa (SB.150) single shot sandwich panel with non-slip coating. Failure propagates along one edge of the rubber pad that simulates a forklift wheel.

The effects of moisture diffusion in the sandwich panels has not been examined. However, recently published literature has addressed this and shown that like birch plywood (Chapter 3), GFRP-end-grain balsa sandwich panels abide by Fickian diffusion [92].

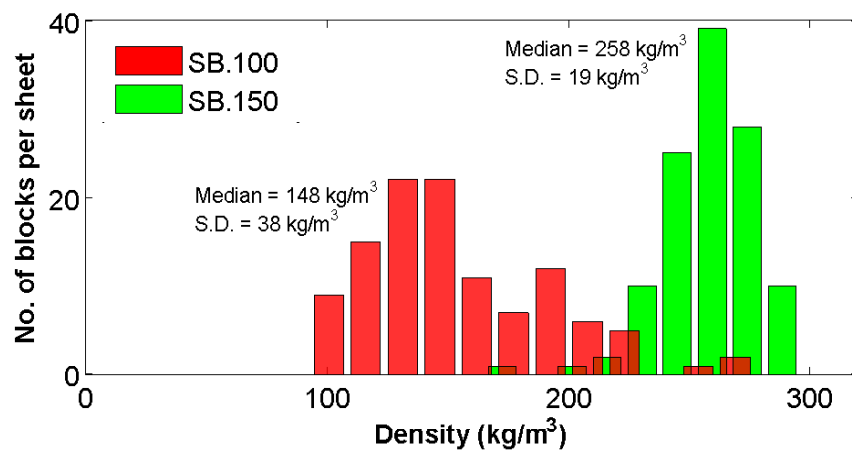


**Fig. 4.20** Histograms of the density of constituent blocks within single sheets of rigid Baltek SB.100 and SB.150 end-grain balsa core. Medians and standard deviations (S.D.) are also shown.

While cost and mechanical performance are the two main concerns that sandwich panel decking needs to satisfy to be used successfully in this application, there are other practical issues that need to be considered. For example, safety dictates that it is desirable to have the exposed surface of the GFRP sandwich panel deck covered or treated with a non-slip

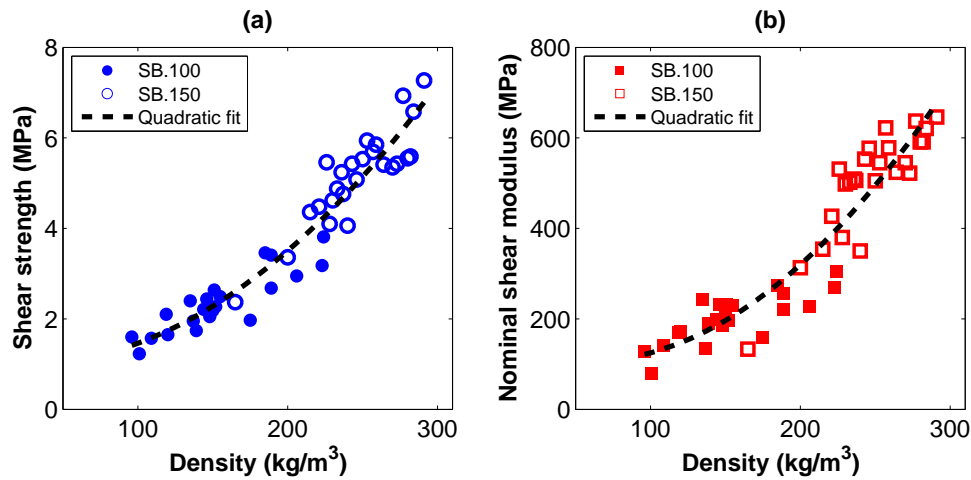


**Fig. 4.21** Variations in (a) shear strength and (b) nominal shear modulus, with density of end-grain balsa core used in sandwich panel construction. Properties determined through ‘hole-punch’ test. Dashed lines correspond to polynomial fits to experimental data.

coating. An abrasion resistant polyamine epoxy coating, commonly spray-applied to bridge decks and helidecks, should work well in this application and was successfully applied to the demonstrator panel (Fig. 4.19).

Since road freight trailers are generally returned to trailer manufacturers for recycling at the end of their service life, the recyclability of the sandwich panel constituent materials also needs to be taken into consideration. This issue of sustainability supports the choice of balsa as a core material over a polymer foam material. While aluminium face sheets are generally more recyclable than GFRP face sheets, the recyclability of fibre reinforced plastics is a focus of much on-going research and is expected to improve within the coming years.

Another important consideration in the application of sandwich panel decking to road freight trailers is the method of joining. Mechanical fastening is the most common form of joining hardwood decking to the trailer beams, though structural adhesives have been successfully used in the past and these can also help to reduce weight [93]. Structural adhesives are the most attractive way to bond a lightweight composite deck to steel trailer beams, though there are some issues that need to be addressed, including: surface preparation of chassis beams, curing time and curing temperature. Nevertheless, these issues have been successfully overcome in other comparable industries (e.g. bridge construction). In addition to these issues, the operating temperature of certain adhesives could be another limiting factor. For example, epoxy adhesives generally have a glass transition temperature of around 50 °C, beyond which their adhesive strength is significantly lower. Finally, it is worth noting that fatigue and impact performance of trailer decking will also require some attention, but this is outside the scope of the current work.

## 4.6 Conclusions

Applying sandwich panels to road freight trailer decking in replacement of conventional hardwood decking has the potential to significantly reduce empty trailer weight, without compromising the structural design of the trailer chassis. The weight saving potential of sandwich panels in this application does not justify a large increase in material cost. Hence, cost, as well as flexural properties, drive material selection in sandwich design. Sandwich panels with woven GFRP face sheets, and a higher density end-grain balsa core satisfy this material selection criterion the most effectively. The chosen sandwich panels presented here are approximately 30% lighter than conventional birch plywood trailer decking, which corresponds to a weight saving of approximately 165 kg in a standard 13.6 m long European flatbed trailer.

Premature core shear failure during three point bend testing is likely to occur in the sandwich panels, should the end-grain balsa core not be sufficiently dense. Hence, in this application it is recommended to use the highest grade (densest) end-grain core available, though there is a slight weight penalty associated with the selection of the densest core. Some practical issues (e.g. the method of joining panels to steel chassis beams) will need to be overcome before sandwich panels can be effectively used in this application. However, the majority of these issues have been successfully resolved in other industries, meaning there should be no significant technical barriers to overcome in applying sandwich panels to road freight trailers. Material and fabrication costs are the main obstacles to the practical uptake of these structures in road freight trailers.

# Chapter 5

## Pultruded GFRP subcomponents

### 5.1 Introduction

It was noted in Chapter 1 that the major downside of composite trailers to-date are increased material and production costs. This suggests that if composites are to be successfully applied to trailers, alternative processing routes should be considered. Pultrusion processing is one such alternative technique that could be employed to avoid tedious manufacturing processes, such as hand lay-up and RTM, used in previous composite trailer projects. Fig. 5.1 compares different composite manufacturing processes in terms of performance and units per annum. It shows that pultrusion processing has the potential to outperform RTM processing in terms of both productivity (units per annum) and component performance. Both of these factors are of utmost importance in trailer design and this suggests that pultrusion processing is worth exploring in this context.

A schematic of the pultrusion process is shown in Fig. 5.2. The first stage of the process involves impregnating dry reinforcing fibres with a low viscosity resin. The impregnated fibres are then drawn through a heated die which shapes the section and cures the resin. A pulling system is used to pull the section along the line and finally the sections are cut to a desired length. The pultrusion process is capable of continuously producing sections with complex shapes, though each section must remain uniform along its length.

Polyester resins are typically used in the pultrusion process, primarily because of their low cost and relatively large processing window. Phenolic-based resin systems have also been successfully employed in the process, though are less common. Phenolic resin systems are advantageous for applications that demand stringent fire and toxic fume emission requirements. Thermoplastic-based systems for the pultrusion process are still under development and these could potentially allow for easier post processing of pultruded members. Glass fibre is by far the most common type of reinforcement used in this process, though carbon fibres are

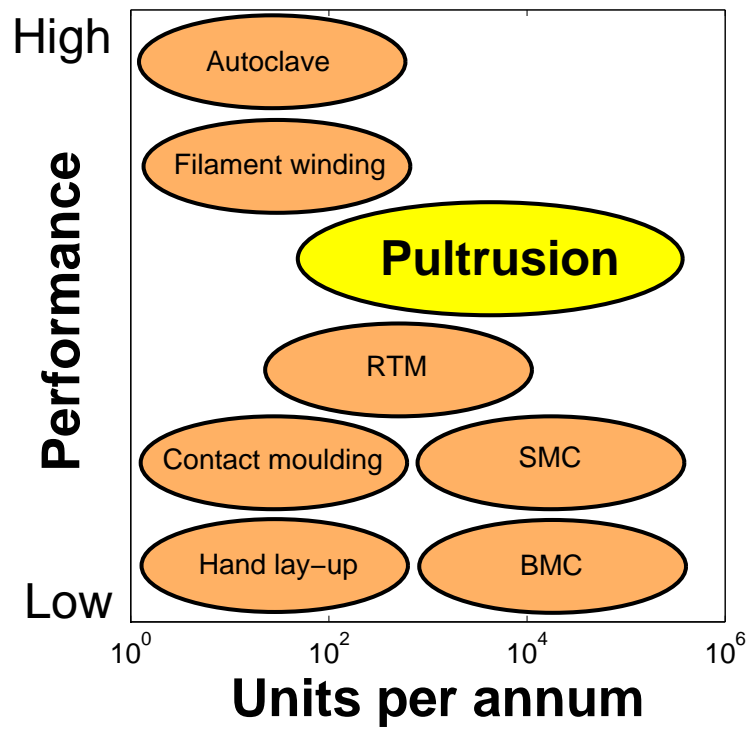


**Fig. 5.1** Composite manufacturing processes in terms of performance and units per annum, adapted from [27].

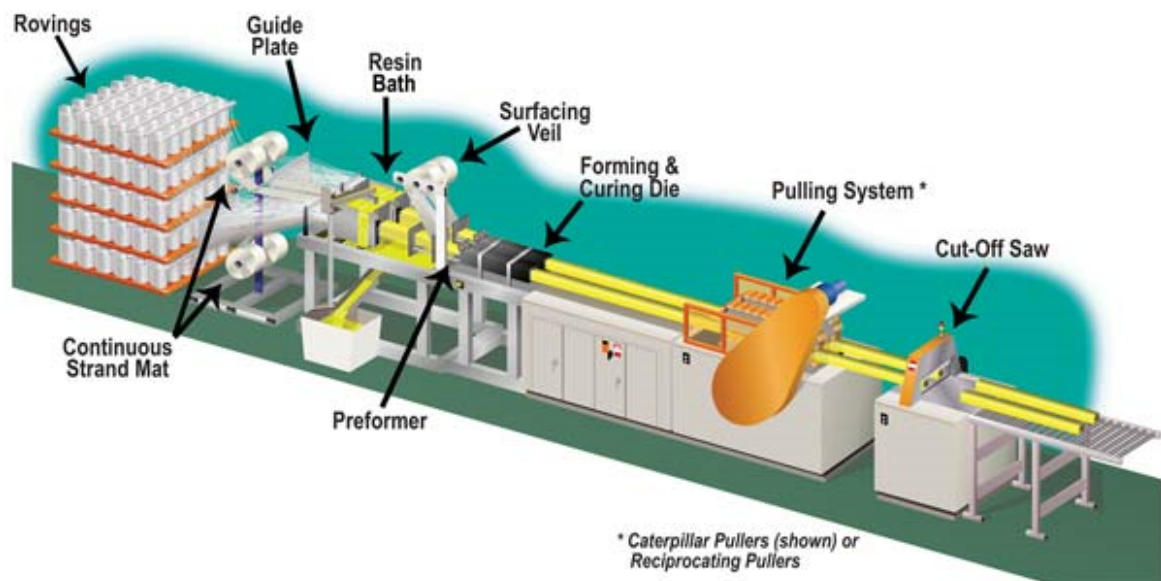


**Fig. 5.2** Schematic of the pultrusion process [28].

sometimes used for applications that require extra stiffness. Unidirectional (UD) fibre rovings provide longitudinal reinforcement, while chopped strand mat (CSM) provides transverse and through-thickness reinforcement. The nature of the process allows for relatively high fibre volume fractions to be achieved, allowing parts with good structural performance to be produced. The fact that it is possible to purchase pultrusions that are certified by the German Building Society, shows the pultrusion process produces sections with predictable quality.

As with the GFRP sandwich panels discussed in Chapter 4, the recyclability of pultruded GFRP sections is one potential drawback to their application. In the case of GFRP pultrusions, the polyester matrix can be burnt off in an oven leaving the glass fibres, which may then be used as short fibre reinforcement in other applications such as cement mixing. The high volume nature of the cement industry makes this a good solution to the problem, though conventional materials are still much more readily recyclable.

The staged integration of pultruded composites into sections of the trailer chassis structure, similar to what has occurred in the development of composite bridges, seems a logical path of exploration in the development of a lightweight yet cost-effective trailer chassis. The aim of this chapter is to explore in more detail the potential application of pultrusions to trailer subcomponents. In particular, pultrusions for use in trailer decking and for transverse structural members in ‘walking-floor’ trailers are examined through multiple existing off-the-shelf pultrusions.

## **5.2 Trailer decking**

### **5.2.1 Choice of off-the-shelf pultrusions**

As previously mentioned, a GFRP pultrusion is a strong candidate for a stiffened panel. The relatively low cost nature of these pultrusions makes them advantageous compared to other kinds of stiffened panels. Indeed, pultrusions have been successfully laid over steel beams in pedestrian bridges, which often have a similar structure to semi-trailers. Two different pultrusions were selected for further analysis. The first pultrusion (Figs. 5.3a and 5.4) is a heavy duty pedestrian bridge deck with a nominal height of 40 mm and is produced by Fiberline Composites, Denmark. This is referred to from herein as ‘Pedestrian Plank’. The second pultrusion (Figs. 5.3b and 5.5) is a pedestrian bridge deck with a nominal height of 28 mm produced by Unicomposite Technology, China. This is referred to from herein as ‘Hollow Decking’. These two decks are chosen to give a broad scope of what a pultruded deck can achieve in terms of cost and mechanical performance. The weight characteristics

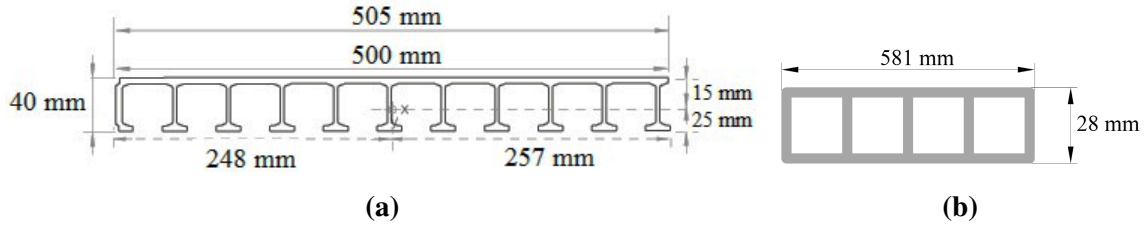


**Fig. 5.3** (a) Dimensions of ‘Pedestrian Plank’ produced by Fiberline, Denmark. Adapted from [29]. (b) Dimensions of ‘Hollow Decking’ produced by Unicomposite Technology, China. Adapted from [30].

**Table 5.1** Comparison of weight characteristics of pultruded GFRP decking compared to birch plywood decking. Total mass calculation assumes a deck area of 27 m<sup>2</sup>.

Deck type	Density (kg/m <sup>3</sup> )	Nominal thickness (mm)	Areal mass (kg/m <sup>2</sup> )	Total mass (kg)	Weight saving (%)
Birch plywood	700	30	21.0	567	-
‘Pedestrian Plank’	1,700	40	17.1	462	19
‘Hollow Decking’	1,800	28	17.3	467	18

of both pultrusions are compared to birch plywood in Table 5.1, and it can be seen that the pultrusions are approximately **19%** lighter than birch plywood.

The chosen pultrusions were first characterised through an analysis of their fibre reinforcement architectures and their fibre volume fractions. To determine the fibre volume fraction through matrix burn-off tests, it was first necessary to determine the density of the composite  $\rho_{comp}$  (Eqn. 5.1). This was done by following a procedure based on BS 2782 Part 6 Method 620A [94]. This procedure requires knowledge of the density of water at room temperature  $\rho_w$  (0.9975 g/cc), the mass of the sample in air  $a$  and the apparent mass of the sample suspended in water  $a_w$ .

$$\rho_{comp} = \rho_w \left( \frac{a}{a - a_w} \right) \quad (5.1)$$

The fibre volume fraction  $v_{fib}$  was then determined through matrix burn-off tests, following a procedure based on ASTM D3171-76 [95]. The matrix burn-off reveals a known mass of fibres  $m_{fib}$  for a given initial mass of composite  $m_{comp}$ . The polyester matrix of all samples is burnt off in a furnace for about 1.5 hours at 150 °C. Assuming that the density of E-glass fibres  $\rho_{fib}$  is 2.6 g/cc, the fibre volume fraction  $v_{fib}$  can then be calculated (Eqn. 5.2). The results of this procedure are shown in Table 5.2. The fibre architectures of the two



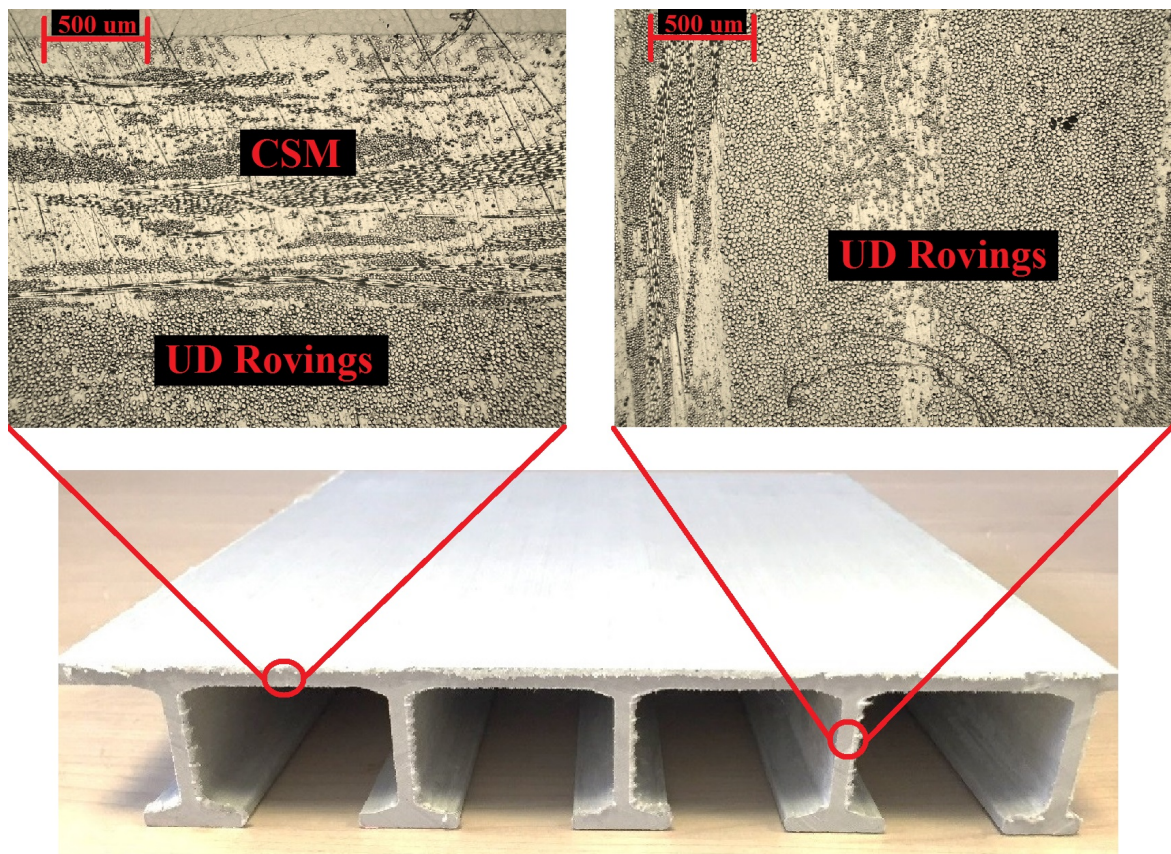


**Fig. 5.4** Micrographs of 40 mm high 'Pedestrian Plank' decking, manufactured by Fiberline Composites, Denmark.

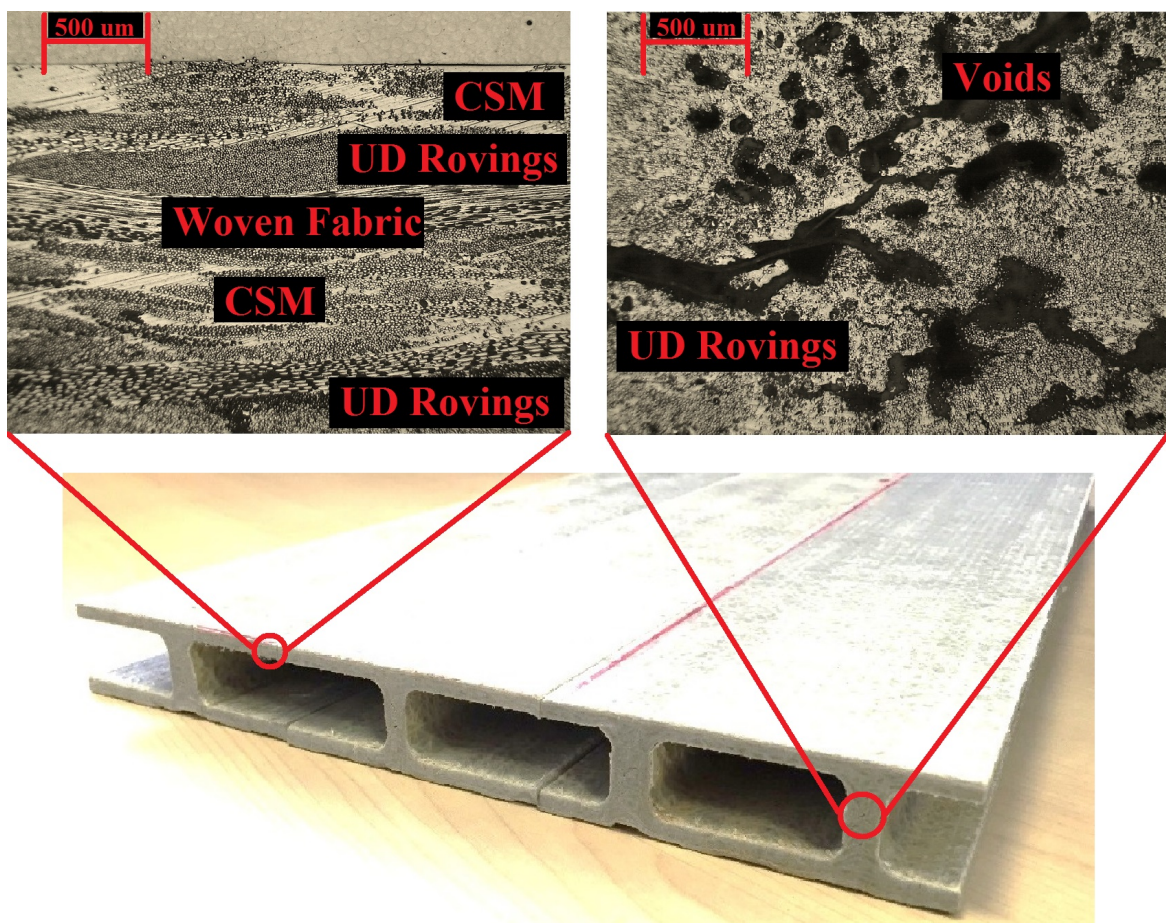


**Fig. 5.5** Micrographs of 28 mm high 'Hollow Decking', manufactured by Unicomposites, China.



**Table 5.2** Fibre reinforcement characteristics of the two pultrusions investigated. The characteristics of the GFRP laminates fabricated by wet hand lay-up in Chapter 4 are also shown for comparison.

	‘Pedestrian Plank’	‘Hollow Decking’	7-ply hand lay-up (Chapter 4)
Fibre architectures	CSM, UD rovings	CSM, UD rovings, woven fabric	Woven fabric
$\rho_{comp}$ (g/cc)	1.7	1.8	1.7
$v_{fib}$	0.40	0.46	0.37

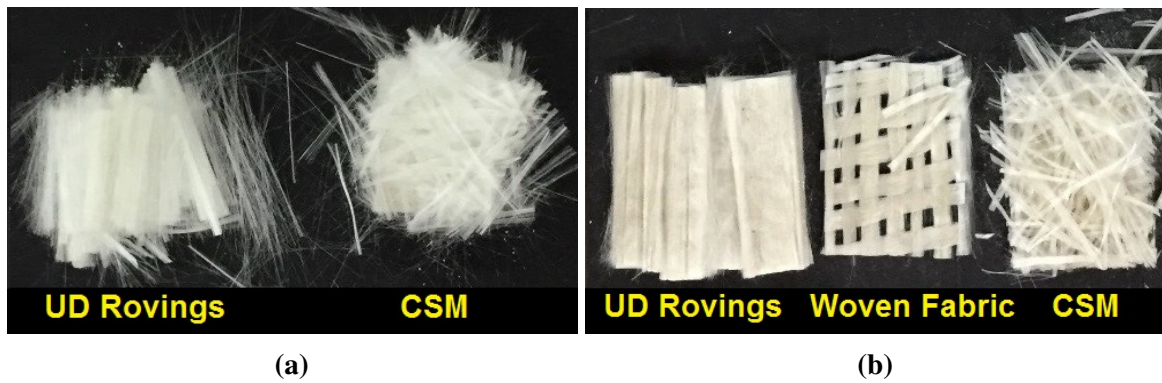


**Fig. 5.6** Fibre architectures recovered during matrix burn-off testing of (a) ‘Pedestrian Plank’ and (b) ‘Hollow Decking’.

different pultrusions recovered during the matrix burn-off are shown in Fig. 5.6.

$$v_{fib} = \frac{m_{fib}\rho_{comp}}{m_{comp}\rho_{fib}} \quad (5.2)$$

### 5.2.2 Damage study and mechanical testing

The two pultrusions were subjected to a similar mechanical testing regime that was performed on the birch plywood decking, described in Chapter 3. This involved; indentation testing, moisture absorption, three point bending flexural testing and abrasive wear testing with a rotary abrasion accelerated wear test machine.

A hardened steel spherical indenter of diameter 40.0 mm was used to indent the ‘Pedestrian Plank’ and the results are shown in Table 5.3. It can be seen that, in contrast to birch plywood decking, GFRP pultrusions have a very high indentation resistance, owing to their high local stiffness.

As with the birch plywood (Section 3.2.3), samples of both pultrusions for flexural testing were soaked inside a water bath and their moisture content determined by the percentage of

**Table 5.3** Indentation testing of ‘Pedestrian Plank’ with a 40.0 mm diameter steel indenter. Note that \* indicates localised fracturing around indentation.

Indentation force (kN)	Plastic work of indentation (J)	Dent depth (mm)
2.0	0.1	0
3.3	2.3	0.06
5.7*	13	0.43

weight gained (Fig. 5.7). It can be seen in Fig. 5.7 that after almost 40 days of soaking, the moisture content in the ‘Pedestrian Plank’ remained below 3%, while the moisture content in the ‘Hollow Decking’ remained below 2%. This is significantly less than the 43% moisture content that was absorbed in birch plywood after a similar soaking time. The pultrusions, like birch plywood, seem to follow Fick’s law of diffusion and this notion is supported by published results from similar studies [96–98].

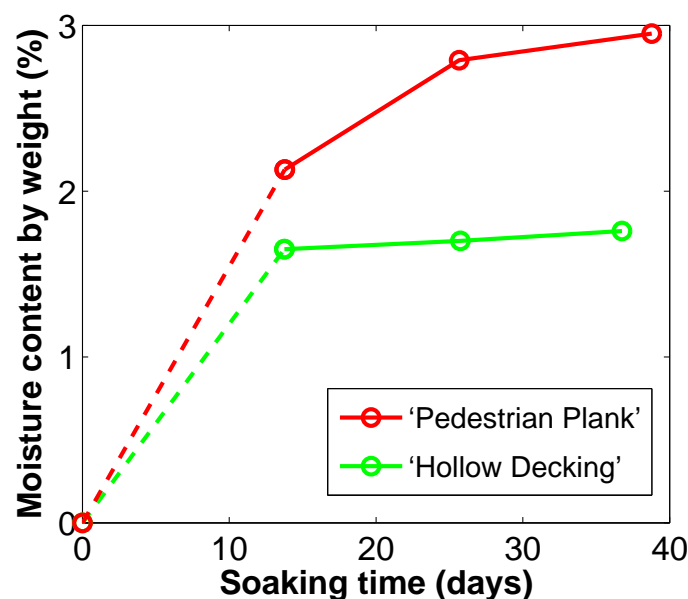


**Fig. 5.7** Moisture content by weight plotted against specimen soaking time for the two GFRP pultrusions.

Three point bending tests (described in Section 3.2.2) were performed to determine the flexural strength and stiffness of undamaged and water soaked pultrusions; results summarised in Fig. 5.8. The results show that the flexural properties of both pultrusions were not greatly affected by severe water damage and that both pultrusions have significantly higher flexural strength and stiffness than birch plywood as found in Chapter 3. However,

the ultimate load of the ‘Hollow Decking’ samples was similar to that of birch plywood and this can be seen in Fig. 5.9, which compares the load-displacement curves of the pultrusion controls and the birch plywood controls. The low flexural strength of the ‘Hollow Decking’ compared with the ‘Pedestrian Plank’ is attributed to a premature shear failure in the web caused by high void content, as seen in Fig. 5.5. The small degradation in the flexural properties of the pultrusions with moisture could be attributed to the loss of low molecular weight components initially present in the polyester resin, which can cause embrittlement of the pultrusions [98].

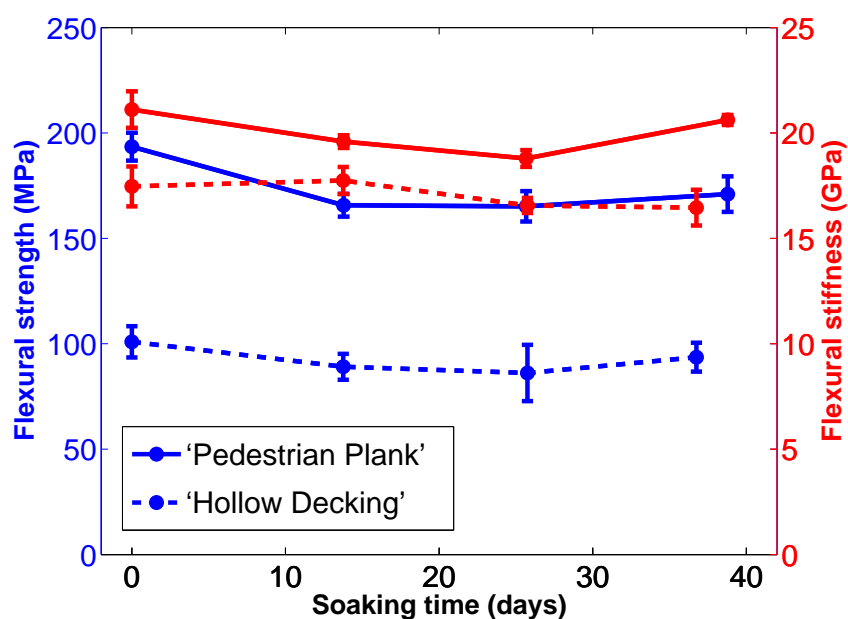


**Fig. 5.8** Flexural strength and stiffness (determined by three point bend tests) of GFRP deck pultrusions plotted against soaking time in days. Error bars indicate standard deviation.

Accelerated abrasive wear testing was performed with the same test set up as described in Chapter 3; results are shown in Fig. 5.10. It can be seen that ‘Hollow Decking’ has worse abrasive wear resistance than uncoated birch plywood. In contrast, the ‘Pedestrian Plank’ was found to have superior abrasive wear resistance. The differences between the tribological performance of the pultrusions can be attributed to the different fibre architectures, polyester resin varieties (which is unknown) and void content [99–102].

Given the smooth nature of the GFRP surfaces, a top coat like that described in Section 4.3 will need to be applied to the pultruded decking to improve abrasive wear performance and increase the coefficient of friction. While it is not investigated here, it has been shown that the presence of woven glass fabric improves the wear performance of neat polyester in each of the three main material directions [99].

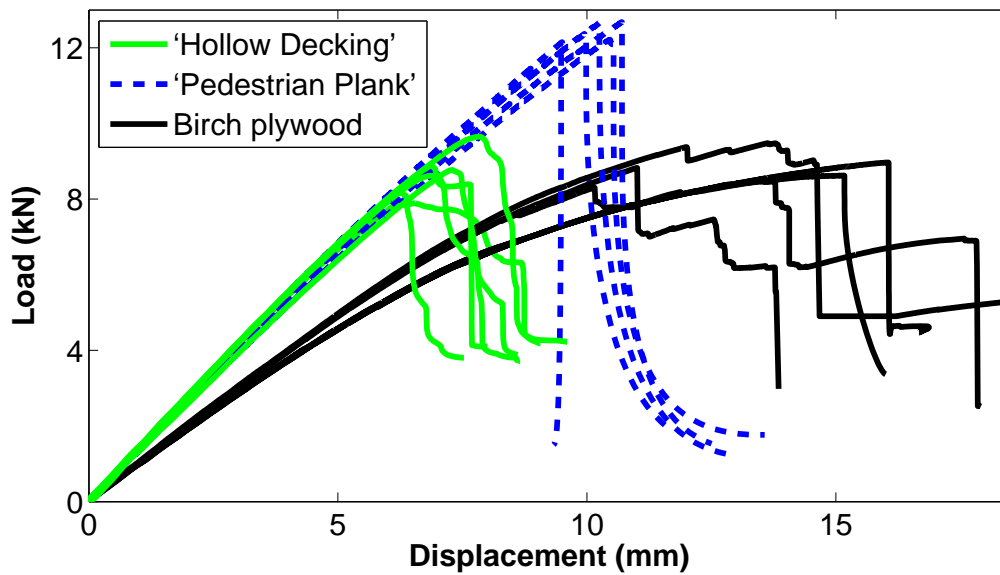


**Fig. 5.9** Load-displacement curves of pultrusion controls compared to birch plywood controls. Note that the nominal width of the birch plywood and 'Hollow Decking' specimens is 95 mm, however the nominal width of the 'Pedestrian Plank' specimens is 50 mm.

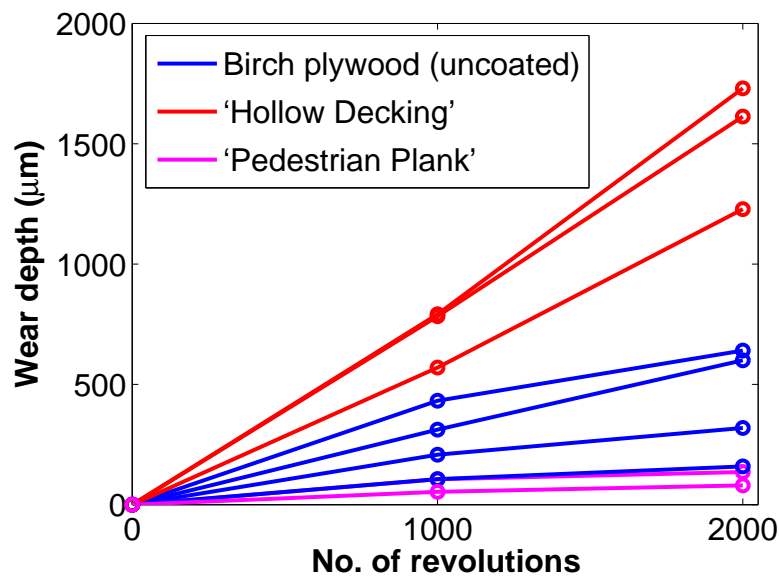


**Fig. 5.10** Maximum wear depth of various uncoated deck materials plotted against number of revolutions of the rotary abrasion machine. Minimum of two repeated tests for each material.

### 5.3 Transverse members in ‘walking-floor’ trailers

Chapter 2 identified ‘walking-floor’ trailers used in bulk haulage as a prime candidate for lightweighting. The aluminium transverse U-beams in these trailers seem like a sensible start-point for lightweighting with pultruded GFRP sections. In a standard 13.6 m ‘walking-floor’ trailer there are typically 29 transverse U-beams (Fig. 5.11), weighing 442 kg total.

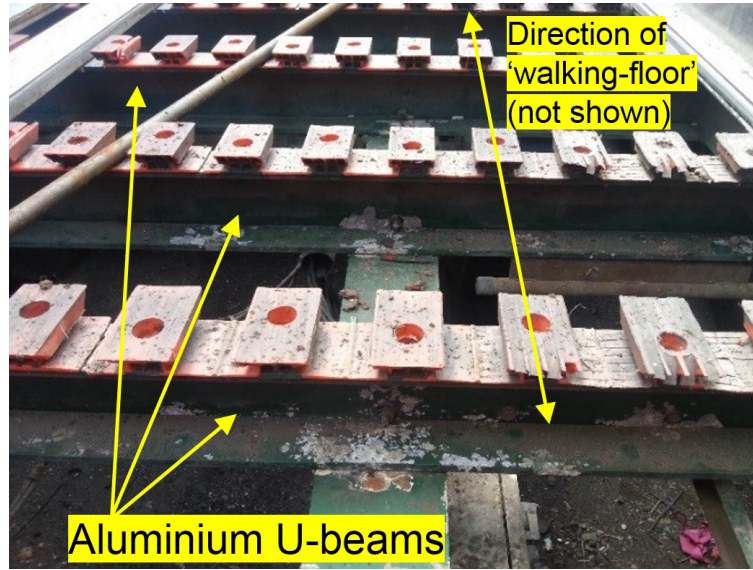


**Fig. 5.11** Transverse aluminium U-beams in ‘walking-floor’ trailers used in bulk haulage are a good candidate for replacement with GFRP pultrusions.

#### 5.3.1 Choice of off-the-shelf pultrusions

‘Walking-floor’ trailers are typically designed to withstand a load of 39,000 kg, though generally operate with a maximum loading of around 28,000 kg. It can be assumed that the flooring over the transverse U-beams distributes the applied load uniformly. This assumption is particularly valid in the case of bulk haulage trailers where payload tends to be spread evenly and is approximately uniform in density. Using these assumptions and knowing that the transverse beams are supported by two longitudinal members that are 1.2 m apart (span length  $l = 1.2$  m), the maximum bending stress  $\sigma$ , shear stress  $\tau$  and deflection  $\delta$ , can all be calculated in the usual manner (Eqns. 5.3 to 5.5). The definition of the terms in these equations are given in the nomenclature section.

$$\sigma = \frac{My}{I} \quad (5.3)$$

**Table 5.4** Comparison of the mechanical performance of two pultruded GFRP sections to the aluminium U-beams used in ‘walking-floor’ trailers. Eqns. 5.3 to 5.5 estimate the mechanical performance of the sections using average material properties taken from [26].

Applied load = 28,000 kg							
Profile Type	Material	Dimensions h × b × t (mm)	Weight (kg/m)	Total weight (kg)	σ (MPa)	τ (MPa)	δ (mm)
U	Al	125 × 65 × 10	6.35	442	67	3.5	0.6
Square	GFRP	120 × 120 × 6	4.95	345	57	2.9	1.5
Rectangle	GFRP	140 × 60 × 6	3.65	254	78	4.6	1.8

$$\tau = \frac{VQ}{It} \quad (5.4)$$

$$\delta = \frac{5ql^4}{384EI} \quad (5.5)$$

The total height of the exiting transverse U-beams (125 mm) is thought to be the principal geometry constraint for new members to conform to. With this in mind, two different pultrusions were selected from the off-the-shelf sections sold by Fiberline Composites, and their mass and performance compared to conventional aluminium U-beams in Table 5.4.

The design guidelines for the strength and stiffness of GFRP pultrusions are well defined in the Fiberline Design Manual [29]. Assuming that long-term (conservative) values of strength and stiffness are required, then the maximum allowable values for stiffness and strength are as follows:

Maximum allowable bending stress = 75 MPa (safety factor = 3.2)

Maximum allowable shear stress = 8 MPa (safety factor = 3.2)

Maximum allowable deflection =  $l / 400 = 1200 / 400 = 3$  mm

It is evident from Table 5.4 that the pultrusions will entail higher levels of deflection than the aluminium members. However, the deflection like the bending stress and shear strength, are all within the maximum allowable values defined by the design guidelines. The exception being in the bending stress of the rectangular profile pultrusion which is slightly higher than the recommended limit. This suggests that the square profile pultrusion would be the best



choice for application here and these could bring a total weight saving of approximately 100 kg. Therefore, despite their less desirable mechanical performance, the rectangular profile could bring a total weight saving of almost 200 kg.

### 5.3.2 Joining

Like in bridges, a significant obstacle to the application of GFRP pultrusions will be creating a robust joint between the pultrusion and steel members. Welded steel brackets and mechanical fasteners are currently used to join the transverse beams to the two longitudinal steel beams. However, there are several issues with transferring traditional bolted joint techniques directly to pultrusions. To this end, the Fiberline Design Manual [29] provides guidance on which bolted configurations are acceptable for each pultruded profile. It also provides guidance on the bolted configurations and loadings that should be avoided, as shown in Fig. 5.12.

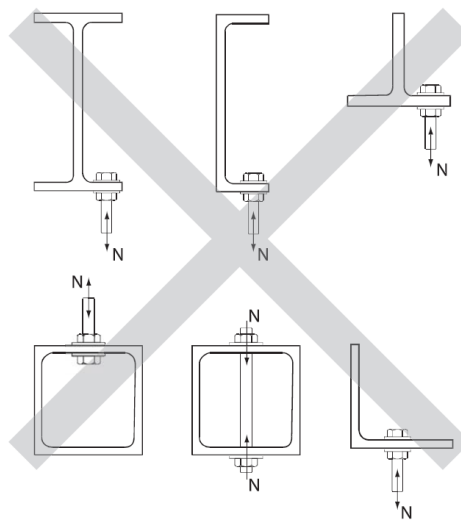


**Fig. 5.12** Bolted joint connections that should be avoided with pultruded GFRP sections, as specified in the Fiberline Design Manual [29].

Adhesive bonding of the pultrusions, on the other hand, could be a more advantageous route for creating a stiff, lightweight joint. Structural adhesives used in joining could also be used to bond nylon wheel tracks to the pultruded members, removing the need for mechanical fasteners and reducing weight even further. While there are problems (such as the effects of surface preparation, joint configuration, adhesive properties and environmental factors) associated with adhesive joints for composite structures, these have been the focus of much recent research (summarised in [103]). Thus, these issues should not significantly hinder the potential application of structural adhesives to trailers, particularly as the technology grows in the future.

## 5.4 Conclusions

The fact that GFRP pultrusions are far less susceptible to moisture and indentation damage is encouraging for their application to trailer decking. Their relatively low material and production costs compared to other composite structures is another promising point for their potential application. However, replacing conventional materials such as hardwood with pultrusions will come with some cost increases. Pultruded GFRP decking would also offer less weight saving benefit compared to the sandwich panel solutions presented in Chapter 4.

The use of pultruded beams to replace aluminium transverse members in ‘walking-floor’ trailers can bring some potential weight saving (up to 200 kg), without significantly compromising mechanical performance. Perhaps more importantly, this route could provide an opportunity for the proof of concept of pultruded sections for use as load bearing members in the trailer chassis. However, mechanical testing has shown that the cheaper pultruded decking manufactured by Unicomposites has significantly less desirable mechanical properties (flexural strength in particular), in comparison to the pultruded decking manufactured by Fiberline Composites. The relatively low flexural strength of the ‘Hollow Decking’ compared with the ‘Pedestrian Plank’ can be attributed to a premature shear failure in the web caused by high void content. Therefore, high quality pultrusions, like those manufactured by Fiberline Composites, should generally be targeted for use in load-bearing subcomponents to avoid this kind of premature failure.

# Chapter 6

## Lightweight chassis design

### 6.1 Introduction

The holistic composite trailer projects discussed in Section 1.2.1 have generally reported similar benefits to each other in terms of weight saving over their steel counterparts. This gives rise to the notion that there is a practical limit on the weight saving potential of composite materials in the context of trailer design, especially when raw material costs and fabrication costs are taken into consideration. The development of a prototype composite trailer like those described in Section 1.1 is outside of the scope of this project. However, an investigation into the potential design space into which a holistic composite trailer could fit will give future lightweighting projects a better understanding as to the limits of weight reduction that can be achieved with composite materials.

The aim of this chapter is to investigate the design space that a composite trailer could fall within, in terms of both weight saving and mechanical performance. To achieve this, work within the chapter is split into three broad areas:

1. A study into the critical load cases to which conventional steel trailers are currently designed is first performed through a literature review and consultation with industry (Section 6.2). Finite element (FE) analysis is applied to the conventional 13.5 m ladder-type trailer chassis used by SDC Trailers.
2. A design methodology similar to that applied by Monroy Aceves *et al.* [31] is described (Section 6.3.1) and then used to investigate steel beam shape optimisation (Section 6.3.2).
3. The design methodology is then expanded to investigate composite-based chassis designs that satisfy the mechanical design constraints while significantly reducing mass

**Table 6.1** Load range for the trailers tested in the FORWARD project [35].

Force	Magnitude (kN)
Total brake force on all trailer axles together	30 – 40
Longitudinal force at the king pin	60 – 100
Vertical force at the king pin	130 – 150
Cornering force over all axles	45 – 60
Cornering force at king pin	30
Torque around trailer axle system	15 – 20

and at the same time, keeping raw material cost increases to a minimum (Sections 6.3.3 and 6.3.4). Trends in the results of the optimisation procedures and issues surrounding practical implementation are also discussed.

## 6.2 Review of chassis load cases and optimisation

### 6.2.1 Literature

A robust lightweight redesign of a trailer chassis requires sound understanding of the in-service loadings such as the forces and moments on the trailer axles and the king pin. This has been the focus of the FORWARD project (Fuel Optimised trailer Referring to Well Assessed Realistic Design loads) performed in the Netherlands in conjunction with multiple European trailer manufacturers [35, 104]. This project examined three different types of 13.6 m tri-axle trailer, including a box trailer, a trailer with a belt unloading system and a flexi-trailer used in container or tank transport. The trailers were fitted with numerous sensors and subjected to a testing regime which characterised normal use over a representative period of time. The payload in each of the three trailers varied from 24 to 28 tonnes and the trailer axle loads in the study were typically between 6 and 8 tonnes per axle. It was found that the maximum decelerations during braking in the testing were around 0.7 g while the maximum lateral accelerations were found to be 0.4 g. A summary of the load range the testing has found for all the trailers is provided in Table 6.1.

In addition, both the ROADLITE trailer project and the CleanMould trailer project described in Section 1.2.1 attempted to benchmark the performance of conventional steel-based trailer designs. Both performed FE simulations on trailers with a Uniformly Distributed Load (UDL) to identify critical areas of the structure. In both cases the goose-neck of the trailer is determined to be the critical area of the structure. The FE simulations in the CleanMould project showed that a 28 tonne UDL across a 13.6 m long trailer causes a

deflection of around 5 mm at the goose-neck when the trailer is running and attached to a tractor unit at the fifth wheel.

One way of reducing trailer chassis weight is via shape optimisation of the conventional ladder-type steel structure and this has been the focus of past research. For example, Kim and Jang [105, 106] developed a novel, lightweight 12.2 m long trailer frame by applying structural optimisation using FE analysis. The design optimisation process used an initial step to obtain an optimum shape topology, followed by a size and shape optimisation step with the Taguchi method to determine detailed dimensions. It was reported that the shape-optimised lightweight frame was 24.5% lighter than the original design and that it had improved bending and torsional rigidities. A major drawback of this approach is in the manufacturability of the complex geometry of the shape-optimised structure compared with the conventional I-beam ladder type-structure.

Indeed there have been other less prominent studies concerning the structural design, analysis and optimisation of a lightweight steel trailer chassis. Yasar and Bircan optimised a steel ladder-type chassis structure using FE analysis and the Taguchi method [107]. Sankar and Yuvaraj performed FE analysis on a 34.4 m steel trailer chassis to locate the critical points in the structure that have the highest stress [108]. Quan-li *et al.* performed a sensitivity analysis on a steel trailer chassis to investigate optimal geometric parameters [109]. Mahmoudi-Kaleybar *et al.* performed a dynamic analysis of a steel ladder-type structure using FE analysis [110]. Guron *et al.* performed a FE analysis to re-design a cross-member bracket within a steel trailer chassis [111].

### 6.2.2 SDC Trailers

It is evident from the literature review that the understanding of critical load cases for lightweight trailer design is an active area of research in itself. Because of this, the critical load cases applied were identified and investigated further with the help of industry partners SDC Trailers. In order of decreasing importance, the critical load cases include:

1. A fully loaded trailer parked resting on its landing legs and the trailer bogie.
2. A fully loaded trailer running on the fifth wheel coupling and the trailer bogie.
3. Torsion of a fully loaded trailer during running.

A 30 tonne UDL represents a fully loaded trailer, estimated using the following considerations:

$$\text{Payload} = \text{Maximum Combination Weight} - \text{Tractor Tare Weight} - \text{Trailer Tare Weight}$$

$$\text{Payload} = 44,000 - 7,500 - 6,500 = 30,000 \text{ kg}$$

The different load cases were investigated through a linear-elastic finite element analysis of a conventional 13.6 m steel chassis performed in Abaqus. The CAD model used in the analysis is a simplified version of a CAD model provided by SDC Trailers Ltd. The two most critical load cases analysed and their corresponding boundary conditions are shown in Fig. 6.1.

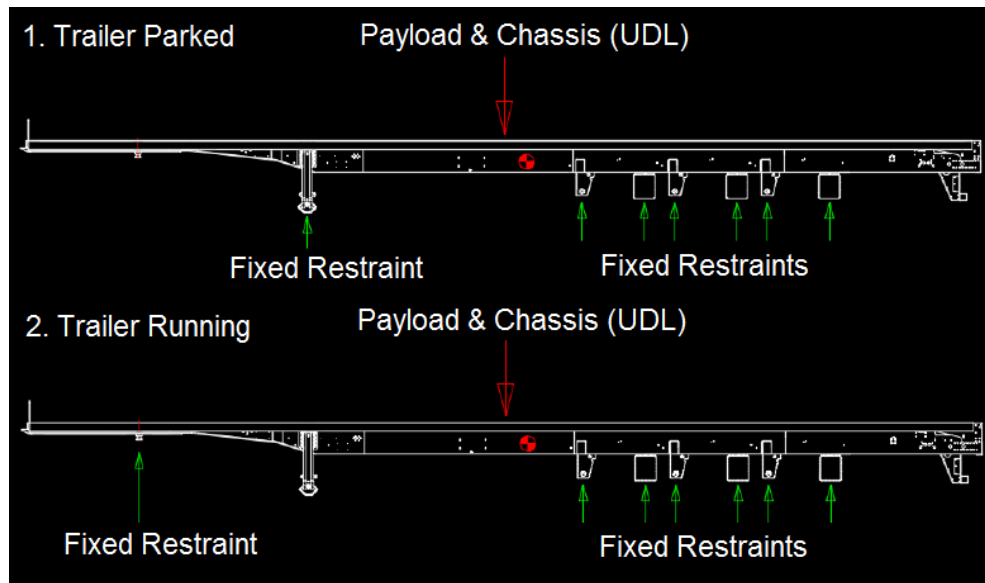


**Fig. 6.1** The two most critical load cases and their corresponding boundary conditions (courtesy of SDC Trailers).

In terms of design constraints, a safety factor of two is typically applied in design by SDC to account for dynamic loading and fatigue, hence the maximum allowable stresses are generally set to half the yield stress of the high strength low alloy steel (YS355) used. It has been noted that additional research on fatigue analysis in the context of trailer design would help in designing lighter chassis [112]. There are no fixed values for maximum allowable deflection, except for the parked and resting on landing legs load case, where the maximum allowable deflection at the front end of the trailer is 50 mm. With regard to torsional stiffness, how much the chassis twists in service varies a great deal due to its make-up and operating conditions. As an approximate criterion, SDC Trailers typically apply a torsional load to cause the chassis to twist by 150 mm (vertical measurement between front and rear diagonal corners) and examine the resulting stress. Because industrial partners have indicated that torsion is far less critical than the other two cases and that it is specific to operating conditions, it has been neglected in this analysis.

In the linear elastic FE analysis, displacement contours and stress plots were created for the two most critical static load cases. The results of the modelling are shown in Figs. 6.2 to 6.4. It can be seen that for both stiffness and strength, the load case of the trailer resting on its landing legs is the most critical. Here the deflection is 50 mm at the front end of the trailer and 2 mm at the rear of the trailer. In this load case, the maximum stress in the main longitudinal beams occurs at the goose-neck in the bottom flange and is approximately 40% of the yield stress, hence within the factor of safety i.e. 50% of the yield stress. In the running on fifth wheel load case the maximum deflection is approximately 4 mm at the goose-neck and the maximum stress is in the main longitudinal beams occurs toward the front end of the trailer and is approximately 20% of the yield stress, which is well within the margin of safety.

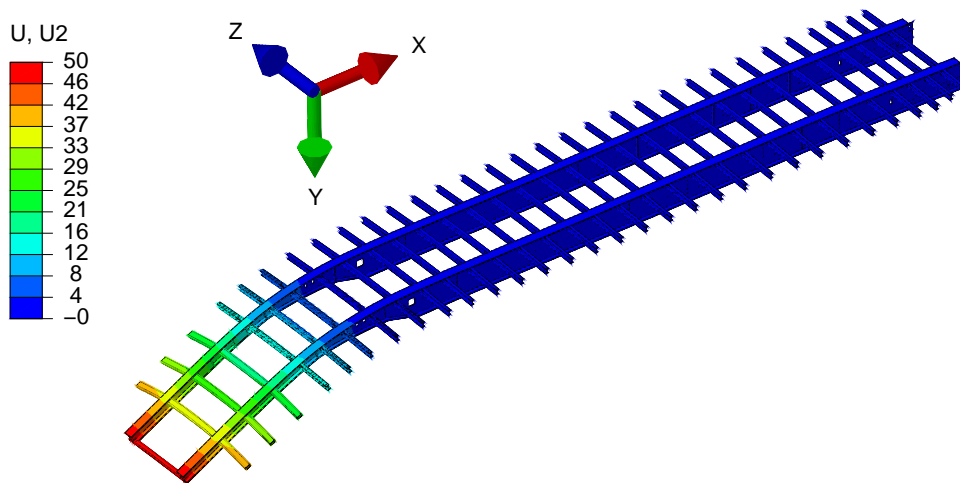


**Fig. 6.2** Displacement contour for the load case of resting on landing legs and trailer bogie (30 tonne UDL).  $U_2$  = displacement in the y-direction in millimetres.

## 6.3 Development of a lightweight chassis

### 6.3.1 Methodology

Since the trailer chassis is a relatively complex shape, it demands a complicated structural analysis, such as FE analysis. Monroy Aceves *et al.* [31] developed a methodology for use in the design of composite structures by combining FE analysis with a graphical optimisation step, as shown in Fig. 6.6. The design problem specification step is used to define the limits on geometry and potential material combinations. A corresponding set of FE analysis input files were generated using Python. These were then submitted to the solver of FE software

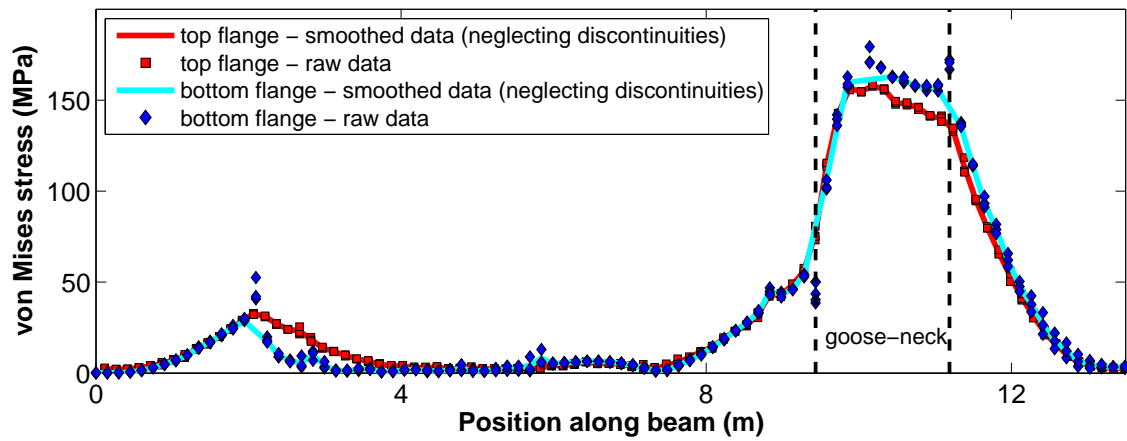


**Fig. 6.3** Stress plot for trailer main beam from the rear (0 m) to the front end (13.5 m) for the load case of resting on landing legs and trailer bogie (30 tonne UDL).

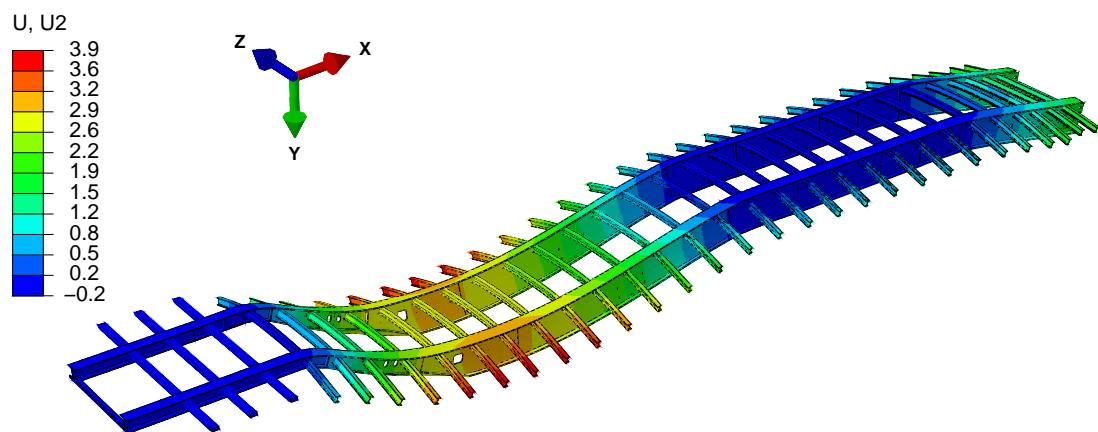


**Fig. 6.4** Displacement contour for the load case of running on fifth wheel and trailer bogie (30 tonnes UDL).  $U_2$  = displacement in the y-direction in millimetres.



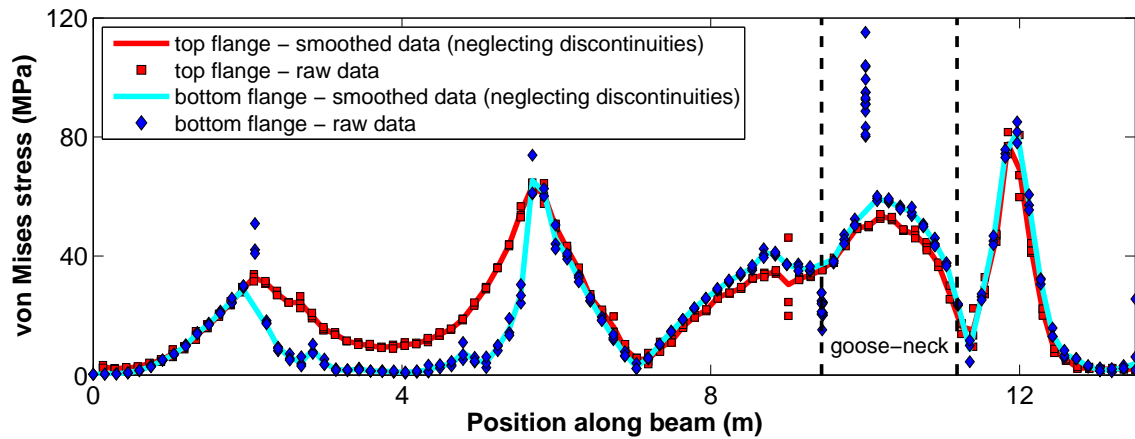


**Fig. 6.5** Stress plot for trailer main beam from the rear (0 m) to the front end (13.5 m) for the load case of running on fifth wheel and trailer bogie (30 tonne UDL).

Abaqus, and results can then be extracted into a database. This was then read in MATLAB and performance maps can be generated which allow for design constraints to be applied, and these help to identify optimal solutions within the allowable design space. While this approach is computationally expensive as it requires many calculations and iterations, it is an effective way of filling out the design space and identifying optimal solutions within the conflicting design constraints. Indeed, advances in desktop computing power make this form of ‘brute-force’ analysis more feasible for use.

The methodology of Monroy Aceves *et al.* was applied here in three separate contexts. Firstly, it was applied to conventional 13.5 m steel longitudinal beams, to investigate geometry changes that could potentially be implemented using existing beam fabrication techniques (Section 6.3.2). It was then used to examine the influence of trailer decking material selection in conjunction with beam sizing and material selection (Section 6.3.3). Finally, the results from Section 6.3.3 are used in Section 6.3.4 to examine in more detail the potential beam geometries and material combinations suited to a wholly composite trailer. In all scenarios investigated, the critical load case of the trailer resting on its landing legs and bogie was examined. The material properties used throughout the FE analysis are provided in Table 6.2. These materials were selected to give a broad scope in terms of mechanical properties (in particular stiffness), weight and raw material cost.

To give an indicator of mechanical performance, front and rear beam displacement, as well as failure index within the 13.5 m longitudinal beam, were all reported. The Tsai-Hill failure criterion (Eqn. 6.1) was applied to the 13.5 m longitudinal I-beam to determine the failure index. Because the FE models each use beam elements to model the longitudinal I-beams, the contributions of stress in the transverse 2-direction along the beam were ne-

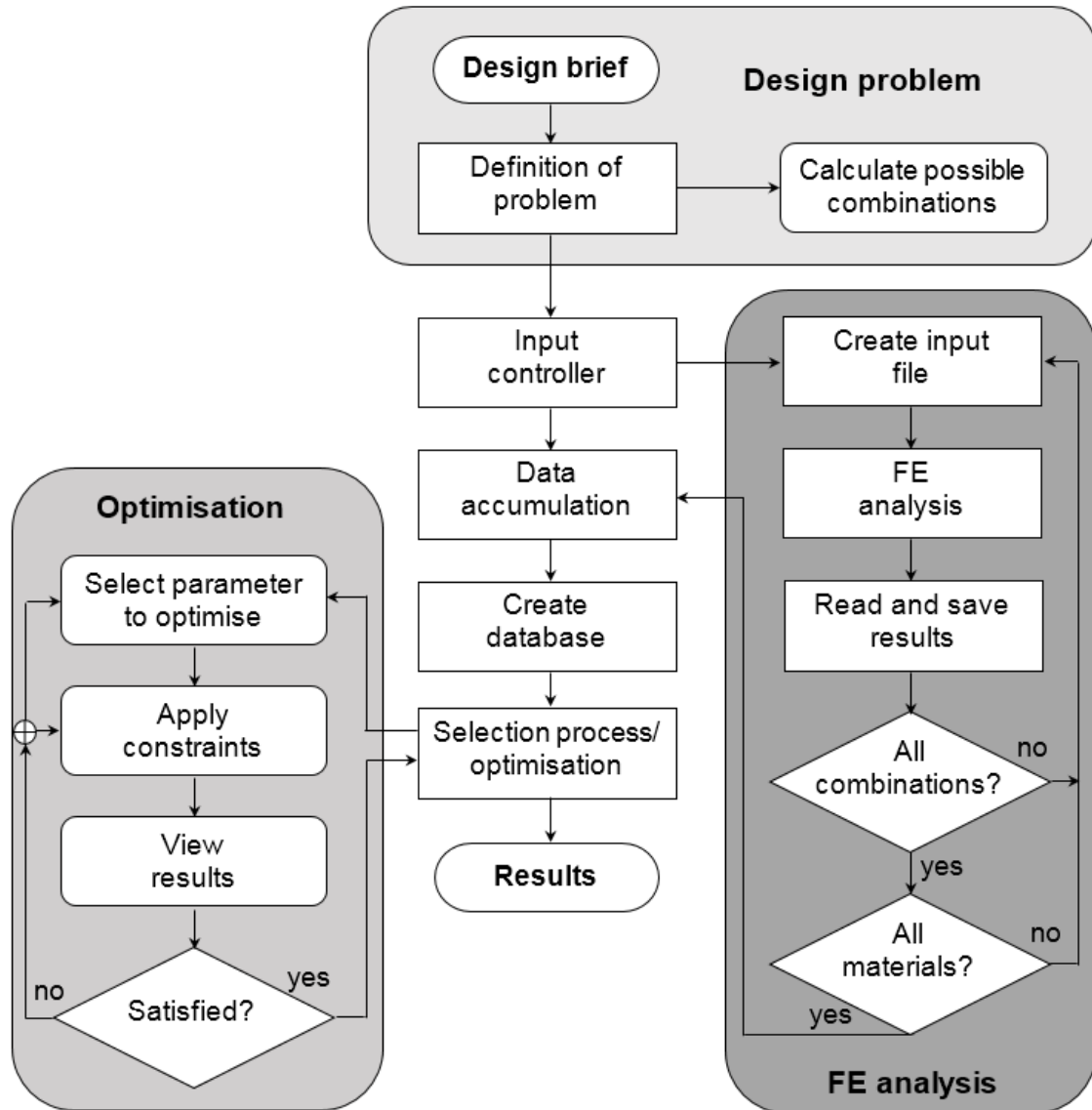


**Fig. 6.6** Design methodology flowchart, adapted from Monroy Aceves *et al.* [31].

**Table 6.2** Material properties used in finite element modelling [26].

Material	$E_1$ (GPa)	$G_{12}$ (GPa)	$\sigma_{1u}$ (MPa)	$\tau_{12u}$ (MPa)	$\rho$ (kg/m <sup>3</sup> )	Cost (£/kg)
Steel (YS355)	200	80	355	210	7,800	0.35
Aluminium	72	27	280	210	2,700	1.4
GFRP	23	3	860	83	1,800	1.2
CFRP	130	6	1,300	62	1,550	24

glected ( $\sigma_2 = 0$ ), simplifying the full Tsai-Hill failure criterion from Eqn. 6.1 to Eqn. 6.2. The failure index can then be written as a percentage (Eqn. 6.3). This failure index is applied to all materials to simplify the automation of the analysis. Since the design of the beam is stiffness-driven, the choice of failure criterion does not impact on the final result of the optimisation procedure. However, it should be noted that the von Mises or Tresca yield criteria would be more appropriate for use with metals.

$$\left(\frac{\sigma_1}{\sigma_{1u}}\right)^2 + \left(\frac{\sigma_2}{\sigma_{2u}}\right)^2 - \frac{\sigma_1 \sigma_2}{\sigma_{1u}^2} + \left(\frac{\tau_{12}}{\tau_{12u}}\right)^2 = 1 \quad (6.1)$$

$$\left(\frac{\sigma_1}{\sigma_{1u}}\right)^2 + \left(\frac{\tau_{12}}{\tau_{12u}}\right)^2 = 1 \quad (6.2)$$

$$\text{FI (\%)} = \left[ \left(\frac{\sigma_1}{\sigma_{1u}}\right)^2 + \left(\frac{\tau_{12}}{\tau_{12u}}\right)^2 \right] \times 100 \quad (6.3)$$

### 6.3.2 Shape optimisation of steel beams

In order to investigate changes that could be potentially implemented to the current ladder-type chassis, the parametric optimisation procedure was first applied to the conventional 13.5 m steel I-beam, which has bending stiffness properties shown in Fig. 6.7. The beam was split into front and rear sections as shown in Fig. 6.8 and modelled with a total of 135 beam elements, corresponding to an element length of 10 cm. Many geometry variations for both the front and the rear of the beam were investigated to determine their effect on beam mass, stiffness and strength. The full set of geometry variations analysed are shown in Table 6.3, along with current beam dimensions. The model assumes that the beam is simply supported at the landing legs and the trailer bogie (toward the rear of the beam) and a uniformly distributed 15 tonne line load was applied, as shown in Fig. 6.8. It was assumed that the present height of the beam (shown in Fig. 6.8) is the critical dimension and this remains constant in all simulations, so as to ensure ease of attachment to the tractor unit and a reasonably sized space envelope.

The results of the analysis are shown in Fig. 6.9 and the key features of the optimised steel beam (model a) found with this procedure are shown in Table 6.4. The bottom left quadrants of each graph depict the design envelope of the beam in accordance with the stiffness and strength requirements currently applied. It is evident in Fig. 6.9 that the shape-optimised

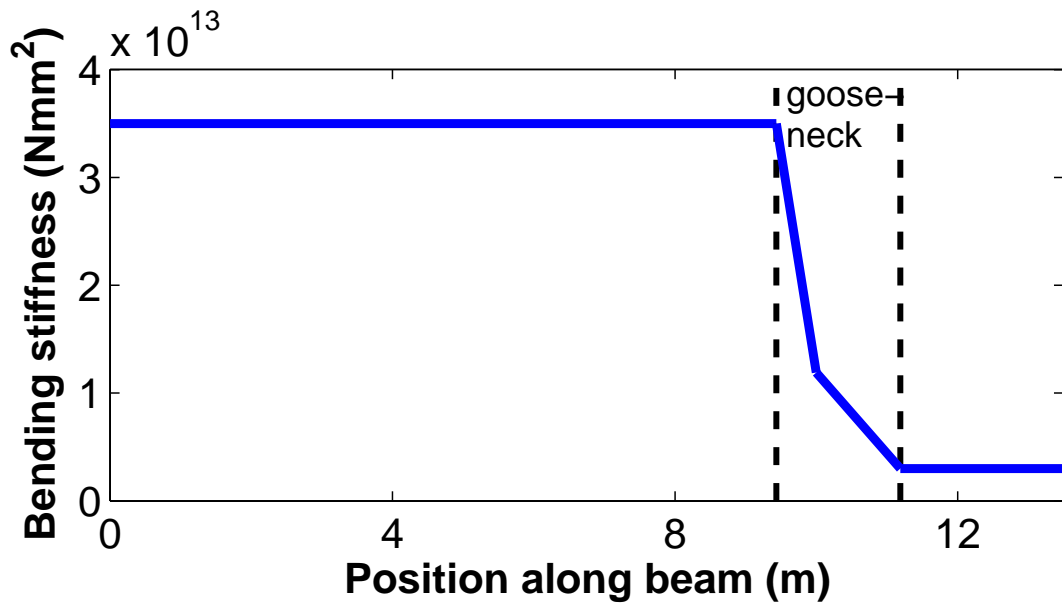


**Fig. 6.7** Beam bending stiffness of the main longitudinal trailer I-beam from the rear (0 m) to the front end (13.5 m).

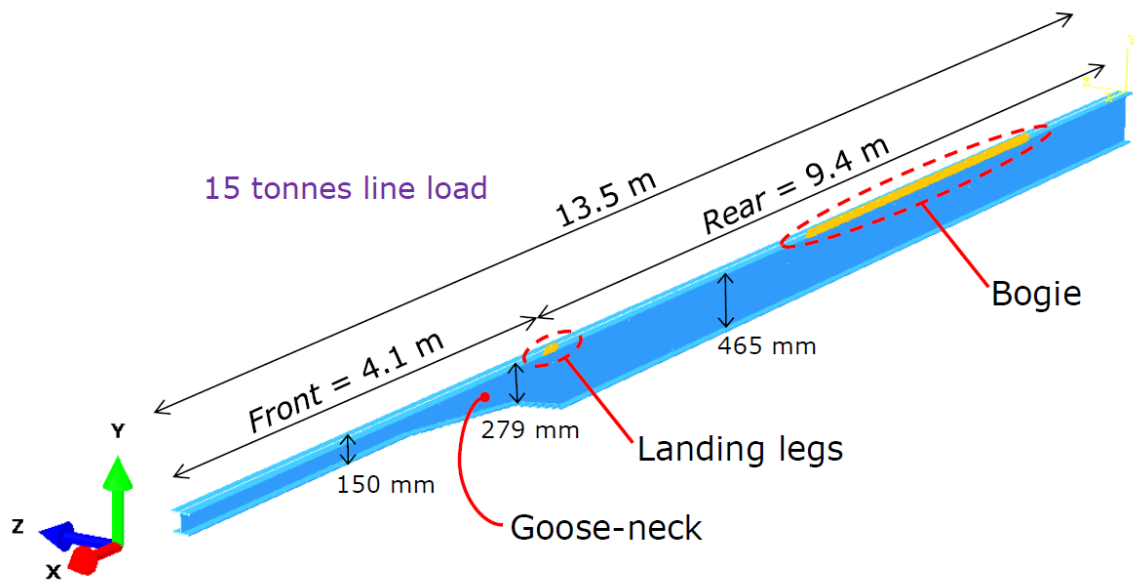


**Fig. 6.8** The geometry, loading and boundary conditions of the parametric FE model of the main longitudinal I-beam developed in Abaqus. The critical heights along the beam at the front, goose-neck and rear are all shown. Note that the x and z directions indicated correspond to the 1 and 2 material directions, respectively.

**Table 6.3** Dimensions of the current typical steel main longitudinal beam and the 5,184 geometry variations analysed with the parametric model in Abaqus.

Beam component	Current dimension (mm)	Modelled dimensions (mm)	Key for Fig. 6.9
Rear flange thickness ( $t_r$ )	10	2.5	Orange
		5	Green
		7.5	Red
		10	Light blue
		12.5	Purple
		15	Dark blue
Front and goose-neck flange thickness ( $t_{fr}$ )	10	2.5	$\triangle$
		5	+
		7.5	$\square$
		10	$\times$
		12.5	$\circ$
		15	$\nabla$
Rear flange width	150 (top)	90, 100, 110, 120	n/a
	130 (bottom)	130, 140, 150, 160 170, 180, 190, 200	
Front and goose-neck flange width	150 (top)	90, 100, 110, 120	n/a
	130 (bottom)	130, 140, 150, 160 170, 180, 190, 200	
Rear web thickness	4	$2/3 \times t_r$	n/a
Front and goose-neck web thickness	6	$2/3 \times t_{fr}$	n/a

**Table 6.4** Critical dimensions of the shape-optimised steel (YS355) I-beam, as shown in Fig. 6.9. The height of the beam at the rear, goose-neck and front sections are defined in Fig. 6.8 and the web thickness was assumed to be two thirds of the flange thickness. Note that the total mass of the current typical 13.5 m steel I-beam is approximately 500 kg.

Model	Rear flange thickness (mm)	Rear flange width (mm)	Front flange thickness (mm)	Front flange width (mm)	Total beam mass (kg)	Weight saving (%)
a	5.0	130	10	180	360	28

beam can reduce longitudinal beam mass by approximately 140 kg (28%), or 280 kg total for the two main longitudinal I-beams combined, while maintaining the desirable level of mechanical performance. The optimised beam has been achieved by reducing the rear flange width and thickness, increasing the front flange width and maintaining the current level of front flange thickness. The results also reiterate that the design of the steel beams for the critical load case is driven by stiffness (displacement at the front and rear of the beam) rather than strength (failure index).

### 6.3.3 Influence of trailer decking on structural properties

The optimisation of the longitudinal I-beams can be expanded to include other materials and combined with a structural decking that removes the need for the transverse members in the conventional ladder-type chassis structure. The resulting structure resembles a stiffened panel as shown in Fig. 6.10. Indeed, such a structure lends itself well to the application of composite materials and could also bring significant aerodynamic improvements. This structure was again modelled in Abaqus to investigate the performance of different materials for use in deck and beams. The different materials and geometries considered for use in the longitudinal I-beams for this scenario are shown in Tables 6.2 and 6.5, respectively. Two decks, differing by an order of magnitude in stiffness, were modelled to illustrate the broad potential of what could be achieved with a structural deck. The I-beam sections were once again modelled with beam elements, while the deck was modelled with a general shell section (with a simplified stiffness matrix  $[D]$ ), that is perfectly connected to the top flanges of the beams. A 30 tonne UDL was applied to the top surface of the deck and the critical load case of the trailer resting on its landing legs and bogie was again examined (Fig. 6.10). The meshing of the model is shown in Fig. 6.11.

The linear elastic response of the deck shell section is governed by Eqn. 6.4, which can be expanded to Eqn. 6.5. The 1, 2 and 3 directions in these equations correspond to the x, z and y directions, respectively, as shown in Fig. 6.10. In these equations, the direct

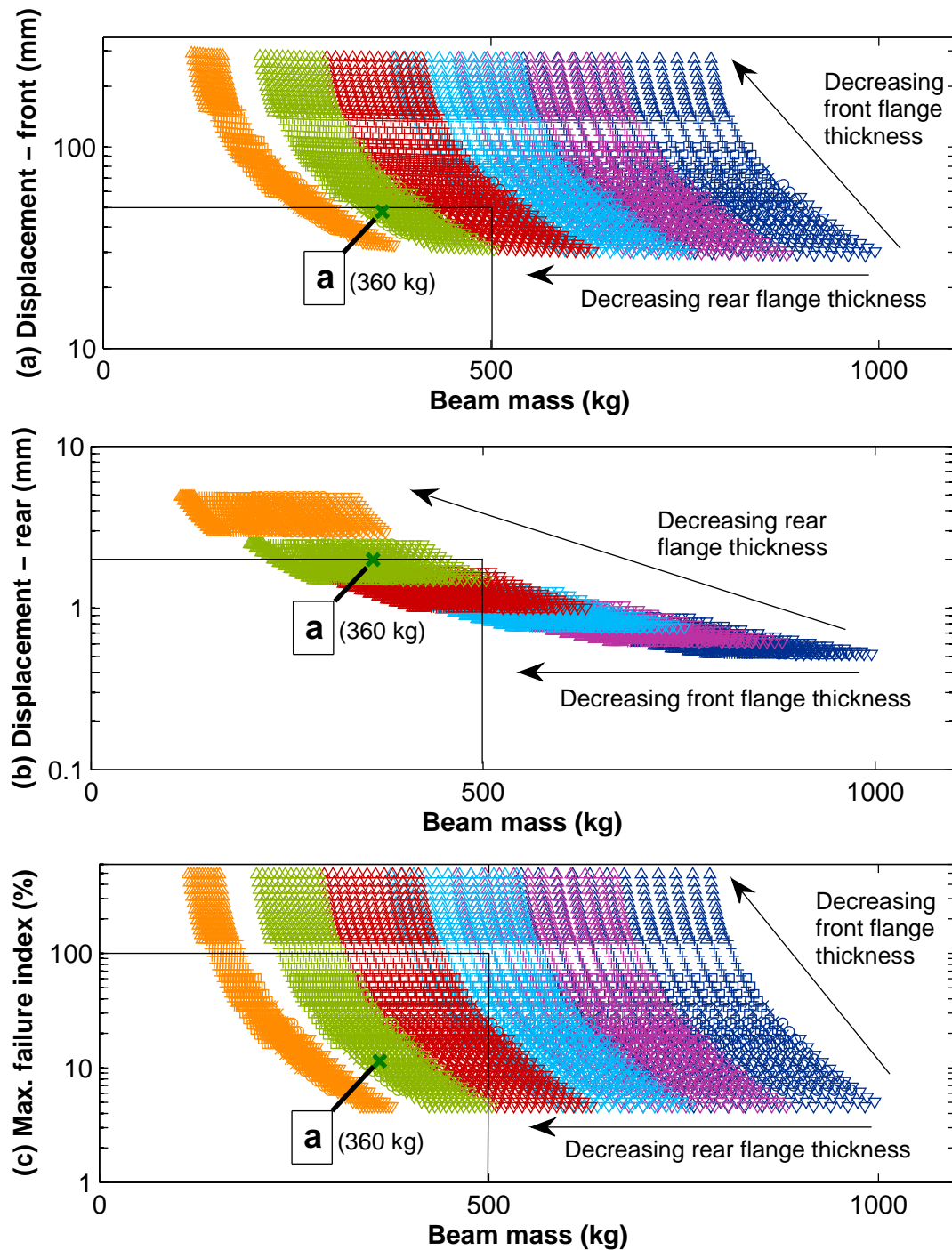


**Fig. 6.9** Displacement of the main longitudinal steel (YS355) I-beam at (a) the front end, (b) the rear end and (c) the maximum failure index (Eqn. 6.3) within the beam, all plotted against beam mass for a 15 tonne uniformly distributed line-load. The design envelope represented by the bottom left quadrant of each graph is established from the mechanical performance of the conventional 500 kg steel I-beam defined in Section 6.2.2. Model ‘a’ is found to be the lightest beam that fits within all three design envelopes. Key for markers in Tables 6.3 and 6.4.

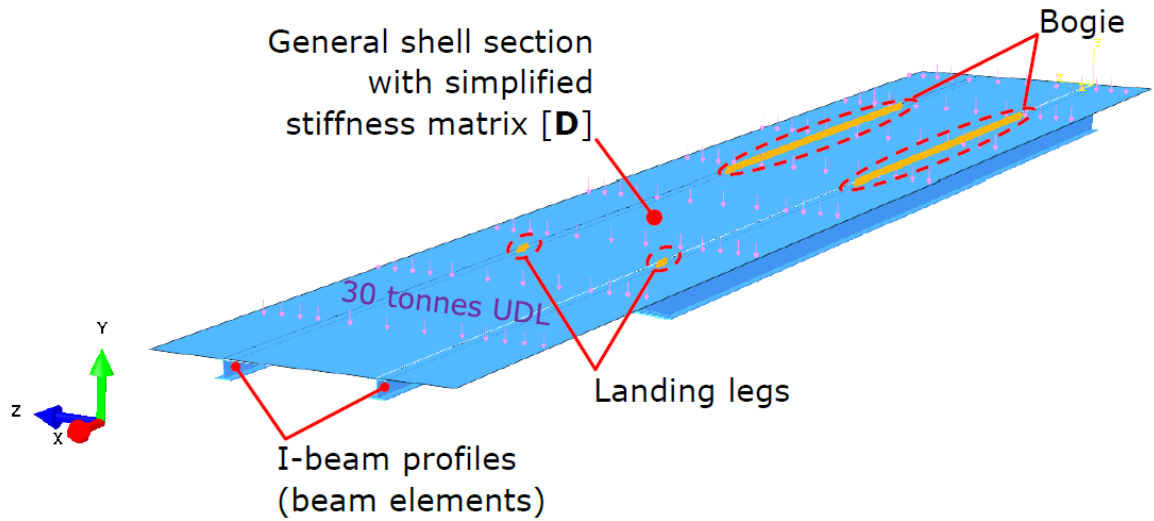


**Fig. 6.10** Parameters of the FE model of the composite trailer. I-beams modelled with beam elements and deck modelled with a general shell section with a simplified stiffness matrix  $[D]$ . A 30 tonne UDL was applied to the top surface of the deck. Note that the  $x$ ,  $z$  and  $y$  directions indicated correspond to the 1, 2 and 3 material directions, respectively.

**Table 6.5** Dimensions of the beams (5,184 geometry variations total) investigated with the two different structural decks of stiffness  $[D]_1$  and  $[D]_2$ . Flange width and thickness remains uniform along the length of the beam.

Beam component	Modelled dimensions (mm)
Flange thickness	5, 10, 15, 20, 25, 30, 35, 40, 45, 50, 55, 60
Flange width	100, 150, 200, 250, 350, 400
Web thickness	$2/3 \times$ flange thickness
Beam height - rear	385, 425, 465
Beam height - front	130, 150
Beam height - goose-neck	279



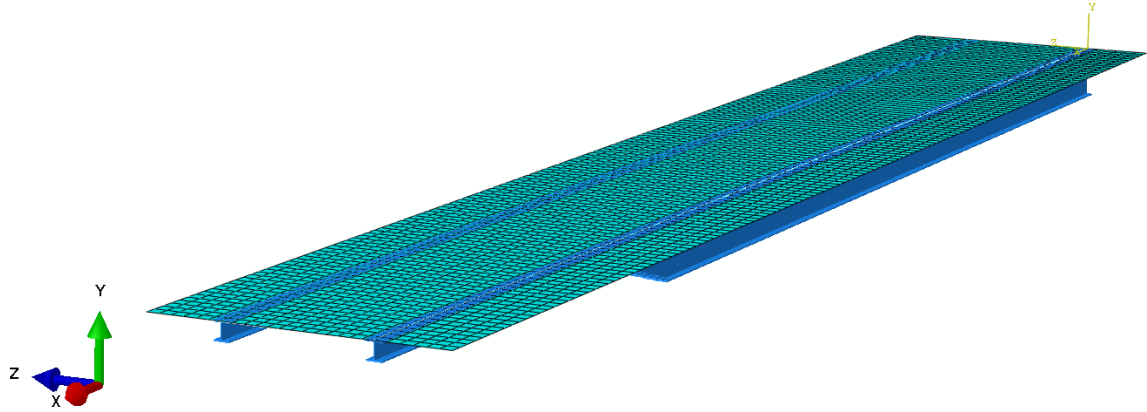


**Fig. 6.11** Meshing of the FE model in Abaqus, with a typical mesh size of 10 cm, corresponding to 135 beam elements per beam and 3,375 shell elements for the decking.

membrane terms come first, then the shear membrane term, then the direct and shear bending terms, with six terms in all. Note that engineering measures of shear membrane strain ( $\gamma_{12}$ ) and twist ( $\kappa_{12}$ ) are used in Abaqus.

$$\{\mathbf{N}\} = [\mathbf{D}] \{\mathbf{E}\} \quad (6.4)$$

where

$\{\mathbf{N}\}$  are the membrane forces per unit length and bending moments per unit length;

$\{\mathbf{E}\}$  are the generalised section strains in the shell, and;

$[\mathbf{D}]$  is the section stiffness matrix.

$$\begin{Bmatrix} N_{11} \\ N_{22} \\ N_{12} \\ M_{11} \\ M_{22} \\ M_{12} \end{Bmatrix} = \begin{bmatrix} D_{11} & D_{12} & D_{13} & D_{14} & D_{15} & D_{16} \\ D_{21} & D_{22} & D_{23} & D_{24} & D_{25} & D_{26} \\ D_{31} & D_{32} & D_{33} & D_{34} & D_{35} & D_{36} \\ D_{41} & D_{42} & D_{43} & D_{44} & D_{45} & D_{46} \\ D_{51} & D_{52} & D_{53} & D_{54} & D_{55} & D_{56} \\ D_{61} & D_{62} & D_{63} & D_{64} & D_{65} & D_{66} \end{bmatrix} \begin{Bmatrix} \varepsilon_{11} \\ \varepsilon_{22} \\ \gamma_{12} \\ \kappa_{11} \\ \kappa_{22} \\ \kappa_{12} \end{Bmatrix} \quad (6.5)$$

The terms of the stiffness matrices for the two different structural decks are defined in Eqns. 6.6 and 6.7. The stiffness matrix  $[\mathbf{D}]_1$  is representative of a pultruded GFRP decking like those discussed in Section 5.2.1. It was assumed the mass of this deck is 440 kg. The stiffness matrix  $[\mathbf{D}]_2$  is representative of quasi-isotropic CFRP-balsa sandwich panel with

5 mm thick face sheets and a 50 mm thick core. The total mass of this deck was calculated to be approximately 910 kg. Note that this deck is an order of magnitude stiffer than the pultruded GFRP decking, and represents an upper limit of stiffness that could be achieved in practical terms using a lightweight structural deck.

$$[\mathbf{D}]_1 : \quad D_{22} = 1.7 \times 10^5 \text{ N/mm}, \quad D_{55} = 3.2 \times 10^7 \text{ Nmm}, \quad D_{11} = D_{33} = D_{44} = D_{66} \approx 0 \quad (6.6)$$

$$[\mathbf{D}]_2 : \quad D_{11} = D_{22} = 1.0 \times 10^6 \text{ N/mm}, \quad D_{44} = D_{55} = 3.0 \times 10^8 \text{ Nmm}, \quad D_{33} = D_{66} \approx 0 \quad (6.7)$$

The results of the modelling procedure for the most critical design constraint, the front end displacement of the beams, are shown in Fig. 6.12. It is evident when comparing Fig. 6.12a and b, that the significantly stiffer decking did not significantly increase the mechanical performance of the structure. This is evident in Fig. 6.12b where the solution clouds have shifted rightward on the graph in comparison to Fig. 6.12a, without having shifted downward enough to include solutions with GFRP based beams, which could bring a substantial cost benefit. This shows that the stiffer decking added a significant amount of weight (approximately 500 kg) to the structure. A CFRP based decking would also be considerably more expensive than a GFRP based decking, reiterating that a lighter, less stiff decking seems to be a more sensible choice. It is also evident from Fig. 6.12 that CFRP beams are the best material choice for lightweight, high performance beams. This is evident through the fact that models with CFRP beams are the most prominent solutions to feature in the light and stiff design envelopes depicted by the boxes in the bottom left quadrants of the graphs. Indeed CFRP composite beams could work well in conjunction with a composite decking, with single shot manufacturing options being a possibility in the future. Composite beams are explored in greater detail in the following section.

### 6.3.4 Optimisation of lightweight composite chassis

Having identified GFRP-based structural decking to be the most advantageous in terms of weight, cost and mechanical performance, additional modelling was performed to examine in more detail composite beam design for use in conjunction with this type of decking. It was also evident from Section 6.3.3 that CFRP beams are the most advantageous in terms of balancing weight reduction and mechanical performance. However, their significantly higher

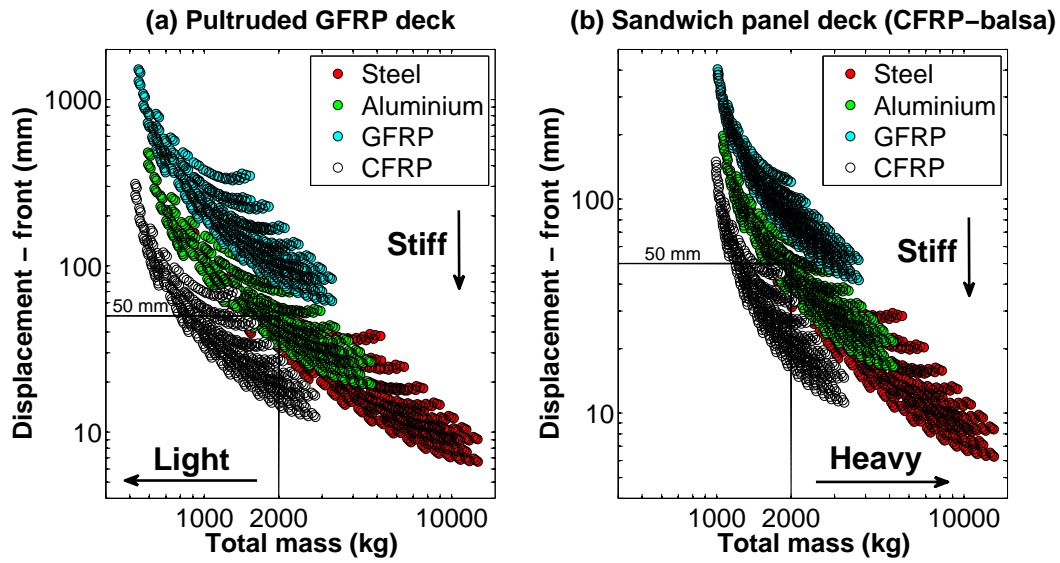


**Fig. 6.12** Displacement of the main longitudinal I-beams (of different materials indicated by different marker colours) at the front end for a 30 tonne UDL, plotted against total chassis mass (combined mass of the beams and decking).

(a) Deck shell stiffness matrix  $[D]_1$ : Pultruded GFRP decking (440 kg).

(b) Deck shell stiffness matrix  $[D]_2$ : CFRP-balsa sandwich panel decking (910 kg).

Note that the total mass of the corresponding current typical steel chassis and hardwood decking is approximately 2,000 kg.

raw material cost needs to be taken into consideration. To this end, additional hypothetical Glass-Carbon beams were modelled, whereby the rear of the beam (as defined in Fig. 6.8) is modelled as GFRP, while the front end of the beam was modelled as CFRP. This strategy was used to reduce weight while keeping raw material cost increase to a minimum, and maintaining mechanical performance. This kind of mixed Glass-Carbon structure could be difficult and costly to achieve with current composite manufacturing technologies, however it may become more feasible with future advancements.

The geometries considered for use in the I-longitudinal beams in this modelling are shown in Table 6.6, while the beam material properties are defined in Table 6.2. The chassis was modelled in the same fashion as in Section 6.3.3 and the deck is defined by the shell stiffness matrix  $[D]_1$ , which was assumed to have a mass of 440 kg.

The results of the modelling and optimisation of the composite chassis are presented in Figs. 6.13 and Table 6.7, respectively. The current stiffness requirements (assumed to be 50 mm and 2 mm of deflection at the front and rear end, respectively) are plotted as horizontal lines in Fig. 6.13a and b. It is evident in Fig. 6.13 that the shape-optimised CFRP beams combined with GFRP decking (model A) could reduce the overall chassis mass by approximately 60% (1207 kg), while meeting the current design constraints for

**Table 6.6** Dimensions of the lightweight composite beams (5,184 total geometry variations) modelled in conjunction with the structural decking defined by the simplified stiffness matrix  $[\mathbf{D}]_1$ .

Beam component	Modelled dimensions (mm)	Key for Fig. 6.14
Rear flange thickness ( $t_r$ )	2.5	Orange
	5	Green
	7.5	Red
	10	Light blue
	12.5	Purple
	15	Dark blue
Front and goose-neck flange thickness ( $t_{fr}$ )	5	$\triangle$
	10	+
	15	$\square$
	20	$\times$
	25	$\circ$
	30	$\nabla$
Rear flange width	150, 250, 350, 450	n/a
	550, 650, 750, 850, 950	
	1050, 1150, 1250	
Front and goose-neck flange width	150, 250, 350, 450	n/a
	550, 650, 750, 850, 950	
	1050, 1150, 1250	
Rear web thickness	$2/3 \times t_r$	n/a
Front and goose-neck web thickness	$2/3 \times t_{fr}$	n/a

**Table 6.7** Critical dimensions of selected composite beams. The height of the beam at the rear, goose-neck and front section are defined in Fig. 6.8 and the web thickness was assumed to be two thirds of the flange thickness. Note that total mass includes 440 kg for decking which could be achieved through either a GFRP pultrusion or sandwich panel.

Model	Rear flange thickness (mm)	Rear flange width (mm)	Front flange thickness (mm)	Front flange width (mm)	Total approx. mass (kg)	Weight saving (%)
A	7.5	450	5.0	650	793	60
A1	7.5	150	5.0	750	674	66
B	12.5	1150	5.0	650	1630	19
B1	7.5	850	5.0	850	1060	47

stiffness and strength. On the other hand, at the current conventional design constraints, the shape-optimised Glass-Carbon beams with GFRP decking (model B) could only reduce overall chassis mass by approximately 19% (370 kg) and would have significantly larger dimensions, as shown in Table 6.7. However, assuming that the maximum allowable rear end displacement could be relaxed from 2 mm to 4 mm (as shown in Fig. 6.13b), shape-optimised Glass-Carbon beams (model B1) become significantly more attractive, as their weight saving potential rises from 19% to 47% (940 kg). By restricting the use of CFRP to the front end only, the overall raw material cost associated with the chassis becomes significantly lower than in the case when CFRP is used in the entire beam (Fig. 6.13d). The largest weight reduction potential was observed in the chassis with shape-optimised CFRP beams with an allowable rear displacement of 4 mm (model A1), as shown in Fig. 6.13. In this case, weight is reduced by approximately 66% (1326 kg).

Trends for beam displacement with beam geometry exist in the same fashion for composite beams (Fig. 6.14), as they did for steel beams (Fig. 6.9). In particular, decreasing the rear flange thickness significantly reduces the total chassis mass.

## 6.4 Conclusions

The current conventional 13.5 m steel ladder-type trailer chassis has been refined over time through experience, rather than empirical data. There are undoubtedly improvements that could be made to the existing structure through a greater understanding of in-service loadings and hence this is the focus of other current research. A better understanding of in-service loadings could be combined well with the FE modelling and steel beam optimisation procedures introduced here to reduce chassis weight even further. It is clear that steel beam

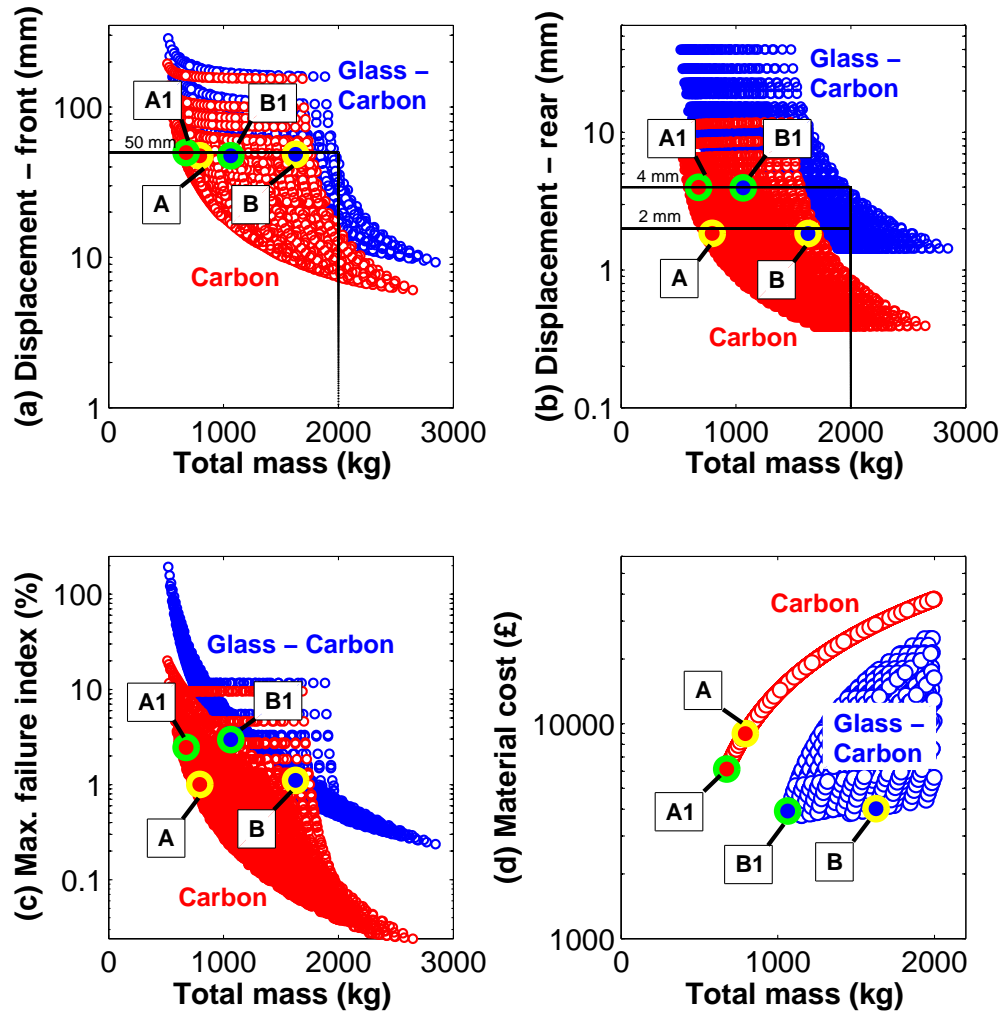


**Fig. 6.13** Performance plots of the composites chassis modelled in Abaqus with a 30 tonne UDL applied to the top surface of the decking. (a) Displacement of the main longitudinal beam at the front end. (b) Displacement of the main longitudinal beam at the rear end. (c) Maximum failure index within the beam. (d) Total raw material cost.

Note that all models assume a deck defined by the shell stiffness matrix  $[D]_1$ : pultruded GFRP decking (440 kg). Red markers indicate CFRP beams and blue markers indicate GFRP at the rear of beam and CFRP at the front end of the beam, as defined in Fig. 6.8. Details of models A, A1, B, and B1 are provided in Table 6.7. Current allowable displacement at the rear of the beam is 2 mm, this could potentially be relaxed to 4 mm to further increase weight savings. The total mass of the corresponding current typical steel chassis and hardwood decking is approximately 2,000 kg.

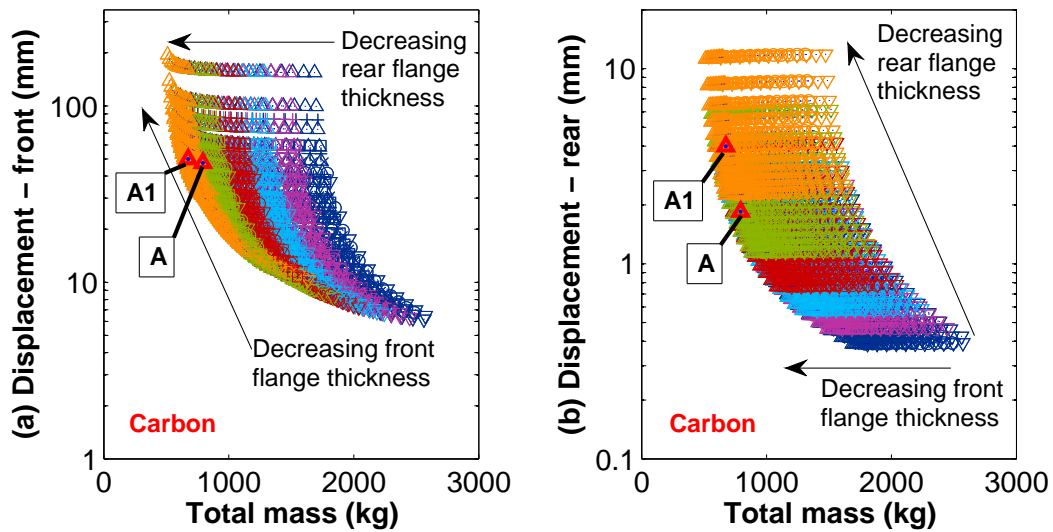


**Fig. 6.14** Trends in performance plots (Fig. 6.13) for the composite chassis with CFRP I-beams modelled in Abaqus. (a) Displacement of the main longitudinal beam at the front end. (b) Displacement of the main longitudinal beam at the rear end. Key see Tables 6.6 and 6.7.

optimisation is a logical first step to chassis weight reduction, as it could be relatively easily implemented by trailer manufacturers and could reduce chassis weight by a total of 280 kg.

More significant weight reductions are more likely to be realised through a wholly composite chassis. While the stiffened panel composite trailer structures presented could be difficult and costly to produce with current composite manufacturing technologies, it may become increasingly feasible with advancements in processing techniques such as pultruding. A composite chassis comprised of CFRP beams and a pultruded GFRP deck could reduce overall trailer weight by up to 1326 kg (67%). However, the high material costs associated with CFRP could dictate that a more desirable approach could be to use CFRP in the front end of the beams and GFRP in the rear end of the beams. FE modelling and optimisation has shown that this structure would reduce trailer weight by approximately 940 kg (47%). It is also clear that reducing the maximum allowable rear end displacement from 2 mm to 4 mm would allow for the most significant levels of weight reduction to be realised.

# Chapter 7

## Conclusions and Future Work

### 7.1 Conclusions

#### 7.1.1 Review of the state-of-the-art

While previous composite trailer projects have failed to gain any significant market acceptance, composites are poised to be used to good effect in the design of road freight trailers. Lessons can be learnt from the success of composites in bridges, which often have a similar structure as road freight trailers. In terms of market acceptance, lightweighting via the subcomponent replacement approach could be considered to be the most prudent first step, as this requires less financial investment in comparison to trailers designed entirely from composites.

#### 7.1.2 Energy consumption and fleet logistics

Lightweighting through the application of composites in trailers used in mass-limited operations can bring significant fuel and energy consumption savings, leading to a reduction in both operation costs and carbon footprint. By considering the mass energy performance index and applying a structured methodology, trailers that will benefit the most from weight reduction can be identified systematically, allowing for lightweighting strategies to be implemented more effectively. Double-deck trailers used in grocery distribution and ‘walking-floor’ trailers used in bulk haulage are both prime examples of HGVs that are suited to lightweighting with composites, as they both typically operate close to their maximum legal weight limit. Drive cycle analysis has shown that reducing the empty weight of these trailers by 30% can cause reductions of up to 18% and 11% in mass energy performance index for double-deck trailers and ‘walking-floor’ trailers, respectively.



### 7.1.3 Lightweight composite subcomponents

Applying composites to trailer subcomponents such as side walls and decking is a logical way to begin the lightweighting process and can be implemented in a short time frame for a modest increase in cost. Replacing plywood panels used in the side-walls of double-deck trailers with readily available polypropylene honeycomb sandwich panels would save approximately 1,000 kg of weight.

#### Trailer decking

Following side walls, Finnish birch plywood decking typically used on many road freight trailers is the next most prudent subcomponent to examine for lightweighting, especially considering there are no existing commercial lightweight deck solutions. Benchmarking the mechanical performance of conventional birch plywood decking is an important first step to developing a competitive lightweight replacement decking. By examining the effects of common types of in-service damage to trailer decking, a stronger case for the application of composite decking can be built. This approach can also provide a practical insight into whether damaged hardwood road freight trailer decking can still withstand in-service loadings. Indentation damage and moisture damage can both have a significant impact on the residual flexural stiffness and strength of birch plywood. While indentation damage can often appear more severe during a visual inspection, it generally has a lesser effect on flexural stiffness and strength compared to moisture damage. On the other hand, composite decking is less susceptible to these forms of service damage and can also have more tailorable mechanical properties.

Sandwich panels and pultrusions are both strong candidates for lightweight deck materials. A sandwich panel with woven GFRP face sheets and an end-grain balsa core is approximately 30% lighter than conventional birch plywood trailer decking. This weight saving corresponds to approximately 165 kg in a standard 13.6 m long trailer. Three point bend testing has shown that these sandwich panels have superior flexural strength and comparable flexural stiffness to birch plywood. Large panel testing confirmed that these panels can withstand roughly four times the forklift wheel load likely to be seen in-service. On the other hand, pultruded GFRP decking offers less weight saving benefit and would only bring a 100 kg weight reduction. However, the mechanical properties, durability and the relatively low cost of the pultrusion process indicate that pultruded decking or transverse members could be the logical first step for using structural composites in trailers.

### 7.1.4 Lightweight composite chassis

A more thorough understanding of trailer in-service loadings will be beneficial to reduce trailer chassis weight. The experience-driven approach to chassis design currently employed by the trailer manufacturing industry is not able to realise the full extent of potential weight savings. However, FE modelling and optimisation can still be implemented to show that significantly lighter steel I-beams could maintain the current desired level of mechanical performance.

It is evident that a ‘clean-slate’ redesign of the conventional ladder-type HGV trailer chassis structure will take a significant amount of time and money to implement in industry. However, it remains the best way to achieve the most significant levels of weight reduction. Optimisation of shape and material selection in chassis design through parametric modelling and FE analysis allows for many different structural configurations to be assessed in terms of both mechanical performance and material cost. This analysis has indicated that up to approximately 1,300 kg (66%) of weight could be saved through a composite re-design of the chassis, using CFRP beams and a pultruded GFRP deck. However, the high material costs associated with CFRP could dictate that a more desirable approach could be to use CFRP in the front end of the beams only and GFRP in the rear end of the beams where stiffness is less critical. FE modelling has shown that mixed GFRP and CFRP beams would reduce trailer weight by approximately 940 kg (47%). As in the case of composite subcomponent design, low-cost materials and manufacturing techniques such as pultrusion processing need to be targeted to ensure cost competitiveness against existing materials. Indeed, material and processing costs can be integrated into the optimisation procedure.

It is clear that lightweight composite trailers will have an increasingly important role in reducing the emissions of the road freight industry.

## 7.2 Future work

While this research has addressed a variety of issues regarding trailer lightweighting, there is still scope for further investigation in the following areas.

The economics of trailer lightweighting was briefly assessed in Section 2.4.3. However, considering that the success of a lightweight composite trailer largely hinges on its economic viability, it would be desirable to undertake a more detailed cost study. Such a study could investigate in detail production and life cycle costs of composite trailers and survey the market to better understand the investment they are willing to make in lightweight trailers. A comprehensive examination of the economic benefit of lightweight fuel tankers for use in the UK would also be of interest.

Joining of composite subcomponents to existing steel chassis beams is another important topic that could be explored in more detail. While this is briefly discussed in Sections 4.5 and 5.3.2, it will be a critical step in the initial uptake of composites in trailers. Without expert consultation, issues are likely to arise since current typical trailer manufacturers do not have significant experience with joining composites. To this end, a potential study could involve testing a range of established composites joining methods by adding composite sections to trailers already in-service and monitoring their performance with time. This would help characterise the most appropriate joining methods and their fatigue performance in this particular application.

Furthermore, a thorough understanding of in-service trailer loadings is crucial for developing lightweight trailers that meet load requirements without being unnecessarily stiff and strong in certain areas. While this is the focus of the FORWARD project mentioned in Section 6.2.1, it is clear that more research could be done in this area, particularly with a focus on the loading requirements specific to the UK. More accurate knowledge of load requirements can be used in conjunction with finite element modelling, allowing for composite solutions to be optimised further, which would in turn provide more scope for weight reduction.

Detailed design and design for manufacture of advanced lightweighting concepts to integrate into the broad solution presented in Chapter 6 is another logical next step for research. For example, corrugated structures and isogrids described in Section 1.2.3 would be good candidates for a detailed analysis in terms of optimising dimensions, materials and manufacturing routes. Prototypes of these structures could be built and tested in the laboratory, before fitting a demonstrator component to a trailer for full proof of concept. The fact that more throughput production routes for composites processing are being developed for other industries (e.g. aerospace) is encouraging, as some of these may be viable for use in the HGV trailer manufacturing industry in the not too distant future.

# References

- [1] J. Verhaeghe, "Introducing an affordable composite trailer to a conservative market - reinforced plastics," 2006. [Online]. Available: <http://www.reinforcedplastics.com/view/4722/introducing-an-affordable-composite-trailer-to-a-conservative-market/>
- [2] M. Turner and G. Boyce, "ROADLITE - Manufacture of a lightweight, cost effective, polymer composite road trailer," in *JSAE Annual Congress*, 2005.
- [3] EPL Composite Solutions, "Development of lightweight, recyclable thermoplastic composite semi-trailer and boat hulls with enhanced performance. Publishable final activity report D27 – final project report." EPL Composite Solutions, Tech. Rep., 2010. [Online]. Available: [http://www.transport-research.info/Upload/Documents/201203/20120314\\_134605\\_69722\\_PublishableFinalActivityReport.pdf](http://www.transport-research.info/Upload/Documents/201203/20120314_134605_69722_PublishableFinalActivityReport.pdf)
- [4] B. Jarvis, "A composite glimpse of the future," pp. 53–54, 2006. [Online]. Available: <http://archive.commercialmotor.com/article/12th-october-2006/52/a-composite-glimpse-of-the-future>
- [5] Trucknews.com, "Wal-Mart WAVES hello to concept truck and trailer." [Online]. Available: <http://www.trucknews.com/products/wal-mart-waves-hello-to-concept-truck>
- [6] R. Kaiser, "Thermosets and thermoplastics set to compete for composite trailer market," *Plastics News Europe*, pp. 14–15, Dec. 2010.
- [7] Lightweight Structures BV, "Lightweight GIGA trailer." [Online]. Available: <http://www.lightweight-structures.com/lightweight-giga-trailer/index.html>
- [8] Evolution Tankers, "Setting the benchmark for chemical transport tankers." [Online]. Available: <http://www.evolutiontankers.com.au/>
- [9] "Spitzer-Eurovrac." [Online]. Available: <http://buzzybeeforum.nl/viewtopic.php?f=124&t=36951>
- [10] Composittransport, "Fiby products." [Online]. Available: <http://www.composittransport.com/?cat=25&lang=en>
- [11] JEC Group, "Composite flooring makes for versatile trailers." [Online]. Available: <http://www.jeccomposites.com/news/composites-news/composite-flooring-makes-versatile-trailers>
- [12] S. Shoukry, G. William, J. Prucz, and T. Evans, "Application of composite sandwich panels in heavy vehicle systems," in *18th International Conference on Composites or Nano Engineering*, Anchorage, Alaska, 2010, pp. 363–364.

- [13] CompositesWorld, “Carbon fiber/ epoxy wheels developed to replace metal wheels on large freight trailers.” [Online]. Available: <http://www.compositesworld.com/articles/carbon-fiberepoxy-wheels-developed-to-replace-metal-wheels-on-large-freight-trailers>
- [14] Gurit, “Wrightbus, new bus for London,” 2008. [Online]. Available: <http://www.gurit.com/files/documents/wrightbuscspdf.pdf>
- [15] Chicagobus.org, “7800-series NABI 45C-LFW- Chicago CTA Bus Photos.” [Online]. Available: <http://chicagobus.org/buses/7800/photos>
- [16] U. K. Vaidya, “Design and manufacture of woven reinforced glass/ polypropylene composites for mass transit floor structure,” *J. Compos. Mater.*, vol. 38, no. 21, pp. 1949–1972, 2004.
- [17] P. B. Potyrała, J. Ramón, and C. Rius, “Use of fibre reinforced polymer composites in bridge construction. State of the art in hybrid and all-composite structures.” Universitat Politècnica de Catalunya, Barcelona, Tech. Rep., 2011.
- [18] NetComposites, “Conference proceedings,” in *2nd International Conference on the Use of Fibre-Reinforced Polymer Composites in Bridge Design*. London, UK: NetComposites, Jan. 2014.
- [19] “Isogrid Composites Canada Inc.” [Online]. Available: <http://www.isogridinc.com/>
- [20] A. Mckinnon, *Green logistics: improving the environmental sustainability of logistics*, 1st ed. London: Kogan Page, 2010.
- [21] K. Glaeser, “Performance of articulated vehicles and road trains regarding road damage and load capacity,” in *11th International Symposium on Heavy Vehicle Transportation Technology*, Melbourne, Australia, 2010.
- [22] A. Odhams, R. Roebuck, Y. Lee, S. Hunt, and D. Cebon, “Factors influencing the energy consumption of road freight transport,” *Proc. Inst. Mech. Eng. Part C-Journal Mech. Eng. Sci.*, vol. 224, no. 9, pp. 1995–2010, 2010.
- [23] S. Mahdi, “MSc Composites lecture: design of composites,” 2013.
- [24] UPM-Kymmene, “WISA-Trans.” [Online]. Available: [http://www.wisaplywood.com/en/downloads/brochures/transport/Documents/WISA-Trans\\_EN\\_fs.pdf](http://www.wisaplywood.com/en/downloads/brochures/transport/Documents/WISA-Trans_EN_fs.pdf)
- [25] D. Zenkert, *An introduction to sandwich construction*, 1st ed. London: Emas Publishing, 1997.
- [26] Granta Design Limited, “CES EduPack,” 2013.
- [27] “Thermosetting composites- processing.” [Online]. Available: <http://www.azom.com/article.aspx?ArticleID=352>
- [28] “Strongwell.” [Online]. Available: <http://www.strongwell.com/>
- [29] Fiberline, “The Fiberline design manual,” 2003. [Online]. Available: [http://fiberline.com/sites/default/files/media/online-tools/190107\\_dm\\_uk.pdf](http://fiberline.com/sites/default/files/media/online-tools/190107_dm_uk.pdf)

- [30] Unicomposite Technology CO., LTD., “Fiberglass decking system- pultruded hollow/open deck panel,” 2016. [Online]. Available: <http://www.unicomposite.com/products/standard-profile/fiberglass-decking-system.html?mydxsbmfkbcclgttm>
- [31] C. Aceves, M. Sutcliffe, M. Ashby, A. Skordos, and C. Rodríguez Román, “Design methodology for composite structures: A small low air-speed wind turbine blade case study,” *Mater. Des.*, vol. 36, pp. 296–305, 2012.
- [32] M. Ashby, *Material selection in mechanical design*, 3rd ed. Oxford: Elsevier, 2005.
- [33] H. Timm, “Automotive CFRP Composites – a new challenge in the competition of Automotive Lightweight Technologies,” in *SAMPE European Summit*, Paris, 2016.
- [34] 3A Composites, “Airex, Baltek, Banova- 3AComposites Core Materials.” [Online]. Available: <http://www.3acorematerials.com/>
- [35] J. Pauwelussen, J. Visscher, M. Merts, and K. Kural, “An integrated testing and model based design approach for semi-trailer weight reduction,” in *11th International Symposium on Heavy Vehicle Transportation Technology*, 2011.
- [36] A. Mckinnon, “Life without trucks: the Impact of a Temporary Disruption of Road Freight Transport on a National Economy,” *J. Bus. Logist.*, vol. 27, no. 2, pp. 227–251, 2006.
- [37] Department for Transport, “Transport statistics Great Britain,” 2012. [Online]. Available: <https://www.gov.uk/government/collections/transport-statistics-great-britain>
- [38] VersaPlast, “VersaPlast/ Panelite – innovative product launch at the CV show,” 2012. [Online]. Available: <http://www.commercialmotor.com/transport-news-brief/payload-is-king>
- [39] “Wabash Composites.” [Online]. Available: <http://www.wabashcomposites.com/products/duraplate-composite-panels/duraplate-sup-reg-sup-panels>
- [40] “Normanton Laminating Services Ltd.” [Online]. Available: <http://www.normanton.co.uk/>
- [41] “Acrosoma.” [Online]. Available: <http://www.acrosoma.com/>
- [42] A. Bentfeld, “Tomorrow’s trailer running gear system,” 2012. [Online]. Available: <http://www.bpw.de/en/media/press/press-archive/eintrag/single/86.html>
- [43] “Freight Wing.” [Online]. Available: <http://www.freightwing.com/>
- [44] ATDynamics, “Fuel-saving ATDynamics trailer tails now an option on Wabash National Trailers.” [Online]. Available: [http://www.atdynamics.com/wabash\\_trailertail.htm](http://www.atdynamics.com/wabash_trailertail.htm)
- [45] L. McIntire, “UPS lightens up- 150 new plastic trucks to save 40% fuel,” 2012. [Online]. Available: <http://blog.ups.com/2012/06/26/ups-lightens-up-150-new-plastic-trucks-to-save-40-fuel-infographic/>

- [46] K. Gleich and J. Te, "Component report for composite bus floor," Birmingham, AL, 2003.
- [47] J. Léonardi and M. Baumgartner, "CO<sub>2</sub> efficiency in road freight transportation: Status quo, measures and potential," *Transp. Res. Part D Transp. Environ.*, vol. 9, no. 6, pp. 451–464, 2004.
- [48] W. Lai, "The effects of eco-driving motivation, knowledge and reward intervention on fuel efficiency," *Transp. Res. Part D Transp. Environ.*, vol. 34, pp. 155–160, 2015.
- [49] C. Yang, D. McCollum, R. McCarthy, and W. Leighty, "Meeting an 80% reduction in greenhouse gas emissions from transportation by 2050: A case study in California," *Transp. Res. Part D Transp. Environ.*, vol. 14, no. 3, pp. 147–156, 2009.
- [50] T. Laclair, "Large scale duty cycle (LSDC) project: tractive energy analysis methodology and results from long-haul truck drive cycle evaluations," Oak Ridge National Laboratory, Tech. Rep. May, 2011. [Online]. Available: <http://info.ornl.gov/sites/publications/files/Pub33189.pdf>
- [51] Department for Transport, "Road freight: domestic and international statistics," 2012. [Online]. Available: [https://www.gov.uk/government/collections/road-freight-domestic-and-international-statistics#group\\_97](https://www.gov.uk/government/collections/road-freight-domestic-and-international-statistics#group_97)
- [52] M. Piecyk and A. McKinnon, "Forecasting the carbon footprint of road freight transport in 2020," *Int. J. Prod. Econ.*, vol. 128, no. 1, pp. 31–42, 2010.
- [53] United Nations, "European agreement concerning the international carriage of dangerous goods by road," 2010. [Online]. Available: <http://www.unece.org/trans/danger/publi/adr/adr2011/11ContentsE.html>
- [54] B. Jujnovich, R. Roebuck, and D. Cebon, "Implementation of active rear steering for a tractor semi-trailer," in *10th Int. Symp. Heavy Veh. Transp. Technol.*, Paris, 2008.
- [55] National Transport Commission, "Australian code for the transport of dangerous goods by road and rail 7th Edition," Melbourne, 2011. [Online]. Available: [www.ntc.gov.au](http://www.ntc.gov.au)
- [56] M. Bysh and I. Dorn, "The generation of internal pressure in tanker rollover (HSE contract research report)," Frazer-Nash Consultancy Ltd, Surrey, Tech. Rep., 1996.
- [57] J. Lu, M. Chorney, and L. Peterson, "Sustainable trailer flooring," *BioResources*, vol. 4, no. 2, pp. 835–849, 2009.
- [58] W. Lewis, "Simulated service testing of wood and wood-base finish flooring," Forest Products Laboratory, Forest Service, U.S. Department of Agriculture, Madison, WI, Tech. Rep., 1971.
- [59] ASTM International, "ASTM D2394-05: Standard methods for simulated service testing of wood and wood-base finish flooring," Philadelphia, PA, 2011.
- [60] H. Heräjärvi, "Static bending properties of Finnish birch wood," *Wood Sci. Technol.*, vol. 37, no. 6, pp. 523–530, 2004.

- [61] UPM-Kymmene, "Handbook of finnish plywood," 2007.
- [62] I. Swaczyna, A. Kedzierski, A. Tomusiak, A. Cichy, and A. Rozanska, "Hardness and wear resistance tests of the wood species most frequently used in flooring panels," *For. Wood Technol.*, vol. 87, no. 76, pp. 82–87, 2011.
- [63] S. Karshenas and J. Feely, "Structural properties of used plywood," *Constr. Build. Mater.*, vol. 10, no. 8, pp. 553–563, 1996.
- [64] S. Knapic, J. MacHado, and H. Pereira, "Properties of cork oak wood related to solid wood flooring performance," *Constr. Build. Mater.*, vol. 30, pp. 569–573, 2012.
- [65] P. Stewart, "Latest innovations in formwork plywood panels," *Concr.*, vol. 39, no. May, pp. 22–24, 2005.
- [66] International Organization for Standardization, "ISO 1496-1: Series 1 freight containers - specification and testing - part 1, general cargo containers," Washington DC, 1990.
- [67] J. Bodig and B. A. Jayne, *Mechanics of wood and wood composites*. Van Nostrand Reinhold, 1982.
- [68] J. Crank, *The mathematics of diffusion*, 2nd ed. Oxford: Clarendon Press, 1975.
- [69] T. Gereke and P. Niemz, "A numerical study on the influence of the bond-line diffusivity on moisture-related stresses and deformations of three-layered spruce cross-laminates," *Wood Mater. Sci. Eng.*, vol. 5, no. 2, pp. 62–66, 2010.
- [70] J. Vinson, *Advanced composite materials: environmental effects*. American Society for Testing and Materials, 1977.
- [71] E. Weppelmann, J. Field, and M. Swain, "Observation, analysis, and simulation of the hysteresis of silicon using ultra-micro-indentation with spherical indenters," *J. Mater. Res.*, vol. 8, no. 04, pp. 830–840, 1993.
- [72] J. Field and M. Swain, "A simple predictive model for spherical indentation," *J. Mater. Res.*, vol. 8, no. 02, pp. 297–306, 1993.
- [73] W. Youngquist and B. Munthe, "The abrasive resistance of wood as determined with the U.S. Navy wear-test machine," 1948.
- [74] I. Hutchings, *Tribology: friction and wear of engineering materials*. Cambridge, UK: Edward Arnold, 1992.
- [75] J. Ruponen, L. Rautkari, T. Belt, and M. Hughes, "Factors influencing properties of parallel laminated binderless bonded plywood manufactured from rotary cut birch (*Betula pendula*)," *Int. Wood Prod. J.*, vol. 5, no. 1, pp. 11–17, 2014.
- [76] L. Cai, "Determination of diffusion coefficients for sub-alpine fir," *Wood Sci. Technol.*, vol. 39, no. 2, pp. 153–162, 2005.
- [77] J. Y. Liu and W. T. Simpson, "Two-stage moisture diffusion in wood with constant transport coefficients," *Dry. Technol.*, vol. 17, no. 1-2, pp. 258–267, 1999.



- [78] M. Sutcliffe, C. Monroy Aceves, W. Stronge, R. Choudhry, and A. Scott, "Moderate speed impact damage to 2D-braided glass-carbon composites," *Compos. Struct.*, vol. 94, no. 5, pp. 1781–1792, 2012.
- [79] H. Heräjärvi, "Variation of basic density and Brinell hardness within mature Finnish *Betula Pendula* and *B. Pubescens* stems," *Wood Fiber Sci.*, vol. 36, no. 2, pp. 216–227, 2004.
- [80] O. Murthy, "Strength and stiffness optimization studies on honeycomb core sandwich panels," *J. Reinf. Plast. Compos.*, vol. 25, no. 6, pp. 663–671, 2005.
- [81] V. Ugale, K. Singh, N. Mishra, and P. Kumar, "Experimental studies on thin sandwich panels under impact and static loading," *J. Reinf. Plast. Compos.*, vol. 32, pp. 420–434, 2012.
- [82] D. F. Caballero, V. R. de la Cruz, J. M. Munoz-Guijosa, and S. Nair, "Ends of sandwich beams subjected to pure bending. Analysis and design," *J. Sandw. Struct. Mater.*, vol. 15, no. 5, pp. 509–522, 2013.
- [83] D. K. Hsu, "Nondestructive evaluation of sandwich structures: a review of some inspection techniques," *J. Sandw. Struct. Mater.*, vol. 11, no. 4, pp. 275–291, 2009.
- [84] O. T. Thomsen, "Sandwich materials for wind turbine blades - present and future," *J. Sandw. Struct. Mater.*, vol. 11, no. 1, pp. 7–26, 2009.
- [85] L. Wang, W. Liu, H. Fang, and L. Wan, "Behavior of sandwich wall panels with GFRP face sheets and a foam-GFRP web core loaded under four-point bending," *J. Compos. Mater.*, vol. 49, no. 22, pp. 2765–2778, 2015.
- [86] U. Vaiday, *Composites for automotive, truck and mass transit: materials, design, manufacturing*. Lancaster, US: DEStech Publications, 2011.
- [87] M. Ashby, T. Evans, N. Fleck, J. Hutchinson, H. Wadley, and L. Gibson, *Metal foams: a design guide*, 1st ed. Burlington: Elsevier Science, 2000.
- [88] C. Steeves and N. Fleck, "Material selection in sandwich beam construction," *Scr. Mater.*, vol. 50, no. 10, pp. 1335–1339, 2004.
- [89] K. Easterling, R. Harrysson, L. Gibson, and M. Ashby, "On the mechanics of balsa and other woods," *Proc. R. Soc. A Math. Phys. Eng. Sci.*, vol. 383, no. 1784, pp. 31–41, 1982.
- [90] M. Borrega and L. J. Gibson, "Mechanics of balsa (*Ochroma pyramidale*) wood," *Mech. Mater.*, vol. 84, pp. 75–90, 2015.
- [91] M. Osei-Antwi, J. De Castro, A. P. Vassilopoulos, and T. Keller, "Shear mechanical characterization of balsa wood as core material of composite sandwich panels," *Constr. Build. Mater.*, vol. 41, pp. 231–238, 2013.
- [92] V. Legrand, L. TranVan, F. Jacquemin, and P. Casari, "Moisture-uptake induced internal stresses in balsa core sandwich composite plate: modeling and experimental," *Compos. Struct.*, vol. 119, pp. 355–364, 2015.

- [93] B. Noonan, "Adhesives for trailer assembly," pp. 38–41, 2009. [Online]. Available: <http://www.assemblymag.com/articles/86655-adhesives-for-trailer-assembly>
- [94] British Standards Institution, "BS 2782:1970 Methods of testing plastics," 1970.
- [95] ASTM International, "ASTM D3171-11: Standard Test Methods for Constituent Content of Composite Materials," Philadelphia, PA, 2014.
- [96] J. Correia and S. Cabral-Fonseca, "Durability of glass fibre reinforced polyester (GFRP) pultruded profiles used in civil engineering applications," *Third International Conference on Composites in Construction*, pp. 1–9, 2005.
- [97] I. Nishizaki and S. Meiarashi, "Long-term deterioration of GFRP in water and moist environment," *J. Compos. Constr.*, vol. 6, no. February, pp. 21–27, 2002.
- [98] A. Apicella, C. Migliaresi, L. Nicodemo, L. Nicolais, L. Iaccarino, and S. Roccotelli, "Water sorption and mechanical properties of a glass-reinforced polyester resin," *Composites*, vol. 13, no. October, pp. 406–410, 1982.
- [99] B. Yousif and N. El-Tayeb, "On the effect of woven glass fabric orientations on wear and friction properties of polyester composite," *Surf. Rev. Lett.*, vol. 14, no. 03, pp. 489–497, 2007.
- [100] —, "Tribological evaluations of polyester composites considering three orientations of CSM glass fibres using BOR machine," *Appl. Compos. Mater.*, vol. 14, no. 2, pp. 105–116, 2007.
- [101] V. Srinivasan, R. Karthikeyan, G. Ganesan, and B. Asaithambi, "Comparative study on the wear behavior of long and short glass fiber reinforced plastics," *Met. Mater. Int.*, vol. 16, no. 2, pp. 205–212, 2010.
- [102] I. Vitez, "Abrasive wear resistance," *Metallurgija*, vol. 47, no. 4, pp. 351–355, 2008.
- [103] M. D. S. Banea L.F.M., "Adhesively bonded joints in composite materials: an overview," *J. Mater. Des. Appl.*, vol. 223, no. 1, pp. 1–18, 2009.
- [104] K. Kural, M. Voskuil, T. Fengnian, and J. Pauwelussen, "Determination of representative loading conditions for effective semitrailer design," *Transport*, vol. 29, no. 4, pp. 363–375, 2014.
- [105] J. Kim and G. Jang, "Development of a lightweight frame for a 40-foot flatbed trailer by using CAE-based structural optimization," *Proc. Inst. Mech. Eng. Part D J. Automob. Eng.*, vol. 225, no. 5, pp. 643–652, 2011.
- [106] J. G. Kim and M. S. Yoon, "Optimal design of lightweight frame for heavy flat-bed trailer by using taguchi method," *Trans. Korean Soc. Mech. Eng. A*, vol. 34, no. 3, pp. 353–359, 2010.
- [107] A. Yasar and P. O. Box, "Design, analysis and optimization of heavy vehicle chassis using finite element analysis," *Int. J. Sci. Technol. Res.*, vol. 1, no. 1, pp. 1–9, 2015.

- [108] S. Murali Sankar and P. Yuvaraj, "Optimization of heavy truck chassis design parameters using FEM," *Int. J. Pure Appl. Res. Eng. Technol.*, vol. 3, no. 4, pp. 333–343, 2014.
- [109] H. Quan-li, T. Lin-hong, and Q. Ling-jin, "Research on optimization design of heavy-duty truck frame based on the sensitivity," in *Int. Assoc. Comput. Sci. Inf. ICCSIT Technol. IEEE Int. Conf. Comput. Sci. Inf.* Chengdu, China: IEEE, 2010.
- [110] M. Mahmoudi-Kaleybar, I. Davoodabadi, V. Visnjic, and a. Ajkar, "Stress and dynamic analysis of optimized trailer chassis," *Teh. Vjesn.*, vol. 21, no. 3, pp. 599–608, 2014.
- [111] B. R. Guron, D. V. Bhope, and P. Y. L. Yenarkar, "Finite element analysis of cross member bracket of truck chassis," *Int. J. Eng. Sci. Res. Technol.*, vol. 2, no. 12, pp. 3432–3438, 2013.
- [112] A. O. Moaaz and N. M. Ghazaly, "A review of the fatigue analysis of heavy duty truck frames," *Am. J. Eng. Res.*, no. 10, pp. 1–6, 2014.
- [113] ASTM International, "ASTM C365/C365M standard test method for flatwise compressive properties of sandwich cores," Philadelphia, PA, 2003.

# Appendix A

## Sandwich panel calculations

### A.1 Flexural rigidity

Flexural rigidity of each sandwich panel, calculated as per [87]:

$$D = \frac{E_f b t_f (t_f + t_c)^2}{2} + \frac{E_f b t_f^3}{6} + \frac{E_c b t_c^3}{12} \quad (\text{A.1})$$

### A.2 Failure collapse loads

Competing collapse modes are calculated using the equations defined by Steeves and Fleck [88]. Core shear failure occurs when the shear strength of the core is exceeded.

$$P_{CS} = 2b(t_f + t_c)\tau_c \quad (\text{A.2})$$

Face yielding occurs when the axial stress in the face sheet reaches the yield strength of the material.

$$P_{FY} = \frac{4bt_f(t_f + t_c)\sigma_f}{l} \quad (\text{A.3})$$

Ductile indentation occurs when the face sheets are assumed to form plastic hinges at the boundaries of the indentation region.

$$P_{ID} = 2bt_f(\sigma_f\sigma_c)^{1/2} \quad (\text{A.4})$$

Elastic indentation occurs when the face sheets remain elastic while the core yields plastically. In this case, the face sheets behave as a beam column upon a non-linear foundation,

which is the core.

$$P_{IE} = bt_f \left( \frac{\pi^2(t_f + t_c)E_f\sigma_f^2}{3l} \right)^{1/3} \quad (\text{A.5})$$

### A.3 Failure mode map methodology

In order to construct sandwich failure mode maps, it is first necessary to define the following non-dimensional material and geometric parameters:

$$\bar{t} = \frac{t_f}{t_c}; \bar{c} = \frac{t_c}{l}; \bar{\sigma} = \frac{\sigma_c}{\sigma_f}; \bar{\tau} = \frac{\tau_c}{\sigma_f}; \bar{E} = \frac{E_c}{\sigma_f}; \text{ and } \bar{\rho} = \frac{\rho_c}{\rho_f}; \quad (\text{A.6})$$

A non-dimensional load index  $\hat{P}$  is defined as

$$\hat{P} = \frac{P}{bl\sigma_f} \quad (\text{A.7})$$

The mass of the sandwich beam  $M$  is calculated as

$$m = bl(2t_f\rho_f + t_c\rho_c) \quad (\text{A.8})$$

and the non-dimensional mass index  $\hat{m}$  is defined by substituting the non-dimensional parameters from Eqn. A.6 into Eqns. A.7 and A.8.

$$\hat{m} = \frac{m}{bl^2\rho_f} = \bar{c}(2\bar{t} + \bar{\rho}) \quad (\text{A.9})$$

The failure loads of the competing collapse modes (Eqns. A.2 to A.5) can also be non-dimensionalised in a similar fashion, as shown in Eqns. A.10 to A.13.

$$\hat{P}_{CS} = 2\bar{\tau}(\bar{t} + 1)\bar{c} \quad (\text{A.10})$$

$$\hat{P}_{FY} = 4\bar{t}(\bar{t} + 1)\bar{c}^2 \quad (\text{A.11})$$

$$\hat{P}_{ID} = 2\bar{t}\bar{c}\bar{\sigma}^{1/2} \quad (\text{A.12})$$

$$\hat{P}_{IE} = \left( \frac{\pi^2 \bar{\sigma}^2 \bar{E}}{3} \right)^{1/3} \bar{t}(\bar{t} + 1)^{1/3} \bar{c}^{4/3} \quad (\text{A.13})$$

Having defined the non-dimensional load indices, failure mode maps can be constructed by first determining the weakest and therefore active failure mode which then gives the dominant failure regimes. The failure mode maps can also be used to optimise the sandwich panel design. The optimisation strategy outlined by Steeves and Fleck [88], finds values of  $\hat{t}$  and  $\hat{c}$  that minimise the mass index  $\hat{m}$  for a given load index  $\hat{P}$ . The trajectory of the minimum mass design then typically lies along the failure mode boundaries, although it can also lie with the elastic indentation domain and the face yield domain. Within the elastic indentation domain, the optimal value of  $\hat{t}$  is given by Eqn. A.14.

$$\bar{t} = \frac{3\bar{\rho}}{2(1 - 2\bar{\rho})} \quad (\text{A.14})$$

Within the face yield domain, the optimal value of  $\hat{t}$  is given by Eqn. A.15.

$$\bar{t} = \frac{\bar{\rho}}{2(1 - \bar{\rho})} \quad (\text{A.15})$$

## Appendix B

### Sandwich panel flexural testing

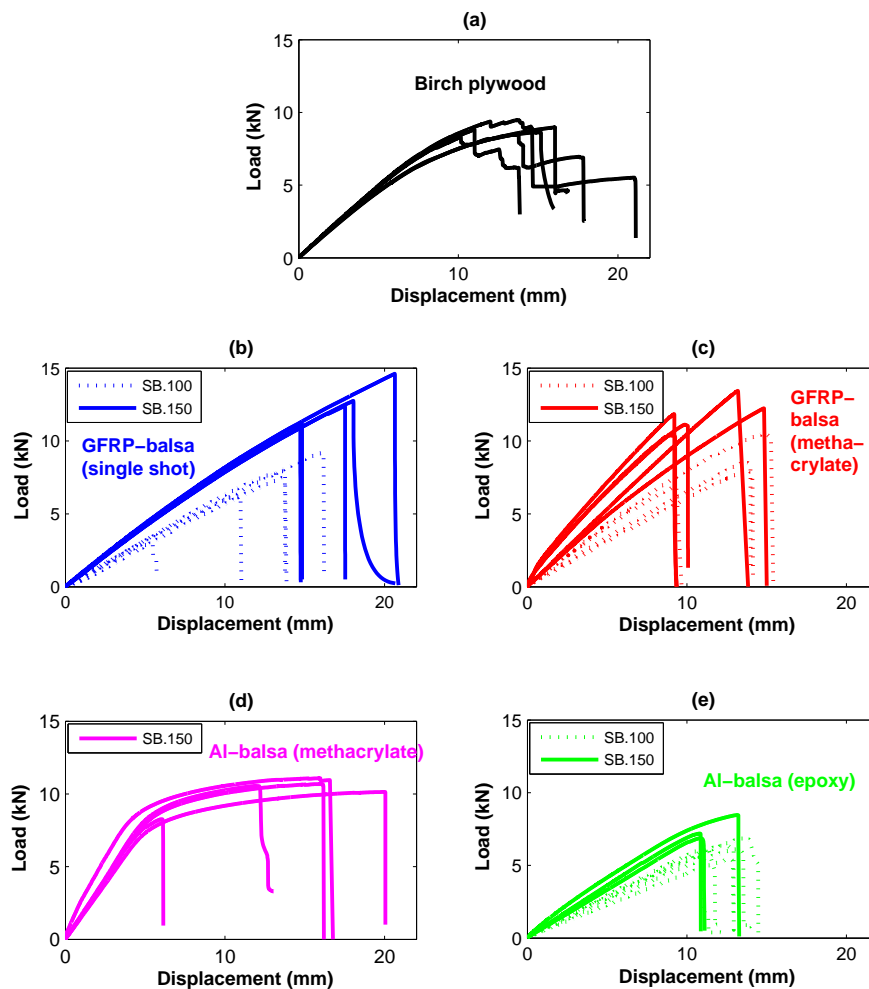


**Fig. B.1** Load-displacement curves of sandwich panels in three point bending compared to birch plywood decking.

# Appendix C

## Balsa micrographs

### C.1 Intermediate density end-grain balsa

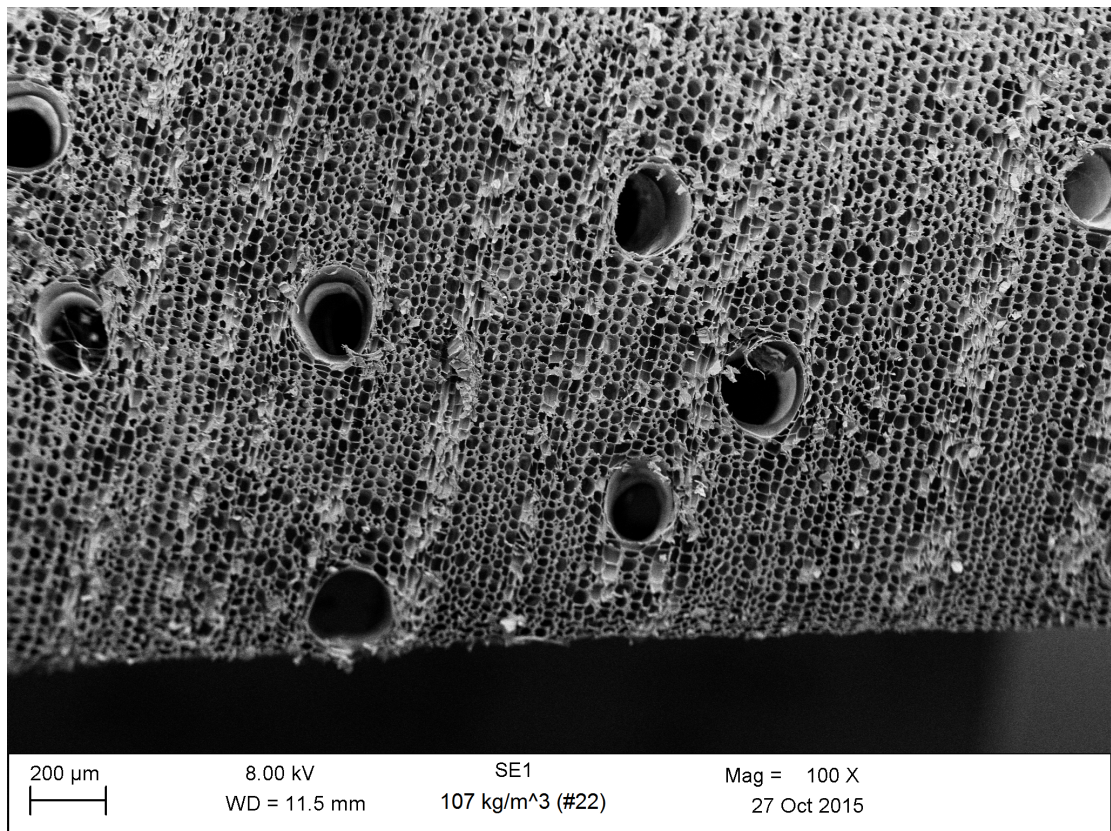


**Fig. C.1** Intermediate density end-grain balsa micro-structure.



## C.2 High density end-grain balsa

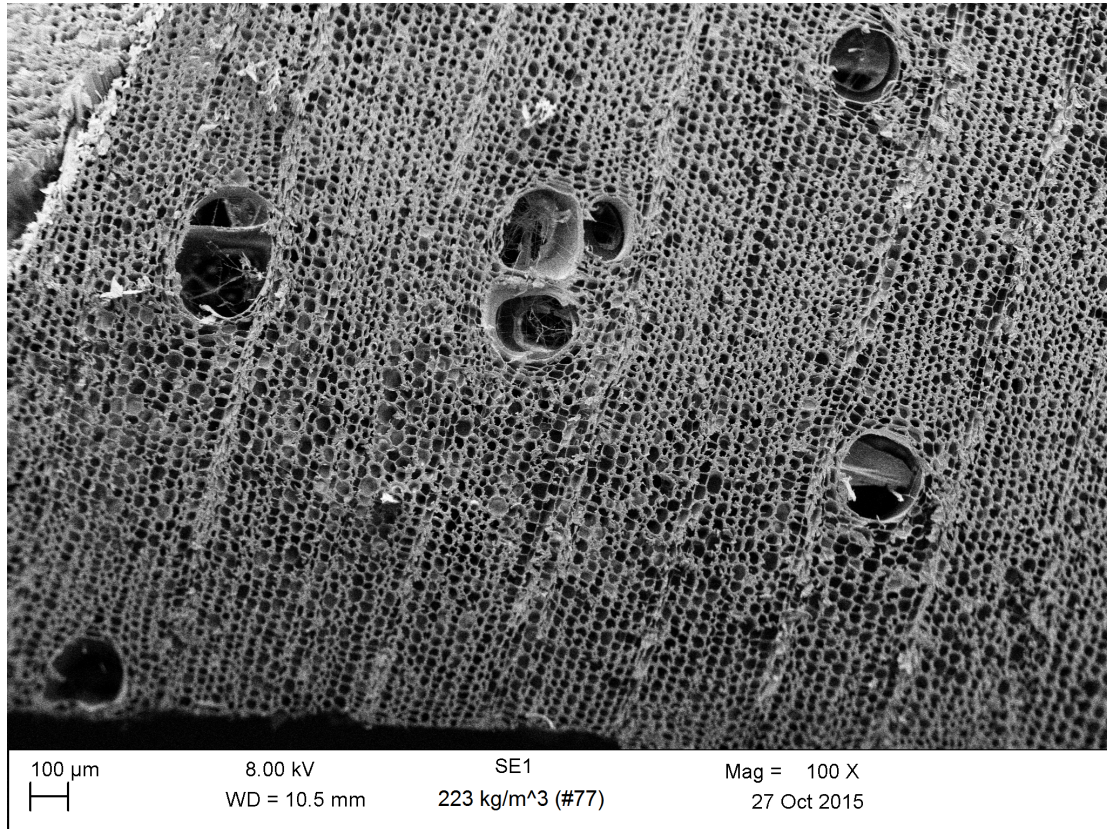


**Fig. C.2** High density end-grain balsa micro-structure.

## Appendix D

### Balsa compression testing

The compressive strength and modulus of the balsa core are determined parallel to the end-grain in accordance with ASTM C365/C365M standard test method for flat-wise compressive properties of sandwich cores [113]. A speed of 0.5 mm/min was used in testing and all specimens tested had nominal dimensions of  $50 \times 50 \times 25$  mm. Compressive properties are plotted against density and trend lines highlight the relationship between the two properties (Fig. D.1).

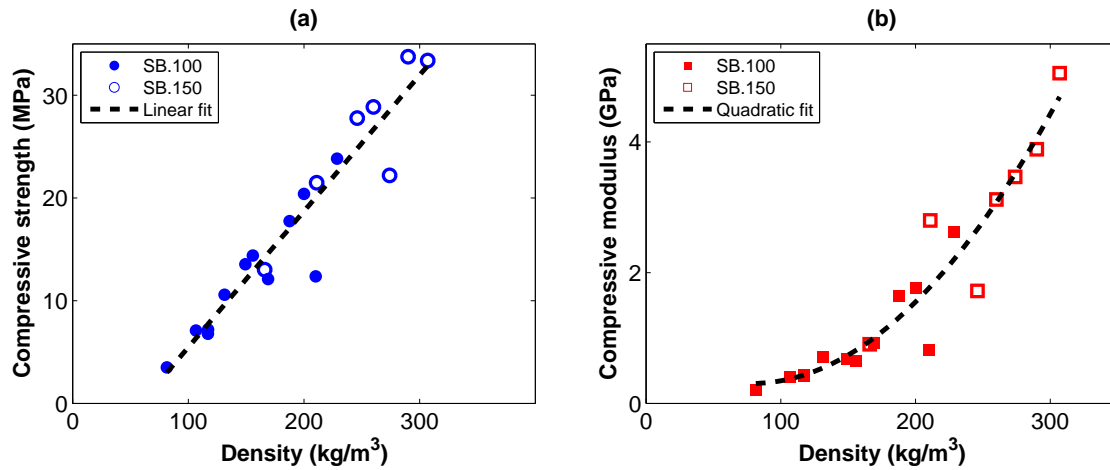


**Fig. D.1** Variations in (a) compressive strength and (b) compressive modulus, with density of end-grain balsa core used in sandwich panel construction. Properties are determined in accordance with ASTM C365/C365M. Dashed lines correspond to polynomial fits to experimental data.